UNIVERSITY OF CALIFORNIA, SAN DIEGO

FtsZ dynamics and the regulation of division site selection by the MinCD division inhibitor in *Bacillus subtilis*

A dissertation submitted in partial satisfaction of the requirements for the degree Doctor of Philosophy

in

Biology

by

James Alan Gregory

Committee in charge:

Professor Kit Pogliano, Chair
Professor Doug Bartlett
Professor Mark Ellisman
Professor E. Peter Geiduschek
Professor Milton Saier
Professor Moselio Schaechter

2009

The Dissertation of James Alan Gregory is approved, and it is acceptable in quality and form for publication on microfilm and electronically:

_____

_____

_____

_____

_____

_____
Chair

Table of Contents

List of Tables and Figures

Chapter 1

Chapter II

Chapter III

Chapter IV

Acknowledgments

Graduate school is an endeavor that I could never have completed without the patience, expertise, and encouragement of many people. The current and former Pogliano lab members, Linda, Xin, Aileen, Ana, Dan, Eric, Alan, Rachel, Ida, James, Shinobu, Jonathon, Stefan, Jennifer, Kenny, Nick, Grace, Tinya, Rachelle, and Anne were instrumental to my research and I would like to thank them for their technical advice and assistance, as well as for providing a work environment that kept me coming back day after day. I am indebted to Eric for showing me that the only limitation in research is your own creativity provided that you are willing to put in the effort to make absurd ideas a reality. I am especially grateful to Alan for the advice and guidance that he has provided even when he clearly knew it was not what I wanted to hear.

This dissertation would not have been possible without the support and enthusiasm of my adviser, Kit Pogliano. Discouragement is an inevitable part of graduate school, but through her actions and attitude, I am constantly reminded of the excitement of discovery and the satisfaction of fulfilling curiosity.

To my family, Mom, Dad, Pat, Michael, and my girlfriend, Mary, thank you for always being there, for I could never have reached this high if I were not standing on the foundation of love and support that you have provided.

The text of Chapter II has been submitted for publication and the dissertation author was the primary author and researcher. I would like to thank Eric Becker, Ida Tuwatananurak, James Jung, and Kit Pogliano for their permission to use this manuscript in my dissertation. The dissertation author was the primary author and researcher.

The text for chapter III is a manuscript that was published on December 15th, 2008, in Genes and Development. I would like to thank Eric Becker and Kit Pogliano for their permission to use this manuscript in my dissertation. The dissertation author was the primary author and researcher.

Curriculum Vitae

2002	Bachelor of Science in Biochemistry, *magna cum laude* Miami University (Oxford, OH)
2002-2003	Massachusetts General Hospital Microarray technician
2004-2007	Teaching Assistant, Division of Biological Sciences, University of California, San Diego
2006-2007	Advanced Placement Chemistry Teacher, San Diego Jewish Academy, San Diego, CA
2007-2008	Head Teaching Assistant, Division of Biological Science, University of California, San Diego
2003-2009	Doctor of Philosophy in Biology, University of California, San Diego

Bjorkbacka, H., Fitzgerald, K.A., Huet, F., Gregory, J.A., Lee, M.A., Ordija, C.M., Dowley, N.E., Golenbock, D.T., Freeman, M.W. The induction of macrophage gene expression by LPS predominantly utilizes Myd88-independent signaling cascades. (2004). Physiol Genomics. Nov. 17; 19(3): 319-330.

Gregory, J.A. Becker, E.C., Pogliano, K. *Bacillus subtilis* MinC destabilizes FtsZ-rings at the new cell poles and contributes to the timing of cell division. (2008). Genes Dev. Dec 15; 22(24): 3475-88.

Abstract of the dissertation

FtsZ dynamics and the regulation of division site selection by the MinCD division inhibitor in *Bacillus subtilis*

by

James Alan Gregory

Doctor of Philosophy in Biology
University of California, San Diego, 2009
Professor Kit Pogliano, Chair

Bacillus subtilis and *Escherichia coli* regulate division site selection through two overlapping systems that together restrict FtsZ-ring assembly to midcell. The first system is nucleoid occlusion, which is mediated by the nonspecific DNA binding protein Noc and SlmA in *B. subtilis* and *E. coli* respectively. Nucleoid occlusion prevents assembly of the Z-ring across the nucleoid. The second system prevents division at the cell poles and is mediated by MinC and MinD (MinCD). In the absence of MinCD, division occurs at the cell poles, resulting in anucleate minicells in both *E. coli* and *B. subtilis*.

The cellular localization of MinCD in *E. coli* and *B. subtilis* is differentially regulated by the unrelated proteins MinE and DivIVA respectively. *B. subtilis* DivIVA

sequesters MinCD to the cell poles, where it interacts with FtsZ to prevent Z-ring assembly. MinE promotes the pole-to-pole oscillation of MinCD that results in a time averaged concentration of MinCD that is highest at the cell poles. The drastic difference between the localization of MinCD in *E. coli* and *B. subtilis* led me to reinvestigate the localization of *B. subtilis* MinCD using new methods.

I constructed a transposon that I call TAGIT (Tn5 Assisted Gene Insertion Technology) to transcriptionally fuse *gfp* to *minCD*. TAGIT randomly inserts *gfp* into a target gene and allows for the rapid identification of in-frame insertions. I utilized TAGIT to construct a library of *gfp-minCD* insertions, from which I isolated a fully functional MinC-GFP that was subsequently integrated at the native chromosomal locus in *B. subtilis* in order to maintain wild type regulation of *minCD*. I then carried out time-lapse epifluorescence microscopy, TIRFM (Total Internal Reflection Fluorescence Microscopy), and SI (Structured Illumination) microscopy of MinC-GFP and FtsZ-GFP to study their cellular localization in growing cells.

I propose a new model of MinC function; MinC prevents FtsZ structures that assemble immediately after cytokinesis at the new cell pole from supporting cell division. The highest concentration of MinC is found at midcell during the last stages of cytokinesis. MinC is then released from the division site thereby placing it in the same region of the cell at the same time that aberrant FtsZ structures assemble. There it disrupts the lateral interactions between FtsZ protofilaments, which promotes FtsZ to relocalize to the midcell, thus ensuring proper placement of the division site.

Chapter I

Introduction

A History of Cell Division in Bacteria

Cell theory states that the functional unit of life is the cell and that all cells are derived from existing cells (Turner, 1940). The ability to divide is therefore essential for the propagation of life that has evolved on Earth. Cell division has evolved to accommodate division in all organisms, regardless of size, shape, or the amount of DNA. Cell division occurs only after the parent cell has duplicated and segregated its DNA. Indeed, the primary purpose for cell division is the maintenance and propagation of genetic material. Each daughter cell possesses identical genetic material as well as the RNA and proteins necessary for future division and therefore the continued survival of the species. A fundamental question in biology is how organisms coordinate cell division with the many of other cellular processes that they must perform (reviewed by (Asato, 2006; Haeusser & Levin, 2008; Hett & Rubin, 2008;Jorgensen&Tyers,2004).

The "simplest" organisms to study this process of cell division are bacteria that possess a single chromosome. In rod shaped bacteria, the cell replicates its DNA and subsequently segregates it by a poorly understood active mechanism. Following DNA segregation, a contractile ring forms at midcell, which then constricts to give rise to two daughter cells, each containing identical copies of the DNA. The contractile ring responsible for division is made up of a complex of proteins; the function of many of

these proteins has yet to be elucidated. The mechanism by which these processes occur is a central question in contemporary biological research.

The bacterial cell cycle

Rod shaped bacteria such as *Escherichia coli* and *Bacillus subtilis* propagate by binary fission, whereby the cell elongates and then divides symmetrically to produce two identical daughter cells (Errington et al, 2003; Ryan & Shapiro, 2003; Slater & Schaechter, 1974). Towards that end, the cell must coordinate a few basic cellular processes: replicating and segregating the chromosome, doubling the cell mass, assembling the necessary machinery for division in the proper position, and finally carrying out cytokinesis. While on the surface this process appears simple, countless studies have demonstrated otherwise; cell division is complicated not only in its regulation, but also the process itself. Furthermore, bacterial cell division is affected by external stimulus such as temperature, nutrient availability, and numerous chemical compounds, which in turn, affect growth rate. The mechanisms by which these regulatory stimuli are integrated into the cell cycle largely remain unknown.

Arthur Henrici published the first studies on bacterial cell division in the 1920's. Henrici conducted numerous studies on freshwater bacteria and was mostly interested in studying natural bacterial communities rather than purified monocultures (Henrici, 1933). He did, however, analyze the growth of *Bacillus megaterium* (Henrici, 1925) and *E. coli* (Henrici, 1928) over time in various media using light microscopy. The results

indicated that bacteria undergo “cytomorphosis,” a term coined by Henrici, whereby cells undergo a series of progressive morphological changes that correlate to the position on a typical bacterial growth curve. For example, bacterial cell size changes depending on growth rate, with growing cells being larger than stationary phase cells. Henrici did not address specific mechanisms of division or cell size regulation, but he did understand that continual observation of cell growth over time was essential for understanding the cell cycle of an organism. This was accomplished either by removing cells from a growing culture at predefined time intervals or by the continuous observation of a group of cells using time-lapse microscopy. Both methods are still used today.

Subsequent studies quantified many of the biochemical changes that different growth rates imposed on the cells. For example, Schaechter et al. were later able to quantify many of the biochemical changes that accompanied different growth rates when they studied the relationship of growth rate with cellular composition and cell size in *Salmonella typhimurium* (Schaechter et al, 1958). In doing so, they discovered that *S. typhimurium* are not simply in a resting or a growing state, but assumed a physiological state that is growth rate dependent and predominantly determined by the growth medium. This physiological state can be measured in terms of mass, RNA, and DNA per cell, which change exponentially with growth rate during steady growth. Furthermore, the physiological state can be either maintained by dilution with fresh media or altered by changing the growth media. Interestingly, the rate of RNA synthesis and mass increases within minutes of switching growth media, but there is

approximately seventy minutes of lag time at 37ºC before changes in the rate of cell division are observed regardless of the growth rate before and after the shift in *S. typhimurium* (Kjeldgaard et al, 1958). These discoveries imply that cell division is not governed by diffusion rates that are determined by the surface to area ratio of a cell (i.e. cell size). Instead, the growth rate must be coupled to the synthesis of proteins required for cell division. This demonstrated a connection between growth rate and the production of proteins required for division, but it provided little insight into the biochemical regulation of cell division.

The first identification of proteins that regulate cell division: the SOS response

The first step toward understanding the biochemical regulation of cell division came from the isolation of the *E. coli lon* mutant (formerly known as *capR*;(Hua & Markovitz, 1972)) that is defective in septation following low doses of ultraviolet (UV) radiation, which causes it to grow in long filaments that eventually lyse (Howard-Flanders et al, 1964). The sensitization of this strain to DNA damage by addition of bromodeoxyuridine suggests that filamentation is a direct consequence of DNA damage (Walker & Pardee, 1967).

The continued study of the link between chromosome replication, DNA damage and cell division led to the characterization of the SOS response (Fig. 1), which has been well characterized in *E. coli* (reviewed by (Butala et al, 2009; Janion, 2008; Walker, 1984)) and partially characterized in *B. subtilis* (reviewed by (Fernandez et al,

2000; Yasbin et al, 1991)). The SOS response is a cellular stress response that promotes DNA repair and increases cell viability in response to DNA damage (Witkin, 1976). Gudas and Pardee put forth the first model for DNA repair in 1975, which proposes that the RecA protein, a DNA dependent ATPase, mediates the SOS response (Gudas & Pardee, 1975). RecA is ATP dependent and catalyzes DNA strand exchange (Shibata et al, 1979) (McEntee et al, 1979) and DNA recombination (Rupp & Howard-Flanders, 1968). Upon DNA damage, single stranded DNA is present in the cell, which activates RecA (Rupp & Howard-Flanders, 1968). Then RecA, in a complex with single stranded DNA and ATP (Phizicky & Roberts, 1981), promotes the autoproteolytic of cleavage LexA (Little, 1984), which is a repressor of the SOS response genes (Little & Harper, 1979; Mizusawa et al, 1983; Mount, 1977). Thus, LexA cleavage induces DNA repair enzymes.

The SOS response in *E. coli* also delays cell division until DNA repair has been completed. Thus, included in the genes that are repressed by LexA is *sulA*, which was discovered while searching for suppressors of *lon* (Gayda et al, 1976). SulA (suppressor of ultraviolet light) provided the link between the SOS response and the arrest of cell division (D'Ari et al, 1979; Huisman & D'Ari, 1981). Overexpression of *sulA* using an inducible promoter is sufficient to arrest cell division (Huisman et al, 1984; Schoemaker et al, 1984), and *sulA* mutants fail to arrest cell division that occurs after UV treatment in *lon* mutants (Gottesman et al, 1981). There was also genetic evidence that SulB, another suppressor of *lon*, was the target of SulA and that SulB may be directly involved in division (Gottesman et al, 1981; Huisman et al, 1984). Indeed, subsequent

research demonstrated a direct interaction between SulA and SulB (Holland & Jones, 1985; Jones & Holland, 1985) and that *sulB* mutations are in fact specific alleles of *ftsZ* (Lutkenhaus, 1983), which encodes a key cell division protein (Lutkenhaus et al, 1980). SulA cannot interact with FtsZ that is coded by the *sulB* allele, and therefore cannot mediate the arrest of cell division by blocking FtsZ polymerization (as described below).

The *lon* gene that was instrumental in discovering the link between DNA damage and cell division, encodes an ATP-dependent protease that allows UV-treated cells to ultimately resume normal growth by degrading SulA (Charette et al, 1984; Goldberg et al, 1994; Mizusawa & Gottesman, 1983). Lon is involved in many cellular processes including protein degradation (Gottesman & Zipser, 1978), lysogeny of temperate phages (Gayda & Markovitz, 1978), and production of capsular polysaccharide (Markovitz, 1964).

The bacterial cousin of tubulin, FtsZ

The extent of cellular organization in bacteria is remarkable, especially when one considers that the volume of most bacteria is just a few cubic microns. The notion that bacteria are simply bags of enzymes was abandoned in the 1990's and has been replaced by a view of the bacterial cells as highly organized cells that contain an elaborate cytoskeleton (reviewed by (Dye & Shapiro, 2007; Graumann, 2007; Moller-Jensen & Lowe, 2005). Arguably the most studied of the cytoskeletal elements in

bacteria is FtsZ (reviewed by (Dajkovic & Lutkenhaus, 2006; Lowe & Amos, 2009; Pichoff & Lutkenhaus, 2007)), which is nearly ubiquitous in bacteria. FtsZ (filament temperature sensitive) got its name from *E. coli* cell division mutants isolated in the 1960's that formed elongated filaments at elevated temperatures because they are unable to divide at nonpermissive temperatures (Hirota et al, 1968; Van De Putte et al, 1964).

FtsZ, the bacterial homologue to eukaryotic tubulins (reviewed (Erickson, 2007; Lowe & Amos, 2009)), plays a critical role in bacterial cell division, as it recruits all other cell division proteins to future division sites. This family of proteins shares the ability to hydrolyze GTP and polymerize in a head to tail fashion. Despite the low overall sequence similarity between FtsZ and tubulin (less than 10% sequence identity), the structures of the core domain of β-tubulin and FtsZ bound to GDP are super-imposable (Lowe, 1998; Lowe & Amos, 1998; Nogales et al, 1998). Sequence alignment demonstrated that the most conserved amino acids are part of the GTP binding pocket, which is formed between two FtsZ monomers in bacteria and between α and β-tubulin in eukaryotes (Erickson, 2007).

Tubulins form linear polymers called protofilaments that assemble into higher order structures called microtubules, which are hollow bundles of protofilaments (reviewed by (Beghin et al, 2007; Desai & Mitchison, 1997; Wade, 2007), (Mitchison, 1992)). Microtubules undergo periods of growing and shrinking called dynamic instability (Mitchison & Kirschner, 1984]. Following GTP hydrolysis, GDP is trapped in the growing microtubule leaving a polymer that is composed of GDP-tubulin. Dynamic instability is a consequence of the inherent instability of GDP-tubulin

polymers, which will rapidly depolymerize in the absence of a stabilizing GTP-tubulin cap. The dynamic instability allows microtubules to perform mechanical work, which is essential for cell polarity {Siegrist, 2007 #1190), chromosome segregation (Bhalla & Dernburg, 2008), cell motility (Mitchell, 2007), and intracellular trafficking (Akhmanova et al, 2009).

FtsZ monomers also assemble into protofilaments (Fig. 2)(Oliva et al, 2004), but these protofilaments do not appear to assemble into microtubules and instead makes lateral interactions to assemble "bundles" of protofilaments, nor is there definitive evidence that they undergo dynamic instability. The crystal structure of FtsZ protofilaments suggests they do not trap GDP, which may explain the absence of dynamic instability (Lowe & Amos, 2000). Biochemical evidence is not definitive, however, with some experiments suggesting that FtsZ protofilaments contain mostly GTP (Romberg & Mitchison, 2004) and others GDP (Scheffers & Driessen, 2002). Lateral interactions have been demonstrated between FtsZ protofilaments *in vitro*, which mediate assembly into tubes, bundles, and sheets of FtsZ protofilaments under certain conditions (Kuchibhatla et al, 2009; Lowe & Amos, 2000; Yu & Margolin, 1997). Bundles of filaments have also been observed in cryoelectron tomography of *Caulobacter crescentus* although it is unclear if the bundles observed were FtsZ (Briegel et al, 2006). It has been postulated that lateral interactions between FtsZ protofilaments may be important for the structural integrity of the Z-ring (Dajkovic et al, 2008), which is a ring-like structure composed of FtsZ that assembles at midcell (see Visualizing FtsZ in bacterial cells).

Assembly of FtsZ and tubulin is cooperative (Mukherjee & Lutkenhaus, 1994) (Chen et al, 2005) (Caplan & Erickson, 2003). Microtubule subunits encounter head to tail interactions as well as lateral interactions during microtubule polymerization therefore addition of a tubulin to a growing microtubule is more favorable than an interaction between two microtubule subunits. There is also a kinetic barrier on initiation of new microtubules, which requires the nucleation factor, γ-tubulin. Together, these barriers to initiation of polymerization prevent aberrant assembly of microtubules in eukaryotic cells. Bacteria do not have a homologue of γ-tubulin and FtsZ does not assemble the striking hollow tubules therefore cooperative assembly cannot be achieved by the same mechanisms. The strongest evidence for the cooperative assembly of FtsZ is the requirement of a critical concentration for GTPase activity and polymerization *in vitro* (Caplan & Erickson, 2003; Huecas & Andreu, 2004). Alternate hypothesis for cooperative assembly of FtsZ have been proposed (Caspar, 1980; Gonzalez et al, 2005; Miraldi et al, 2008). In these models, a conformational change (Fig. 2B) in FtsZ polymers is proposed to result in a higher affinity interaction with FtsZ monomers than interactions between monomeric FtsZ therefore polymerization is favored over nucleation.

Possibly the most significant difference between FtsZ and tubulins is their divergence in function. Cytokinesis in bacteria is dependent on FtsZ whereas cytokinesis in eukaryotes is largely mediated by actins (Barr & Gruneberg, 2007). The origin of this divergence is unclear, but it has been postulated that a redundant copy of FtsZ in an ancient eukaryotic cell allowed it to evolve a role in chromosome segregation

(Erickson, 2007). TubZ, which is distantly related to FtsZ and Tubulin, ensures the stability of pBtoxis, a low copy plasmid in *Bacillus thuringiensis* and is an example of a bacterial tubulin that is functionally similar to eukaryotic tubulins that are involved in DNA segregation (Larsen et al, 2007). FtsZ is highly conserved, even among divergent organisms, with 41% identity between *E. coli* and *B. subtilis* FtsZ. A reasonable conclusion is that FtsZ is evolutionarily constrained because it must maintain a particular three-dimensional structure to be viable for cell division. A redundant copy of FtsZ would not be confined by the same restraints.

Visualizing FtsZ in bacterial cells

Prior to the 1990's, the study of FtsZ was largely confined to biochemists who analyzed the function of proteins *in vitro,* and geneticists who were using relatively primitive microscopy techniques to study cell division mutants. In fact, a review of *E. coli* cell division in 1993 stated that the present microscopy techniques lacked the sensitivity and resolution necessary to study the cellular distribution of proteins in bacteria (de Boer, 1993). The limitations of microscopy were clearly a large hurdle to overcome for microbiologists, but an equal hurdle was the view that bacteria were simply bags of enzymes lacking in subcellular organization, so there was not much to be gained by cell biological studies. Ironically, one year prior to de Boer's review, Douglas Prasher published a paper that elucidated the structure of the *Aequorea victoria* Green Fluorescent Protein (GFP) (Prasher et al, 1992). Two years later he would express GFP in *E. coli* and make the cells fluoresce when illuminated with light at 488

nanometers (Chalfie et al, 1994). He also proposed that GFP might be a suitable marker to track protein localization *in vivo*. The use of fluorescence microscopy to study the subcellular localization of proteins in bacterial cells was first demonstrated in 1993, when studies from Lucy Shapiro's lab demonstrated the polar localization of the chemoreceptor complex in *E. coli* (Maddock & Shapiro, 1993) and in 1995, when Rich Losick's lab demonstrated the specific localization of proteins to cell division sites (Arigoni et al, 1995).

A modern view of bacterial cell division

FtsZ localizes to future division sites in *E. coli*, *B. subtilis*, and all other organisms in which it has been localized using immunoelectronmicroscopy (Bi & Lutkenhaus, 1991), immunofluorescence, (Levin & Losick, 1996) or GFP fusions (Ma et al, 1996). In *E. coli*, expression of the wild type *ftsZ* was necessary because FtsZ-GFP could not complement an *ftsZ-* strain, while in *B. subtilis*, the expression of FtsZ-GFP by itself was possible, but accompanied by a temperature sensitive phenotype. This suggested that fusing GFP to FtsZ interferes with FtsZ function. Despite this drawback, FtsZ-GFP allows researchers to directly visualize FtsZ in live cells in order to address Z-ring dynamics, Z-ring constriction, and FtsZ movement during the cell cycle and development.

These studies have revealed that FtsZ is highly dynamic. FRAP (fluorescence recovery after photobleaching) experiments of Z-rings, in which FtsZ-GFP in the Z-ring

was bleached using a laser, revealed that the fluorescence of the Z-ring recovers, indicating that unbleached FtsZ-GFP from the cytoplasm is rapidly incorporated into the Z-ring (Anderson et al, 2004; Stricker et al, 2002). This suggests the exchange of FtsZ monomers or protofilaments from the cytoplasm with the Z-ring, or the rearrangement of FtsZ protofilaments within the Z-ring, since only half of the Z-ring was bleached in these experiments. Remarkably, the half-time of recovery of the Z-ring is the same in *E. coli* and *B. subtilis*. One limitation of these studies is that they did not discriminate between dividing and non-dividing cells, making it unclear if FtsZ turnover is identical before and after cell division. Thus, the published studies of FtsZ dynamics using FRAP did not fully harness the potential of this method to investigate mechanisms of constriction, nor did they illuminate the mechanism for turnover within the Z-ring.

There are several possible mechanisms for constriction. First, in eukaryotes it is common for a motor protein to drive the sliding action between two adjacent filaments (reviewed by (Bramhill, 1997)). In theory, FtsZ filaments sliding across one another would decrease the length between their distal ends thus providing a constrictive force. However, no cytoskeleton-associated motor proteins have been identified in bacterial cells. Second, FtsZ might simply be a scaffold that recruits other proteins that direct the inward growth of the septum. For example, the Z-ring positioned at midcell recruits proteins involved in PG biosynthesis (reviewed by (Scheffers & Pinho, 2005)), which might mediate cell constriction through synthesis of the cell wall. Third, it is possible that a conformational switch between straight and bent FtsZ protofilaments might

provide the force necessary for constriction by bringing the ends of a single protofilaments, and the membrane to which it is attached, closer together (Ghosh & Sain, 2008). In keeping with this model, recent data from cryoelectron tomography of FtsZ protofilaments in *Caulobacter crescentus* favors a conformational switch from straight to bent protofilaments as the driving force (Li et al, 2007). Recent crystallographic data refutes this hypothesis on the grounds that there is no observable nucleotide-dependent switch from straight to bent protofilaments (Oliva et al, 2007). Reconstitution of Z-rings in tubular liposomes demonstrates that FtsZ can produce visible constrictions when a membrane anchor is provided, suggesting that FtsZ generates a constrictive force (Osawa et al, 2008), or that the diameter of Z-rings is smaller than the liposomes and the membrane anchor pulls the liposome inward. Thus, the models for constriction are dependent on membrane-anchored FtsZ protofilaments, which are pushed or pulled inward by an unknown mechanism.

The Z-ring in the daughter cell begins to assemble while the parent cell is in the final stages of cytokinesis (Sun & Margolin, 1998), relocalizing to the midpoint of the new daughter cells. Relocalization of FtsZ has been proposed to occur through an extended helical structure that has been observed *in vitro* (Lowe & Amos, 2000), as well as in living vegetative cells (Michie et al, 2006; Peters et al, 2007; Thanedar & Margolin, 2004), and sporulating cells (Ben-Yehuda & Losick, 2002). A helical intermediate could be formed by polymerization emanating from the completed septa or by the movement of a coil by a spring-like mechanism. This model proposes that the helical structure would reassemble or collapse into a ring at the nascent division site. In

contrast to this model, my studies of FtsZ-GFP (Chapter IV) suggests that FtsZ moves about the cell as short membrane associated protofilaments. These protofilaments are highly dynamic and appear to coalesce into a Z-ring at midcell. Consistent with this model of Z-ring assembly, cryoelectron tomography of *Caulobacter crescentus* revealed a Z-ring that is composed of multiple protofilaments (Li et al, 2007).

Spatial Regulation of FtsZ-ring assembly and divisome maturation

There is abundant evidence that Z-ring ring assembly is spatially regulated to ensure that the divisome is positioned at midcell. Indeed, unstressed *E. coli* and *B. subtilis* cells spatially regulate FtsZ assembly by two systems: the Min system and the nucleoid occlusion proteins (SlmA and Noc). Together these systems confine cell division to the midcell by preventing cell division at the cell poles (Min) and over the chromosome (SlmA, Noc) (Fig. 3).

The widely conserved MinCD proteins, which spatially regulate cell division in a variety of organisms (Lutkenhaus, 2007; Mazouni et al, 2004; Ramirez-Arcos et al, 2001; Rothfield et al, 2005; Szeto et al, 2001), prevent division at the cell poles that would result in production of anucleate minicells. MinC inhibits division at the cell poles through a direct interaction with FtsZ that perturbs the lateral interactions between FtsZ protofilaments in *E. coli* (Dajkovic et al, 2008; Shen & Lutkenhaus, 2009) and *B. subtilis* (Scheffers, 2008), which might destabilize Z-rings or compromise interactions between the Z-ring and the late division proteins. *In vivo,* MinC exists as a dimer and is

composed of an N- and C-terminal domain that are responsible for direct interaction with FtsZ and dimerization, respectively (Cordell & Lowe, 2001; Hu & Lutkenhaus, 2000). Overproduced MinC can inhibit cell division in *E. coli* (de Boer et al, 1992) and *B. subtilis* (Levin et al, 2001), but only when expressed at 15-50X greater levels than the normal physiological concentration. This suggests that MinC must be properly localized to be a potent cell division inhibitor. This localization is mediated by MinD, which sequesters MinC to the membrane through a conserved C-terminal amphipathic helix (Szeto et al, 2002; Zhou & Lutkenhaus, 2004) and localizes MinC (as described below), thereby increasing the concentration of MinC on the membrane. MinD is a ParA-like ATPase and is the most highly conserved of the Min proteins (Szeto et al, 2002). Mutations in the ATP binding domain cause mislocalization of MinD and concurrent mislocalization of MinC (Hayashi et al, 2001). This suggests that the ATP binding activity of MinD is essential for membrane binding and localization of MinC.

The localization of MinCD in *E. coli* (Fig. 3A) and *B. subtilis* (Fig. 3B) are drastically different despite their conservation and nearly identical cellular functions in both organisms. First, MinCD localization is mediated by the unrelated proteins MinE and DivIVA in *E. coli* and *B. subtilis* respectively. In *E. coli*, MinE promotes MinD ATPase activity, which drives a periodic oscillation of MinCD from one cell pole to the other cell pole (Zhao et al, 1995). Mathematical modeling of *E. coli* MinCD dynamics shows that the oscillatory behavior results in a time average concentration of MinCD that is highest at the cell poles, where it must prevent cell division (Howard, 2004). Prior to my thesis work, it was thought that *B. subtilis* DivIVA sequesters MinCD to the

cell poles (Marston & Errington, 1999; Marston et al, 1998), via the recently identified MinJ linker protein (Bramkamp et al, 2008; Patrick & Kearns, 2008). In this view, the stable polar localization of B. subtilis MinC achieves the same aim as oscillation of *E. coli* MinC, providing a high enough concentration of MinC to prevent polar FtsZ-ring formation. However, my studies (Chapter III) have shown that MinC in not stably associated with the cell poles and predominantly localizes to the nascent division sites. Furthermore, my studies indicated that *B. subtilis* MinC is highly dynamic leaving newly completed septa and moving towards midcell, but I found no evidence of oscillatory behavior (Fig. 4). My data indicate that in *B. subtilis*, MinC prevents normally transient FtsZ structures that assemble immediately after cytokinesis adjacent to the completed septum from supporting cell division. This is consistent with recent biochemical studies, which demonstrate that MinC acts by disrupting the lateral interactions between FtsZ protofilaments.

A process known as nucleoid occlusion provides a second means negative regulation of cell division, by preventing FtsZ from assembling over the chromosome (Mulder & Woldringh, 1989; Woldringh et al, 1991; Yu & Margolin, 1999). The recently discovered nonspecific DNA binding proteins, Noc and SlmA, mediate nucleoid occlusion in *B. subtilis* (Wu & Errington, 2004) and *E. coli* (Bernhardt & de Boer, 2005) respectively. Mutations in *noc* (*yyaA*) and *slmA* were identified as synthetically lethal with mutations in *minCD* and depletion of either *slmA* or *noc* in a *minCD* strain causes severe defects in cell division, although single mutants in *noc* or *slmA* have no obvious phenotype under normal growth conditions. GFP fusions to Noc

and SlmA localize to the nucleoid suggesting both are nonspecific DNA binding proteins, although GFP-SlmA showed some affinity for the polar proximal regions of the chromosome. Consistent with being a division inhibitor, overexpression of *slmA* and *yyaA* inhibits cell division although the mechanism of inhibition of FtsZ assembly remains unknown.

Evidence for other spatial regulation mechanisms

EzrA is a *B. subtilis* transmembrane protein thought to decrease the critical concentration of FtsZ required for polymerization *in vivo* based on the observation that deleting *ezrA* results in polar Z-rings and suppression of the temperature sensitive *ftsZ* alleles at nonpermissive temperatures. Biochemical data suggests that EzrA prevents FtsZ polymerization without affecting FtsZ GTPase activity (Haeusser et al, 2004), suggesting that it might act in a similar manner to MinC by disrupting the lateral interactions between FtsZ protofilaments or by capping FtsZ protofilaments and preventing elongation. Unlike MinCD, EzrA colocalizes with FtsZ and is recruited to the division site immediately after Z-ring formation through a direct interaction with FtsZ (Haeusser et al, 2007). EzrA's function at midcell, while unclear, is genetically separable from its role as a spatial regulator of Z-ring assembly. Ezra contains a conserved C-terminal patch of amino acids known as the QNR patch (Haeusser et al, 2007). Mutations in the QNR patch prevent Ezra from localizing to midcell, but do not affect its role in preventing polar Z-rings, which suggests that EzrA has two distinct functions *in vivo*.

Regulation of FtsZ polymerization and Z-ring assembly

Similar to microtubules, FtsZ assembly is regulated to ensure that the correct balance between polymerization and disassembly is achieved (reviewed by (Dajkovic & Lutkenhaus, 2006; Errington et al, 2003; Goehring & Beckwith, 2005; Margolin, 2005; Romberg & Levin, 2003). This regulation is accomplished by both negative and positive regulatory proteins (Fig. 5). While progress has been made in understanding the mechanism by which individual proteins affect Z-polymerization *in vitro* and *in vivo*, it remains unclear how the activities of these proteins are coordinated or regulated to achieve the correct spatial and temporal regulation of cell division.

Key negative regulators of FtsZ polymerization include the *E. coli* proteins SulA, MinCD, and SlmA and the *B. subtilis* proteins EzrA, Noc, MinCD, ClpX, and UgtP. Three of these proteins, MinCD, Noc, and SlmA are principally involved in restricting FtsZ-ring assembly to the midcell (see spatial regulation of FtsZ ring assembly) or, in the case of MinCD, in preventing non-polar FtsZ rings from maturing into divisomes and initiating cell division. SulA, the effector of the E. coli SOS response, inhibits FtsZ polymerization by binding to and sequestering FtsZ monomers thereby preventing cell division (Trusca et al, 1998). DNA damage activates RecA, which in turn promotes autolytic cleavage of the LexA repressor thereby allowing transcription of the SOS response genes including SulA. ClpX, an ATPase and bacterial chaperone protein (Zolkiewski, 2006), was identified as a negative regulator of FtsZ polymerization in a screen for mutations that rescue the temperature sensitivity of FtsZ-

GFP in *B. subtilis*, but the mechanism or circumstances under which this regulation is important remain unclear (Haeusser et al, 2009; Weart et al, 2005). UgtP, the last protein in the glucolipid biosynthesis pathway, negatively impacts FtsZ assembly during rapid growth (Weart et al, 2007). Mutations in the enzymes of the glucolipid synthesis pathway cause rapidly growing cells to be unusually short compared to wild type cells suggesting that division occurs too early. UgtP-YFP localizes to the division site in response to elevated UDP-glucose levels, which is a metabolic indicator of rapid growth. Biochemical experiments suggest that UgtP directly interacts with FtsZ to inhibit FtsZ assembly. Initial studies of mutations in *E. coli* glucolipid biosynthesis suggest that UgtP might be a conserved link between growth rate and cell division.

The exact mechanisms by which EzrA, MinCD, ClpX, and Noc affect Z-ring assembly in living cells are largely unknown. In part, this is a reflection of our lack of understanding into the mechanism of FtsZ polymerization and assembly into Z-rings *in vivo*, which involves numerous positive regulators of FtsZ assembly that are essential for Z-ring assembly. For example, how does EzrA prevent division at the cell poles while allowing FtsZ assembly at the midcell despite a direct interaction with FtsZ during the early stages of Z-ring assembly. We also do not yet understand how the recruitment order of FtsZ regulatory proteins to midcell affects their activity. Is the divisome where their activity is needed or do they act at another time and place during the cell cycle?

The positive regulators of FtsZ assembly are less well understood, but appear to promote FtsZ assembly by anchoring FtsZ to the membrane or by promoting bundling

of FtsZ protofilamets. It has been postulated that ZipA and FtsA facilitate Z-ring assembly in *E. coli* through a direct interaction with a conserved C-terminal domain FtsZ that recruit FtsZ to the membrane (Moreira et al, 2006; Wang et al, 1997). ZipA is a membrane protein (Hale & de Boer, 1999) whereas FtsA is an actin-like ATPase that is targeted to the membrane through a C-terminal amphipathic helix (Pichoff & Lutkenhaus, 2005). The absence of both proteins abolishes Z-ring formation, but inactivation of either protein arrests cell division despite Z-ring assembly [Pichoff, 2002 #1053}, suggesting that both are necessary for a stable divisome. Like *E. coli*, *B. subtilis* FtsA has been proposed to mediate FtsZ association with the cell membrane along with YlmF (Ishikawa et al, 2006; Jensen et al, 2005). Neither of these proteins is essential for cell division, but mutations in *ylmF* are synthetically lethal with *ftsA*, which suggests that they possess partially redundant functions. Unlike YlmF, the absence of FtsA has a deleterious effect on Z-ring assembly (Beall & Lutkenhaus, 1992) suggesting that FtsA serves a more critical role in FtsZ assembly. The membrane binding activity of FtsA, ZipA, and YlmF suggests that they anchor FtsZ, a soluble protein, to the membrane and that this activity is required for Z-ring formation, perhaps simply by increasing the concentration of FtsZ above the critical concentration for polymerization

FtsZ protofilaments assemble into sheets and ribbons *in vitro* (Lowe & Amos, 2000; Romberg et al, 2001) and ZapA (FtsZ associated protein) has been shown to enhance this phenomenon in *B. subtilis* and *E. coli* (Addinall et al, 2005; Gueiros-Filho & Losick, 2002), suggesting that it promotes bundling or stabilizes these structures.

Consistent with this hypothesis, overexpression of ZapA can suppress MinCD induced filamentation *in vivo* (Gueiros-Filho & Losick, 2002) and counteract the destabilizing action of MinC on FtsZ bundling *in vitro* (Scheffers, 2008). The absence of ZapA is lethal in cells producing less than normal levels of FtsZ. Recently, ZapB was discovered in *E. coli* (Ebersbach et al, 2008). Inactivation of ZapB results in misshaped Z-rings and a delay in cell division whereas overexpression causes condensation of the nucleoid. Both ZapA and ZapB interact directly with FtsZ and localize to the Z-ring early in divisome assembly where they likely promote Z-ring assembly by enhancing the lateral interactions between FtsZ protofilaments or by stabilizing Z-rings.

Maturation of the Z-ring to a divisome

The assembled Z-ring recruits additional proteins that are involved in cell division to the future site of septation. The protein complex that assembles with the Z-ring to promote efficient cytokinesis is called the divisome (reviewed by (Errington et al, 2003; Harry et al, 2006; Ryan & Shapiro, 2003; Vicente et al, 2006; Weiss, 2004)). For simplicity, the recruitment of proteins to the divisome of *E. coli* and *B. subtilis* will be discussed separately.

The earliest proteins recruited to the *E. coli* divisome ('early' division proteins) are those that regulate Z-ring assembly, including FtsA, ZapA, ZapB, and ZipA. All of these except for ZapA and ZapB have been shown to be required for recruitment of the other divisome proteins to the midcell. The 'late' division proteins include FtsK, FtsQ,

FtsL, FtsB (YgbQ), FtsW, FtsI, FtsN, FtsEX, and AmiC. An early model of divisome assembly proposed that protein recruitment was semi linear (reviewed by (Buddelmeijer & Beckwith, 2002)) although this seemed unlikely after an extensive two-hybrid analysis of the protein interactions in the divisome revealed a network of interactions between the proteins in the divisome (Di Lallo et al, 2003). Furthermore, assembly appears to be cooperative as pairs of division proteins are often more effective at recruiting interacting proteins than either could alone (Karimova et al, 2005).

The current model of divisome recruitment proposes an inside out approach whereby the cytoplasmic side of the ring is assembled first at the cell membrane, followed by proteins that function in part as a periplasmic connecter to the last group of proteins, the peptidoglycan (PG) biosynthesis machinery (Vicente & Rico, 2006). The initial recruitment of the cytoplasmic side of the divisome includes FtsZ, ZipA, FtsA, FtsEX, and FtsK. FtsZ, ZipA, and FtsA simultaneously localize to the midcell (Pichoff & Lutkenhaus, 2002; Rueda et al, 2003) followed by FtsEX, a predicted ABC transporter that is essential only in salt free media, (Schmidt et al, 2004) and finally FtsK, a DNA translocase. Next, the periplasmic connecter (FtsQ, FtsL, and FtsB) forms a complex (Buddelmeijer & Beckwith, 2004) that is recruited by FtsK through a direct interaction between FtsK and FtsQ (Grenga et al, 2008). The main function of FtsQ, which contains separate domains in the membrane and periplasm, may be to connect the cytoplasmic side of the Z-ring to the periplasmic PG biosynthesis machinery (van den Ent et al, 2008). The PG biosynthesis machinery complex, FtsI and FtsW, is recruited next, followed by FtsN (Addinall et al, 1997).

There is evidence that the order of recruitment does not fully describe the interactions that take place in the divisome. Surprisingly, FtsA fused to DivIVA, which localizes to the cell poles, can artificially recruit FtsI to the cell poles, but it is unclear if FtsA can recruit FtsI to the division site in the absence of the other division proteins (Corbin et al, 2004). Furthermore, several interactions were demonstrated by an *in vivo* two-hybrid analysis that would not be predicted by the order of assembly presented here (Di Lallo et al, 2003). The importance of the order of recruitment is unclear. For example, the periplasmic connector (FtsQ, FtsL, FtsB) and the PG biosynthesis machinery (FtsI, FtsW) can be artificially recruited in reverse order by prematurely targeting FtsI and FtsW to the divisome by fusing them to ZapA (Goehring et al, 2006). It has been postulated that the order of assembly could contribute to the cooperative assembly of the divisome, which likely prevents weaker interactions from mediating aberrant assembly of the divisome complexes (Karimova et al, 2005).

The recruitment of *B. subtilis* divisome proteins has not been characterized to the same extent as *E. coli*. Thus far, these proteins have been characterized as 'early' division proteins (FtsA, ZapA, YlmF, and EzrA), which encompass the cytoplasmic side of the divisome, or 'late' (GpsB, FtsL, DivIB, DivIC, FtsW, Pbp1 (*ponA*), Pbp2B, and DivIVA) division proteins, which are the periplasmic connector proteins and the PG biosynthetic machinery. Recent studies using timelapse microscopy in synchronized *B. subtilis* cells suggests the lag between recruitment of the 'early' and 'late' division proteins in approximately twenty percent of the cell cycle (Gamba et al, 2009).

The early division proteins appear to arrive at midcell simultaneously and their assembly is dependent on FtsZ, but not on the late division proteins or each other (Gueiros-Filho & Losick, 2002; Haeusser et al, 2007; Ishikawa et al, 2006; Jensen et al, 2005). Similar to *E. coli*, these proteins anchor FtsZ to the membrane and regulate Z-ring assembly, although unlike their *E. coli* counterparts, none appear to be essential for division, suggesting at least partially overlapping function. Mutations in *ezrA* and *zapA* are synthetically lethal despite having antagonistic biochemical effects on Z-ring assembly (Gueiros-Filho & Losick, 2002), which suggests that one or the other is required for recruiting the 'late' division proteins. YlmF was classified as a 'late' division protein because it is involved in septation (Hamoen et al, 2006), but is here classified as an 'early' division protein because it localizes to the divisome independently of the late division proteins Pbp2B and FtsL (Hamoen et al, 2006), and because it regulates Z-ring assembly (Ishikawa et al, 2006; Singh et al, 2008).

The 'late' division proteins GspB, FtsW, and DivIVA appear to localize to midcell simultaneously (Gamba et al, 2009), which suggests that all of the late division proteins might localize in this manner. Pbp1, GspB, and DivIB are dispensable for growth and therefore not required for the recruitment of the late division proteins (Claessen et al, 2008; Harry & Wake, 1997; Scheffers & Errington, 2004). DivIB, DivC, FtsL, and Pbp2B appear to be codependent for recruitment to the divisome (Errington et al, 2003), but the dependencies of the remaining late division proteins have not been fully elucidated. FtsL is naturally unstable *in vivo*, which is exacerbated by the absence of DivIB at higher temperatures (Daniel & Errington, 2000; Katis et al,

2000). Furthermore, in the absence of FtsL, DivIC is rapidly degraded. Several lines of evidence suggest that FtsL may play a role in the regulation of cell division (Bramkamp et al, 2006). First, the rapid turnover of FtsL suggests that FtsL may be the limiting reagent in cell division. Second, the DNA replication initiation factor DnaA regulates the transcription of FtsL (Goranov et al, 2005). Third, YluC, a potential RIP (regulated intramembrane proteolysis) protease, mediates the turnover of FtsL. YluC degradation of FtsL could provide a molecular on/off switch by modulating the amount of FtsL present in the cell. FtsL is required for the localization of Pbp2B and therefore the absence of FtsL might stall division by preventing the recruitment of Pbp2B, which is required for septal PG biosynthesis.

Pbp1 and Pbp2B are responsible for septal PG biosynthesis during cytokinesis (Scheffers et al, 2004). Pbp1 studies demonstrate that it also localizes to positions of PG synthesis in elongating cells as well suggesting it has dual roles in division and elongation (Claessen et al, 2008). EzrA (in addition to its role in regulating FtsZ polymerization) and GspB have been proposed to mediate the switch between septal and lateral PG synthesis, respectively although severe growth defects are only seen in the double mutant, which suggests that they are partially redundant (Claessen et al, 2008). Pbp2B is a transpeptidase and is the only PBP that localizes solely to the septum (Scheffers et al, 2004). Pbp2B and is required for cell division and depletion results in filamentous cells that contain Z-rings and division sites that have stalled during cytokinesis, which suggests that Pbp2B is required for the inward growth of the septum (Daniel et al, 2000).

The biochemical function of many of the late division proteins is unknown. For example, DivIB and DivIC are essential for the stability of FtsL and all of them are required for division, but no biochemical activity has been identified for any of them. FtsW is a membrane protein that belongs to the SEDS (shape, elongation, division, sporulation) family of proteins and is a paralogue of SpoVE and RodA, which are required for cortex PG biosynthesis during sporulation (Vasudevan et al, 2007) and cell shape in *B. subtilis* respectively (Henriques et al, 1998). These studies and others on *E. coli* FtsW suggest that it is required for PG biosynthesis during division, but the exact role is unclear. Finally, DivIVA is required for the localization of the division inhibitor, MinCD, to midcell (Gregory et al, 2008), but likely plays a more direct role in division as MinC and MinD are not required for division.

Conclusions and Perspectives

The preponderance of FtsZ-regulating proteins is evidence that proper FtsZ dynamics is paramount in bacteria, but how these regulators are coordinated to ensure that division occurs at the proper place and time during the cell cycle is unclear. Clearly some of these regulator proteins are themselves spatially regulated. For example, Noc, which prevents cell division over the chromosome also localizes to the chromosomes. Others are coordinated with growth (UgtP) or DNA damage (SulA) to ensure that the proper amount of protein is produced at the correct time. However, the mechanism by which the activity of other regulatory proteins is regulated remains unclear. Notable among these proteins are EzrA and MinC, which negatively regulate cell division, yet

localize to midcell prior to cytokinesis. This conundrum raises the possibility that the predominant subcellular localization of a protein might not accurately reflect where it is biologically active. Interactions with other proteins, possibly those in the divisome, may be required for their activity or for inactivation. For example, EzrA may not promote disassembly of the Z-ring at midcell due to interactions with other proteins in the divisome, which prevent it from effectively inhibiting Z-ring assembly.

The characterization of FtsZ regulatory protein localization throughout the cell cycle, in conjunction with biochemical and structural studies, will be required to elucidate the mechanisms for the regulation of Z-ring assembly. Accomplishing this goal will require the use of *gfp* fusions that are expressed from their native signal sequences and visualized by fluorescence microscopy in growing cells as well as by fluorescence methods that allow for higher temporal and spatial resolution in living cells, including TIRF, SI, PALM, and STORM (Schermelleh et al, 2008) (Axelrod, 2003; Heintzmann & Ficz, 2006; Shroff et al, 2007). These methods make it possible to visualize dynamic proteins, such as FtsZ protofilaments, and determine the stoichiometry of proteins in the divisome.

Figures

Figure 1. Induction of the SOS response genes, including SulA, in response to DNA damage. (A) During normal growth, the LexA repressor binds and represses the expression of the SOS response genes. FtsZ assembles at midcell and cell division proceeds normally. (B) Upon DNA damage, RecA is stimulated by single stranded DNA and promotes the autoproteolysis of LexA, thus the SOS response genes are derepressed. SulA is produced and binds to FtsZ thereby inhibiting FtsZ assembly and arresting cell division. (C) Lon degrades SulA following DNA repair, allowing FtsZ assembly and cell division to resume.

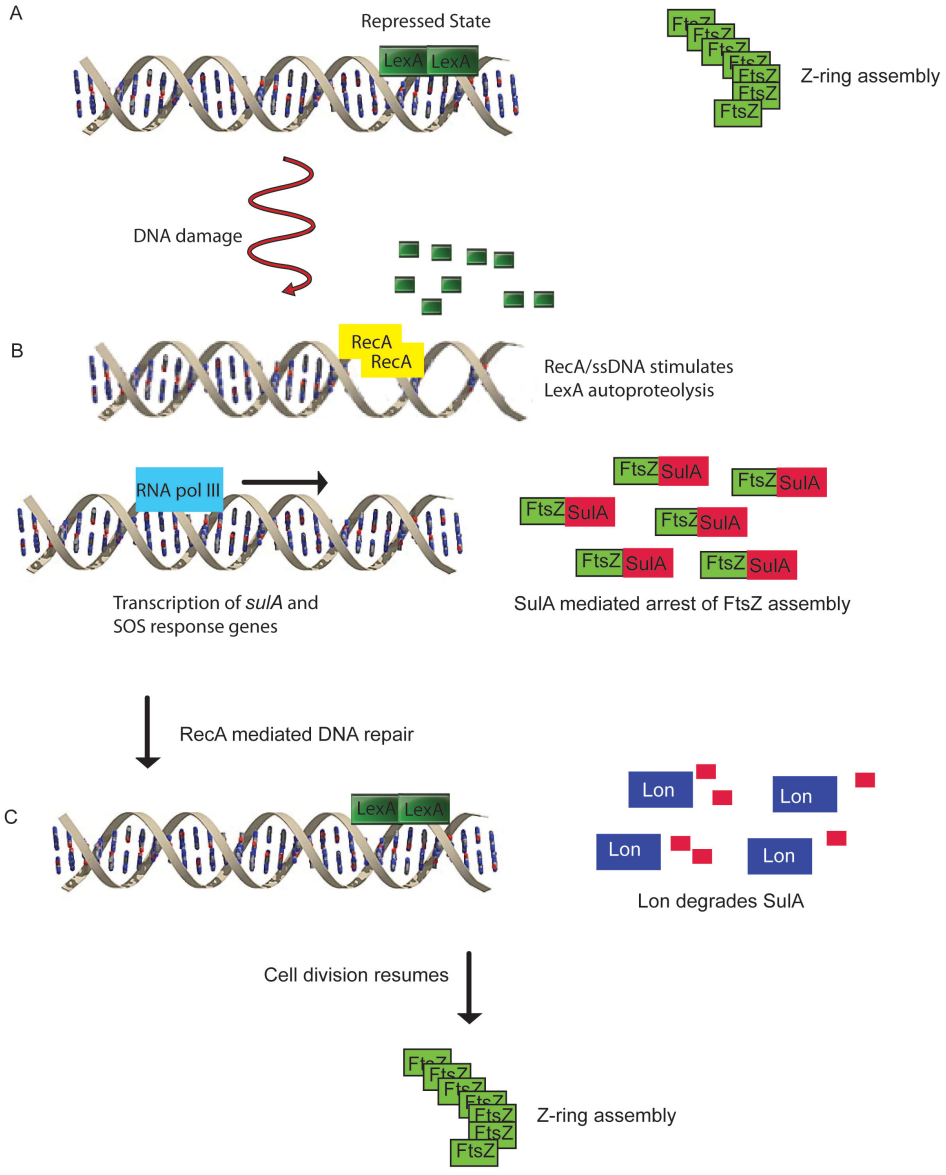
A
Repressed State
LexA
LexA
FtsZ
FtsZ
FtsZ
FtsZ
FtsZ
FtsZ
FtsZ
Z-ring assembly
DNA damage
B
RecA
RecA
RecA/ssDNA stimulates
LexA autoproteolysis
RNA pol III
FtsZ SulA
FtsZ SulA
FtsZ SulA
FtsZ SulA
FtsZ SulA
FtsZ SulA
Transcription of sulA and
SOS response genes
SulA mediated arrest of FtsZ assembly
RecA mediated DNA repair
C
LexA
LexA
Lon
Lon
Lon
Lon
Lon degrades SulA
Cell division resumes
FtsZ
FtsZ
FtsZ
FtsZ
FtsZ
FtsZ
FtsZ
Z-ring assembly

Figure 2. Proposed model of FtsZ polymerization and bundling. The slow step in FtsZ assembly is (A) the assembly of an unknown number of FtsZ monomers into a short protofilament followed by a (B) conformational change. (C) The conformational change favors polymerization of this short protofilament over the assembly of new protofilaments. (D) The lateral interactions between protofilaments mediates the assembly FtsZ protofilament bundles, which ultimately (E) assemble into the Z-ring at midcell.

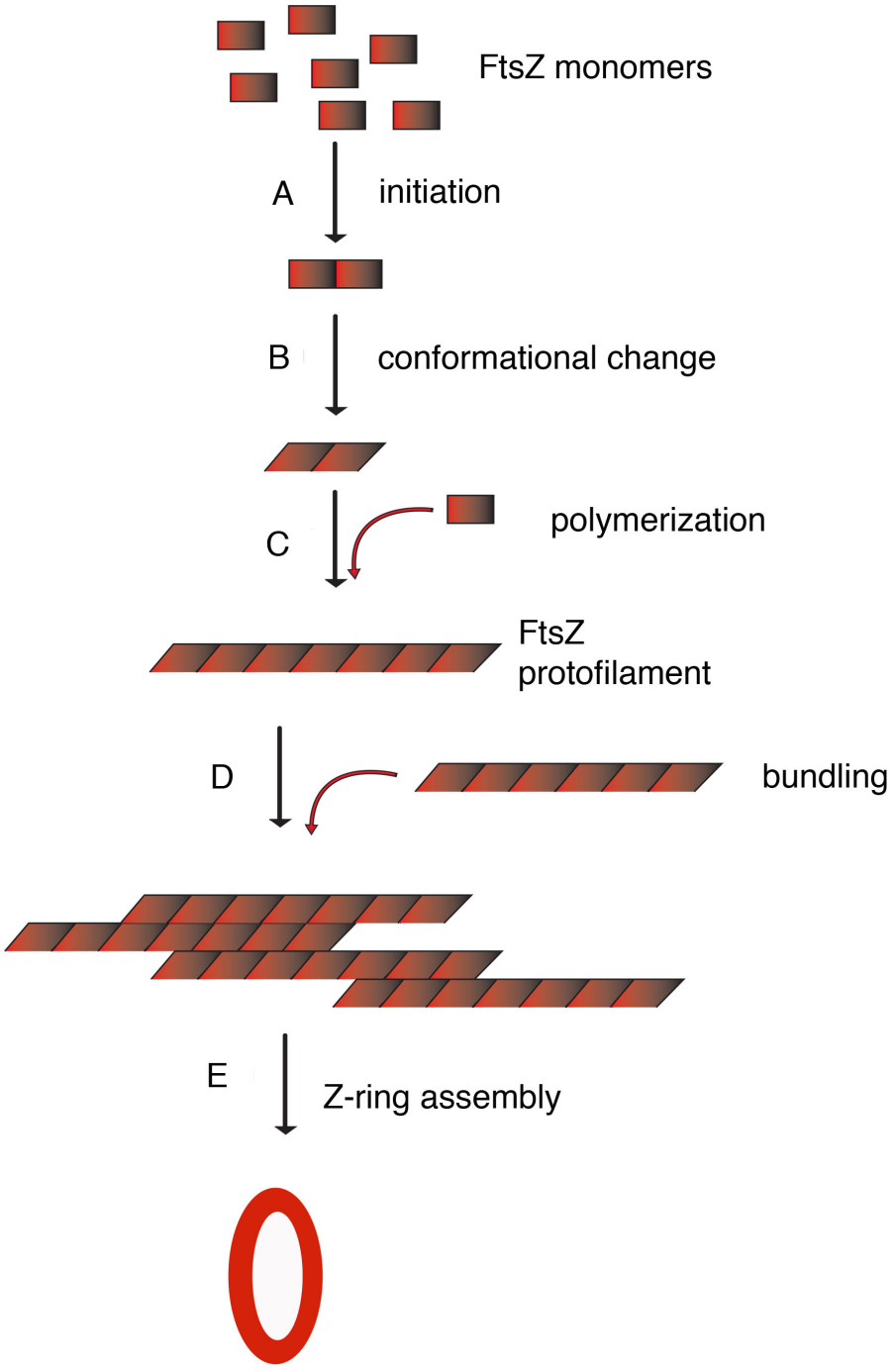
FtsZ monomers
A
initiation
B
conformational change
C
polymerization
FtsZ
protofilament
D
bundling
E
Z-ring assembly

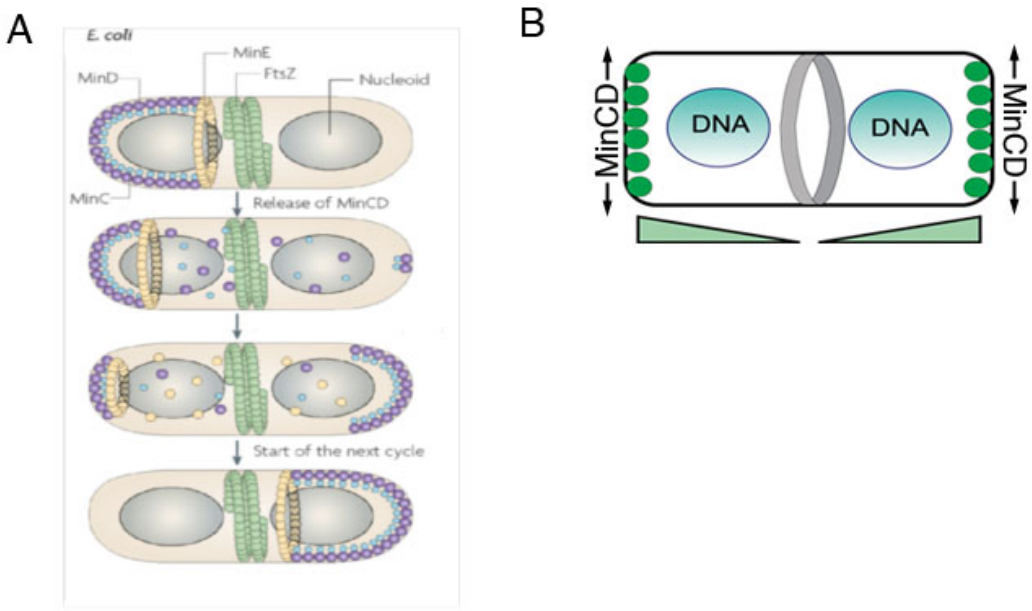

Figure 3. Models of the topological regulation of MinCD in E. coli and B. subtilis. Z-ring assembly is restricted to the midcell by the combined action of MinCD and nucleoid occlusion. (A) In E. coli, the MinE ring stimulates the ATPase activity of MinD, which drives the periodic oscillation of MinCD from pole to pole. The Z-ring assembles at midcell where the effective concentration of MinCD is the lowest (figure from (Thanbichler & Shapiro, 2008)). (B) In B. subtilis, DivIVA anchors MinCD to the cell poles, which results in a concentration gradient of MinC that is lowest at the midcell, thus restricting Z-ring assembly to the midcell (figure from (Gregory et al, 2008)).

Figure 4. Summary of MinC dynamics in B. subtilis and a proposed role for MinC in relocalization of FtsZ from new cell poles (Gregory et al, 2008). (A) MinC (red) localizes to septa before septal biogenesis, rotating around sites of active cell division (top cell) and constricting as septal biogenesis completes (middle cell). After septation is complete, it leaves the new pole and moves to mid-cell. (B) Model for the role of MinC (yellow) in relocalization of FtsZ (green filaments) during the cell cycle. Chromosomes are shown in cyan. Cells 1 and 2 show the formation of an FtsZ ring at mid-cell from short FtsZ protofilaments (green filaments) (Li et al. 2007; Osawa et al. 2008), cells 3 and 4 show the onset of septal biogenesis and the recruitment of MinC (yellow) to the active divisome (solid green ring). As septation completes (cells 4 and 5), FtsZ is released from the new cell pole and accumulates in ring-like structures near the cell pole that is destabilized by MinC. (C) In the absence of MinC, these normally transient structures persist and are used for cell division.

A Summary of MinC dynamics

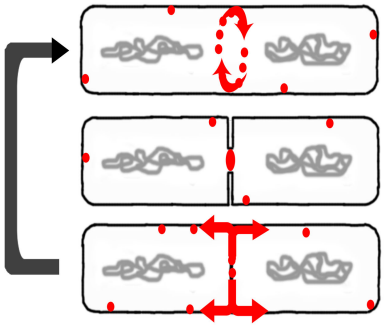

B wildtype

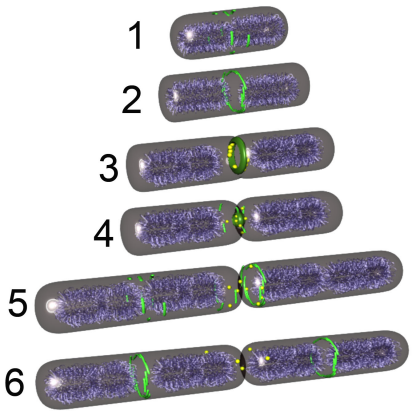

C *minCD*

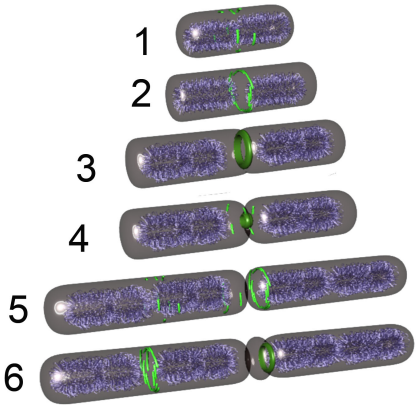

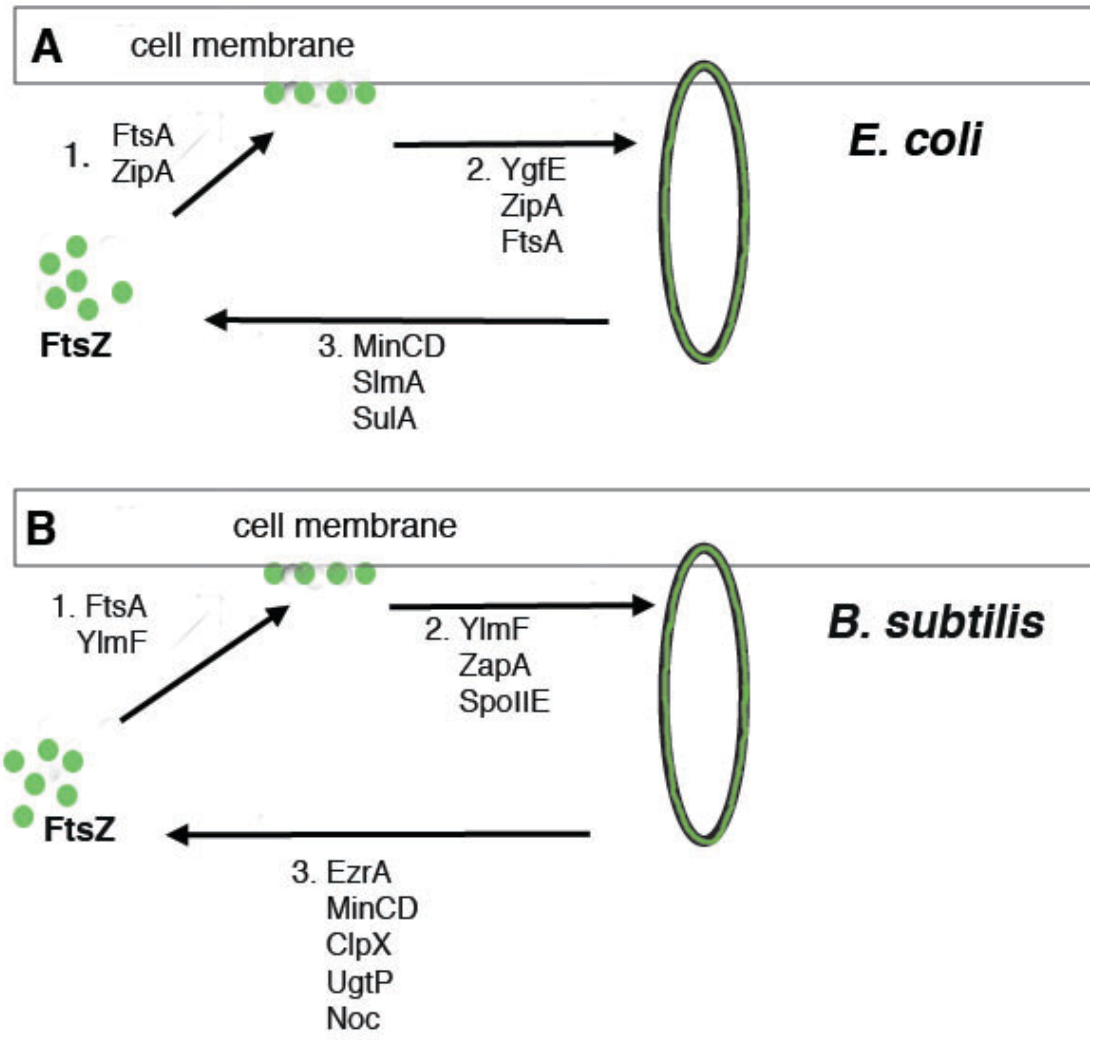

Figure 5. Summary of the positive and negative regulators of FtsZ assembly in (A) *E. coli* and (B) *B. subtilis*. Proteins involved in step one are thought to anchor FtsZ to the membrane while the proteins in step 2 and 3 are positive and negative regulators of Z-ring assembly respectively.

Chapter II

Transposon Assisted Gene Insertion Technology (TAGIT): A tool for generating GFP fusion proteins

Abstract

We constructed a transposon (transposon assisted gene insertion technology, or TAGIT) that allows the random insertion of *gfp* (or other genes) into chromosomal loci without disrupting operon structure or regulation. TAGIT is a modified Tn5 transposon that uses KanR to select for insertions on the chromosome or plasmid, β-galactosidase to identify in-frame gene fusions, and Cre recombinase to excise the *kanR* and *lacZ* genes *in vivo*. The resulting *gfp* insertions maintain target gene reading frame (to the 5' and 3' of *gfp*) and are integrated at the native chromosomal locus, thereby maintaining native expression signals. Libraries can be screened to identify GFP insertions that maintain target protein function at native expression levels, allowing more trustworthy localization studies. We here use TAGIT to generate a library of GFP insertions in the *Escherichia coli* lactose repressor (LacI) and to identify fully functional GFP insertions and partially functional insertions that bind DNA but fail to repress the lacZ operon.

Introduction

The latest advances in optical microscopy enable fluorescently tagged proteins to be observed with subdiffraction-limited spatial resolution and outstanding temporal resolution. The combination of Photo Activated Localization Microscopy (PALM) and Stochastic Optical Reconstruction Microscopy (STORM) provides a ten-fold gain in spatial resolution and allows individual proteins to be counted (Bates et al, 2007; Betzig et al, 2006; Heintzmann & Ficz, 2007; Manley et al, 2008; Shroff et al, 2008). However, achieving the maximum gain from these promising methods requires that the behavior of the fluorescently-tagged fusion protein accurately represents that of the native protein.

Studies of protein localization in living cells are often compromised by protein overproduction or by partially functional fusion proteins (reviewed by (Margolin, 2000; Wang et al, 2008)). Examples of partially functional fusion proteins include GFP fusions to the *Bacillus subtilis* engulfment proteins, which cause synergistic engulfment defects (Aung et al, 2007) and GFP fusions to FtsZ, which are temperature sensitive in most species, including *B. subtilis* (Levin et al, 1999). Co-expressing tagged and untagged proteins is a frequently-used solution that makes it impossible to use PALM/STORM techniques to quantify the number of molecules at a particular location, since the complex will be a mixture of untagged and tagged protein. Overexpression can also cause misleading protein localization. A two-fold overexpression of a partially functional GFP-SpoIIQ fusion protein changes its localization (Broder & Pogliano, 2006). Overexpression of *B. subtilis* MinC causes it

to accumulate at the cell poles (Marston & Errington, 1999; Marston et al, 1998), although when produced under its native expression controls MinC localizes to midcell (Gregory et al, 2008). Furthermore, even modest overproduction of some proteins, particularly those involved in signal transduction and cell division, can have deleterious effects on cell viability and on cellular architecture.

The ideal strategy for imaging studies is to have fully functional fluorescent fusion proteins produced from a gene in its native chromosomal context. This is difficult to achieve using existing technologies, which typically use conventional molecular biology techniques to fuse *gfp* to the 5' or 3' end of the target gene (Datsenko & Wanner, 2000; Kaltwasser et al, 2002; Yu et al, 2000). It is particularly difficult to maintain appropriate expression of genes encoded in bacterial operons, which can be transcribed from several promoters and in which translation of consecutive genes can depend on overlapping translation signals.

We developed a method for the random insertion of *gfp* into target genes in their normal chromosomal context, without disrupting expression of upstream or downstream genes. This method, which we call TAGIT (transposon assisted gene insertion technology), allows rapid isolation of in-frame hybrid genes (Figure 1). The resulting genes encode "sandwich" fusion proteins in which GFP is inserted into the middle of a protein; we call these fusions "GFP insertions" (abbreviated GFPi), to distinguish them from N- or C-terminal GFP fusions. The feasibility of sandwich fusions was originally demonstrated for MalF, an integral membrane protein component of the maltose-maltodextrin transport system (Ehrmann et al, 1990).

Insertion of alkaline phosphotase into MalF produced a hybrid protein retaining both alkaline phosphatase and maltose transport activities. GFP is well-suited for the construction of sandwich fusions, because its N- and C-termini are close to one another (Prasher et al, 1992). We built TAGIT to take advantage of this feature and to facilitate the construction of GFP sandwich fusions expressed from the native chromosomal locus to avoid protein overproduction artifacts.

TAGIT offers several advantages over previously published GFP transposons (Lambertsen et al, 2004; Merkulov & Boeke, 1998; Osawa & Erickson, 2005; Pinheiro et al, 2008; Sheridan et al, 2002; Sheridan & Hughes, 2004). First, TAGIT includes the *lacZ* gene to allow the rapid identification of in-frame insertions and significantly reduce the number of insertions screened. Second, TAGIT allows removal of the selectable marker necessary to isolate transposition events and *lacZ* using the Cre recombinase (Abremski & Hoess, 1984) rather than restriction enzymes. Cre is functional in bacterial and eukaryotic cells and therefore allows excision of selectable markers on the chromosome of living cells. Thus, TAGIT generates fluorescent insertion genes that maintain their native expression signals rather than utilizing inducible promoters. Together these modifications eliminate the time and resource intensive processes of identifying in-frame fusions with DNA sequencing and excising selectable markers *in vitro* using restriction endonucleases, which hinders future efforts to integrate the fusions into chromosomal loci.

We previously used TAGIT to isolate two functional GFP insertions in *B. subtilis* MinC (Gregory et al, 2008), but these insertions were close to the N-terminus

of MinC. To demonstrate that TAGIT can be used to isolate internal insertions of GFP into a target protein, we tested TAGIT on the *E. coli* lactose repressor (LacI). LacI is an ideal candidate because of extensive studies of its function, structure, and regulation (Lewis, 2005; Suckow et al, 1996; Wilson et al, 2007). Epitope insertion mutagenesis of *lacI* identified linker regions that tolerate a 31 amino acid insertion (Nelson et al, 1997), which might also tolerate GFP insertion. After constructing a library of LacI-GFP insertion proteins (LacI-GFPi) using TAGIT, we identified six sites in LacI that are tolerant to GFP insertion, including those previously identified by epitope insertion mutagenesis. We also isolated several insertions that maintained the ability to bind to the *lac* operator, but were unable to repress the *lac* operon. These partially functional LacI-GFPi proteins could potentially be used to track chromosome dynamics without the affects on chromosome segregation sometimes observed for fully functional LacI-GFP fusions (Lau et al, 2003).

Results

Construction of TAGIT

TAGIT consists of five elements that together allow identification of in-frame insertions and the subsequent *in vivo* removal of marker genes to construct a library of *gfp* insertions within a target gene (Fig. 1). (1) At either end of TAGIT are the optimized minimal inverted repeats (19 bp mosaic ends; ME) that allow the hyperactive Tn5 transposase to mediate transposition (Goryshin et al, 1998). (2) Near the 5' end of TAGIT is the *'lacZ* gene, which lacks translational initiation sequences,

such that β-galactosidase is only expressed after insertion into an open reading frame. (3) Encoded downstream of *'lacZ* is an aminoglycoside phosphotransferase (*kan*) gene, which confers resistance to kanamycin (KanR) in both *B. subtilis* and *E. coli*, allowing selection for transpositions in either organism. (4) Near the 3' end of TAGIT is the *gfp* gene, which also lacks translational initiation sequences. (5) Finally, two *loxP* sites are within the transposon, the first immediately upstream of *'lacZ* and the second immediately downstream of *kan* and upstream of *gfp*. These *loxP* sites allow Cre recombinase (Abremski et al, 1986) to mediate excision of *'lacZ* and *kan* either *in vivo* or *in vitro*. The delivery vector for TAGIT, pTAGIT-1, contains the R6Kγ origin of replication, which functions only in *E. coli* strains expressing the *pir* gene (Gregory et al, 2008; Wu et al, 1992).

TAGIT-1 (the first version of TAGIT) contains a single open reading frame extending through the leftward ME and *loxP* site into *'lacZ*. This ensures that β-galactosidase will be expressed only if TAGIT has inserted into an expressed open reading frame. In addition, the rightward *loxP* site is in the same reading frame as the leftward *loxP* site, and this reading frame continues through *gfp* and the rightward ME, into the target gene. Thus, after Cre-mediated excision, the *gfp* gene maintains the same reading frame as the excised *lacZ* gene, and translation continues out of *gfp* and into the 3' end of the target gene. The resulting genes therefore encode 'sandwich' fusion proteins; we call these fusions "GFP insertions", to distinguish them from conventional N- or C-terminal fusions.

Isolating GFP insertions in LacI

We previously used TAGIT-1 to construct *gfp* insertions into the *B. subtilis minCD* operon (Gregory et al, 2008). We found that the β-galactosidase activity provided a reliable indication of in-frame TAGIT-1 insertions on the *B. subtilis* chromosome. However, when we attempted to use TAGIT-1 to isolate in-frame insertions on *E. coli* plasmids, we found that both in-frame and out-of-frame TAGIT insertions produced indistinguishable β-galactosidase activity. We solved this issue by first mutagenizing pTAGIT-1 to change an internal ATG codon at codon 3 of *lacZ*, which provides a potential internal translational initiation codon to GCG (which encodes alanine) and by lowering the copy number of the plasmid by using an *E. coli pcnB* strain (Lopilato et al, 1986). We named the resulting transposon TAGIT-2.

We performed *in vitro* transposition with pTAGIT-2 into the $lacI^q$ containing plasmids pEB363 and pEB364 (which have *lacI* inserted in opposite orientations relative to the plasmid backbone) using purified Tn5 transposase (Goryshin et al, 1998). The resulting insertion library was transformed into the *pcnB* strain KJ622, selecting for KanR on plates containing the β-gal indicator X-gal. DNA sequencing revealed that all 57 blue colonies contained insertions in the same reading frame as *lacI*. The 30 unique insertion sites were distributed throughout *lacI* and provided sufficient coverage of LacI (Fig. 2) for comparison with previously constructed epitope insertion mutants of LacI (Nelson et al, 1997). One of the *gfp* insertions (LacI-144-GFPi) was in-frame on the 5' side of *gfp*, but out of frame on the 3' side of *gfp*, thereby producing a protein containing the first 144 amino acids of LacI followed by

GFP, because the frame shift resulted in a stop codon following the 3' end of *gfp*. Thus, the incorporation of *'lacZ* into TAGIT facilitates the rapid identification of in-frame *gfp* insertions thereby reducing the cost and effort required to identify in-frame insertions.

We excised *kan* and *'lacZ in vivo* with Cre recombinase (Abremski & Hoess, 1984) by transforming the plasmids into an *E. coli* strain that transiently expresses Cre (Materials and Methods). The transformants were selected on ampicillin (bla is encoded on the plasmid backbone) and tested for kanamycin sensitivity to ensure that excision had occurred. Successful excision occurred in approximately 80% of transformants (data not shown). We used Cre for excision of *kan* and *'lacZ* because the 21 base pair *loxP* sites are unlikely to be present in the target gene. It also eliminates the time consuming process of isolating plasmid DNA, performing a restriction digest, and transforming *E. coli* with the ligated plasmid. Finally, restriction enzymes must be used *in vitro* on plasmid DNA and ultimately results in the loss of the selectable marker, thus eliminating the possibility of integrating the gene into the native chromosomal locus. Cre can be expressed *in vivo* after integration of the modified gene into the native locus, thereby leaving the chromosomal structure intact and maintaining the native expression signals.

Test of the LacI-GFP insertion proteins for function

We first tested if the LacI-GFP insertion proteins were able to repress the *lacZYA* operon in *E. coli* strain CSH140, in which a *lacI* mutation renders expression constitutive (Miller, 1972). We transformed CSH140 with the control plasmids pEB363 or pEB364 (in opposite orientations) and the TAGIT-2 constructed GFP insertions and performed β-galactosidase assays on strains cultured in the absence of lactose or IPTG. Repression activity was calculated as the ratio of the β-galactosidase activity (Miller units) produced by the parent strain (CSH140) to that of the transformant. LacI produced from pEB363 and pEB364 repressed the *lac* operon with equivalent efficiency and the combined data is shown in Table 1 for the LacI+ control. Six of the thirty unique LacI-GFPi proteins repressed the *lac* operon at least two-fold over background (GFP insertions at amino acid 158, 221, 312, 315, 320, and 351), with the most active, LacI-312-GFPi, showing a repression activity of 3,100. Five of the six of repression-competent GFP insertions were also induced by IPTG, increasing ß-galactosidase activity 2-1500 fold, with only LacI-320-GFPi showing no induction. We conclude that six of our GFP insertions retained a significant amount of repression activity and that all but one of these is inducible.

Relative protein abundance of LacI-GFP insertion proteins

The insertion of GFP into domains of LacI critical for folding might decrease the stability and accumulation of the LacI-GFPi proteins thereby decreasing repression activity. To determine if reduced protein accumulation was solely responsible for

decreased repression activity, we quantified the amount of protein being produced by each *lacI-gfp* insertion. Protein samples were prepared from each strain for in-gel detection of GFP (Drew et al, 2006) and accumulation was quantified using a Typhoon 9400 (Materials and Methods). We observed one major band of ~70 kD in all samples except the frame-shift mutant LacI-144-GFP (which migrated at ~50 kD). There was little variability in the apparent size of LacI-GFPi proteins and little evidence of degradation products (Figure 2B). The amount of protein varied approximately twenty-fold across all the samples, but protein levels did not correlate with repression activity (Table 1). For example, the highest and lowest protein levels (LacI-27-GFPi and LacI-99-GFPi respectively) were observed for nonfunctional proteins, while the repression activity of LacI-320-GFPi was down nearly 300-fold compared to LacI-312-GFPi despite greater protein accumulation relative to LacI-312-GFPi. We conclude that the repression activity of each insertion protein due to the position at which GFP is inserted, not to the level at which the protein accumulates.

Localization of LacI-GFP insertion proteins

We next tested the ability of the LacI-GFPi proteins to bind the *lac* operator (*lacO*) in living cells. We introduced TAGIT-2 derived *lacI-gfp* insertion alleles into an *E. coli* strain that contains tandem copies of *lacO* integrated near the chromosomal origin of replication (*oriC*)(Lau et al, 2003). LacI-GFPi proteins that are capable of binding *lacO* should assemble discrete foci near *oriC*, which is located near the 1/4 and 3/4 positions of the cell after chromosome replication. Fluorescence

microscopy(Gregory et al, 2008) demonstrated three classes of localization (Figure 3; Figure S1 shows localization of all LacI-GFPi proteins). One class showed irregularly sized foci that were typically either randomly positioned or localized near each cell pole (Fig. 3A) that are likely inclusion bodies. Some GFP insertions appeared to contain both inclusion bodies and DNA bound foci, perhaps because some protein molecules did not fold efficiently and aggregate to form inclusion bodies (Fig. S1, insertions 283 and 285). A second class showed cytoplasmic fluorescence, which likely indicates that the proteins failed to bind *lacO* (Fig. 3B). A third class showed fluorescent foci that were associated with the DNA and regularly spaced within the cells, as would be expected for proteins that bound the *oriC*-proximal *lacO* array (Fig. 3C-F). This class included all of the LacI-GFPi proteins that repressed the lactose operon. Surprisingly it also included several fusions that failed to repress the lactose operon (Fig. 3C), including GFP insertions at amino acid 93, 133, 143, 191, and 240, suggesting that these proteins were able to bind *lacO*, but could not mediate repression. We conclude that many GFP insertions in LacI maintain both GFP fluorescence and the ability of LacI to bind *lacO* DNA.

LacI-GFPi proteins that disrupt cell division

Studies of chromosome and plasmid dynamics during cell growth have become increasingly dependent on the ability to track movement of DNA by fusing GFP to DNA binding proteins that recognize specific DNA sequences. LacI-GFP has been used extensively for such studies, but it can cause defects in cell division when a *lacO*

array is integrated into the chromosome (Lau et al, 2003). Indeed, we noted that many of the repression competent insertions showed various degrees of filamentation during growth (Fig. 3F; Fig. S1). Increasing growth temperature generally exacerbated this phenotype. However, several of our newly isolated GFP insertions alleviate the filamentation associated with *lacO* arrays and localized to DNA associated foci, including insertions at amino acid 93, 133, 143, 191, 221, 240 (Fig. 3C-D). These GFP insertions could provide ideal tools for non-disruptive DNA tagging experiments.

Discussion

We successfully used TAGIT to randomly generate *gfp* insertions into the *E. coli* lactose repressor (LacI) and identified LacI-GFPi proteins that maintain GFP fluorescence and various levels of LacI repressor activity. The incorporation of the *'lacZ* gene into TAGIT facilitated the rapid identification of 57 in-frame *gfp* insertions into *lacI*, which represented 30 unique insertion sites across *lacI*. The effect of GFP insertion on LacI activity was largely consistent with genetic and structural information available for LacI (Lewis, 2005; Suckow et al, 1996; Wilson et al, 2007). The most active LacI-GFPi protein contained GFP inserted after amino acid 312, 48 amino acids before the end of the protein. Therefore LacI activity was best preserved when GFP was inserted within the protein, not at the conventional N- or C-terminal positions. We also isolated LacI-GFPi proteins that lost the ability to repress the lactose operon, but retained the ability to bind a *lacO* array integrated into the *E. coli* chromosome. These proteins alleviate the filamentation associated with more active LacI-GFP fusions and therefore could provide a less disruptive method to track movement of chromosome loci. Thus, TAGIT is a useful molecular tool that can be used to rapidly generate a library of GFP insertion proteins, which can subsequently be screened to isolate fully functional GFP insertion proteins as well as mutant proteins with novel biological activities.

Analysis of LacI-GFPi proteins

We characterized thirty unique GFP insertions in the lactose repressor. Not surprisingly, most GFP insertions produced nonfunctional proteins. However, several retained LacI repressor activity while others bound DNA but failed to repress the *lac* operon. In the next section, we analyze the insertions with respect to the domain structure of the LacI protein (Fig. 4A) (Lewis, 2005; Lewis et al, 1996; Suckow et al, 1996; Wilson et al, 2007).

DNA binding domain. The N-terminus of LacI consists of four helices that together comprise the DNA binding domain (residues 1-62; not shown in Fig. 4A) of LacI and a linker to the core domain(Lewis et al, 1996). This region has been previously identified as sensitive to mutation and substitution. We therefore expected this region to be intolerant of GFP insertion. Indeed, the four insertions we isolated in this domain (GFP insertions at amino acid 8, 14, 27, and 40) showed no repression activity and localized to the cytoplasm or inclusion bodies. LacI-27-GFPi and LacI-40-GFPi had the highest relative protein accumulation, which could account for the presence of inclusion bodies.

Inducer binding domain. The inducer-binding domain of LacI contains two separate subdomains of similar structure, the N-terminal core domain (residues 61-163 and 293-320) and the C-terminal subdomain (residues 164-292). Both domains contribute to a six stranded parallel β–sheet located between four alpha helices (Lewis, 2005). The N-terminal core domain contains four regions that are highly tolerant to

substitutions (amino acids 100-112, 129-145, 151-160, and 305-318 (Markiewicz et al, 1994)) and to epitope insertions at amino acids152 and 317 (Nelson et al, 1997). We therefore predicted that these regions were likely to tolerate GFP insertion. Indeed, LacI-312-GFPi (Fig. 4B and 4C) is the most active repressor that we isolated from our screen and the repression activity of LacI-315-GFPi is just two-fold lower than LacI-312-GFPi. Interestingly, LacI-320-GFPi is approximately 300 fold less active than LacI-312-GFPi, which correlates well with a decreased tolerance for substitution from residues 319-330 (Suckow et al, 1996). LacI-320-GFPi is nearly unresponsive to the inducer IPTG, suggesting that it interferes with lactose binding.

We expected LacI to be tolerant of insertions in the hinge region between the N- and C-terminal core domains(Nelson et al, 1997; Suckow et al, 1996), but the repression activity of LacI-158-GFPi is down three orders of magnitude from LacI-312-GFPi. Residues 151-158 of LacI form a mutationally tolerant hinge that connects the N-terminal core domain to the C-terminal core domain that is in close spatial proximity to the loop that contains residue 312. It is likely that the 237 codon GFP insertion in this region is more detrimental to protein function than the 31 codon epitope insertion (Nelson et al, 1997) because it is much larger.

Dimerization interface. The functional unit of LacI is a tetramer comprised of a dimer of dimers. Proteins that assemble into dimers, tetramers, polymers, etc. pose a greater challenge when identifying sites that can tolerate GFP insertion. Four principle clusters of amino acids are involved in dimerization (159-163, 221-226, 251-259, 280-285)(Lewis et al, 1996; Suckow et al, 1996). We were surprised to find that an

insertion near one of these sites, LacI-221-GFPi, retains some repression activity. The crystal structure of LacI reveals that amino acid 221 is at the end of a short linker region adjacent to the second alpha helix of the C-terminal core domain. It is possible that the long linker connecting LacI to GFP encoded by TAGIT may be sufficiently flexible to allow LacI dimerization.

Tetramerization domain. In LacI-351-GFPi, GFP is inserted nine amino acids from the C-terminus (Fig. 4B and 4C) and is almost equivalent to the C-terminal GFP fusion protein typically used to localize DNA molecules in living cells. As expected, LacI-351-GFPi can repress the lactose operon, but it was less active than LacI-312-GFPi. Hence, the optimal site for GFP insertion is not at the N- or C-terminus and would therefore have been very difficult to identify using conventional GFP tagging methods.

Potential utility of repression defective LacI-GFPi mutants

LacI-GFP fusions are commonly used to track the movement of plasmids or chromosome loci into which arrays of lactose operators have been integrated. Tracking the movement of chromosomes in growing cells using this method poses challenges because *lacI-gfp* can cause growth defects when expressed in cells that contain a chromosomal *lacO* array (Lau et al, 2003). We found this to be the case for GFP insertions at amino acids 158, 283, 288, 312, 315, and 351 of LacI, and we found that filamentation was exacerbated by increased growth temperature (from room

temperature to 30ºC). We identified several LacI-GFPi proteins that alleviate these problems. GFP insertion proteins at amino acid 133, 143, 191, and 240 of LacI were unable to repress the lactose operon, but nevertheless retained sufficient DNA binding activity to localize as *lacO* array-associated foci (Fig. 3, Fig. S1).

Acknowledgements

This research was supported by a grant from the National Institute of Health (GM 57045) and from the University of California at San Diego Academic Senate. We thank Dr. William Reznikoff (University of Wisconsin) for providing Tn5 transposase, and Dr. Alan Derman for comments on the manuscript.

Author Contributions

J.G. designed and performed the experiments, the data anaylsis, and wrote the article. E.B. designed and performed experiments. I.T. and J.J. performed experiments. K.P. contributed the article.

Materials and Methods

Strains, reagents, and recombinant DNA techniques

The following *E. coli* strains were used in this study: CSH140(Miller, 1992), IL06(Lau et al, 2003), DH5∝(Hanahan, 1983), Top10 (Invitrogen), and KJ622(Abanes-De Mello et al, 2002). Restriction enzymes were purchased from New England Biolabs. Tn5 transposase was a gift from Dr. William Reznikoff (University of Wisconsin). DNA digestion and ligation reactions and transformations of *E. coli* were performed according to standard protocols (Ausebel FM, 1992). Cultures were grown in Luria broth (LB) or M63 supplemented with 0.2% glucose or 1 mm IPTG as appropriate. When required, antibiotics were used at the following concentration: kanamycin (50 μg/ml), ampicillin (100 μg/ml).

Construction of pTAGIT-1 and pTAGIT-2.

Plasmid pTAGIT-2 was constructed in the following manner. Plasmid pMDS12 (Sharp & Pogliano, 2002) was digested with the restriction enzymes BamHI and SpeI to isolate the fragment corresponding to the superbright *gfp* gene (Cormack et al, 1996). This fragment was gel purified and then ligated to a BamHI and SphI digested pUC19 vector (Yanisch-Perron et al, 1985) to yield pEB49. Next, we introduced the *kanR* gene with its native promoter from plasmid pEB9. Plasmid pEB9 was constructed by amplifying the *kanR* gene from pDG364 (Karmazyn-Campelli et al, 1992) by PCR using primers EB15 and EB16, which create a fragment containing

the *kanR* gene flanked by *loxP* sites. This fragment was digested with the restriction enzymes BamHI and SpeI and ligated to pMDS73 (Sharp & Pogliano, 2002) that had also been digested with BamHI and SpeI to give pEB9. The *kanR loxP* fragment was amplified using PCR from pEB9 using primers EB106 and EB128. This fragment was digested with SpeI and NotI, gel purified, and then ligated to pEB49 that had been digested with SpeI and NotI to give pEB118. The *loxP 'lacZ* fragment was amplified by PCR from pEB9 using primers EB105 and EB127. This fragment was cloned into pCR3.2-topo blunt (Invitrogen) and subsequently isolated by restriction digest with SpeI and AscI. We then constructed plasmid pEB123 by cloning the *loxP 'lacZ* fragment into SpeI and AscI digested pEB118. Plasmid pEB123 contains all the parts of TAGIT except for the ME (hyperactive mosaic end) that are recognized by the Tn5 transposase. To introduce the ME's we used primers JG10 and EB143, both of which contain the ME sequence, to amplify TAGIT from pEB123. This fragment was then poly A-tailed using Taq polymerase and ligated to SmaI digested pUC19 that had been poly T-tailed in the same manner to give plasmid pEB163. Plasmid pTAGIT-1 was constructed by digesting pEB163 with KpnI and SphI and ligating it to the conditional R6K-α origin of replication (Dennis & Zylstra, 1998), a modified origin from the R6K plasmid (Kolter et al, 1978). The R6K-α origin was amplified by PCR with primers EB180 and EB181 from plasmid pRL27 (Larsen et al, 2002). To ensure that blue colonies were the result of in frame transpositions we used primers JG119 and JG120 to change the methionine codon near the 5' end of *'lacZ* to a codon corresponding to

alanine using the Quick-Change Site-Directed Mutagenesis protocol (Stratagene, La Jolla, CA).

Construction of *lacI-gfpi* library

The target plasmids, pEB363 and pEB364, were constructed by amplifying and cloning *lacI*^{q} from pMUTIN-GFP+ (Kaltwasser et al, 2002) into the pSMART vector (Lucigen) using primers EB231 and EB232. The two target plasmids contain the *lacI*^{q} insert in the opposite orientation. *In vitro* transposition was carried out using pTAGIT-2 and either pEB363 or pEB364 using Tn5 transposase. The transposition was transformed into XL-10 Gold competent cells (Stratagene) and plated on LB with kanamycin. The resulting transformants were pooled and plasmid DNA was isolated using QIAprep miniprep columns (Qiagen). The resulting plasmid DNA was transformed into the *pcnB* strain KJ622 and plated on LB with kanamycin and X-Gal. Blue colonies were purified and plasmid DNA was prepared and transformed into Strataclone Solopack competent cells (Stratagene). This strain transiently expresses Cre recombinase and successfully excises the *kanR* and *'lacZ* genes in approximately 80% of transformants. After Cre mediated excision, plasmid DNA corresponding to each of the blue colonies was prepped and sequenced using primers JG33 (downstream) and EB46 (upstream) to determine the position of *gfp* insertion in *lacI*.

β-galactosidase assays

β-galactosidase activity was measured as Miller units in strain CSH140 transformed with each *lacI-gfpi* plasmid separately, pEB363, and pEB364. β-galactosidase activity was identical in CSH140 containing pEB363 or pEB364. Strains were grown overnight in LB ampicillin. Cultures of LB with ampicillin with or without IPTG (1 mM) were then inoculated with 20 μl of the overnight and grown to an OD_{600} of 0.4 – 0.6. Assays were then carried out as described(Kleina & Miller, 1990). The strain harboring *lacI-221-gfpi* was grown in M63 salts supplemented with glucose to ensure the retention of the F plasmid that contains the lactose operon. Optical densities were measured with a Beckman DU640 spectrophotometer. Repression activity was calculated as the ratio of the β-Galactosidase activity of CSH140 to the β-galactosidase activity of CSH140 containing the appropriate plasmid grown in the appropriate media.

Quantification of LacI-GFP insertion protein levels by in-gel fluorescence

Protein accumulation of LacI-GFPi protein was measured by in-gel fluorescence (Drew et al, 2006). The same strains used to measure β-Galactosidase activity were grown in LB with ampicillin to an OD_{600} of 0.5. Approximately 1.0 OD_{600} of cells were pelleted by centrifugation and resuspended in 100 μl of SB buffer (140mM Tris-HCl pH 8.8, 14% glycerol, 3.5 mM EDTA, 0.02% bromophenol blue, 0.05 M DTT, 4% SDS) Samples were analyzed by 12.5% SDS-PAGE and scanned using a Typhoon 9400 variable mode imager followed by coomassie staining.

Quantification was performed using ImageQuant 5.2. Relative protein levels were reported as a ratio of the fluorescence of each sample to the fluorescence of LacI-99-GFPi, which had the lowest protein accumulation of all the samples.

Microscopy

Strains were prepared by transforming strain IL06 with each *lacI-gfpi* plasmid. Transformants were grown on LB with ampicillin and IPTG. All microscopy was performed using LB agar pads without antibiotics as described previously (Gregory et al, 2008) at 30ºC or at room temperature. Images were acquired using an Applied Precision Spectris microscope and deconvolved using softWoRx version 3.3.6 software (Applied Precision). Figures were assembled with Photoshop CS.

3D cartoon model

The three-dimensional structure of the lactose repressor (PDB ID: 1LBI and PDB ID: 1LBG; (Lewis et al, 1996) was manipulated using Visual Molecular Dynamics (VMD ver. 1.8.6).

This chapter has been submitted for publication and the dissertation author was the primary author and researcher. I would like to thank Eric Becker, Ida Tuwatananurak, James Jung, and Kit Pogliano for their permission to use this manuscript in my dissertation. The dissertation author was the primary author and researcher.

Tables

Table 1. *in vivo* activities and accumulation of LacI-GFP insertion proteins

Strain	Repression Activity[1]	Inducibility[2]	Relative Protein Level[3]	Localization
LacI+	16,500 ± 5800	74.4 ± 7.1	NA	NA
LacI8-GFPi	0.814 ± 0.03	ND	6.84	Cytoplasmic
LacI14-GFPi	0.921 ± 0.09	ND	14.2	Cytoplasmic
LacI27-GFPi	0.867 ± 0.04	ND	23.0	Inclusion bodies
LacI40-GFPi	0.916 ± 0.10	ND	20.5	Inclusion bodies
LacI63-GFPi	1.03 ± 0.12	ND	5.19	Inclusion bodies
LacI74-GFPi	0.812 ± 0.05	ND	3.04	Cytoplasmic
LacI85-GFPi	1.27 ± 0.64	ND	5.83	Inclusion bodies
LacI93-GFPi	0.908 ± 0.16	ND	8.97	DNA foci
LacI97-GFPi	0.928 ± 0.09	ND	1.83	Cytoplasmic
LacI99-GFPi	0.979 ± 0.12	ND	1.00	Cytoplasmic
LacI114-GFPi	0.924 ± 0.12	ND	7.68	Cytoplasmic
LacI120-GFPi	0.890 ± 0.10	ND	8.50	Cytoplasmic
LacI133-GFPi	1.19 ± 0.42	ND	12.1	DNA foci
LacI143-GFPi	1.10 ± 0.13	ND	5.34	DNA foci
LacI144-GFPi	1.14 ± 0.31	ND	10.9	Cytoplasmic
LacI158-GFPi	2.31 ± 0.42	0.863 ± 0.05	11.7	DNA foci
LacI175-GFPi	0.978 ± 0.07	ND	2.01	Cytoplasmic
LacI176-GFPi	1.02 ± 0.08	ND	1.47	Cytoplasmic
LacI191-GFPi	0.984 ± 0.12	ND	3.49	DNA foci
LacI221-GFPi	7.95 ± 0.54	0.789 ± 0.48	3.42	DNA foci
LacI240-GFPi	1.14 ± 0.10	ND	6.33	DNA foci
LacI248-GFPi	1.23 ± 0.04	ND	3.34	Cytoplasmic
LacI265-GFPi	1.27 ± 0.10	ND	4.29	Cytoplasmic
LacI283-GFPi	1.27 ± 0.09	ND	9.91	DNA foci, inclusion bodies
LacI288-GFPi	1.14 ± 0.05	ND	7.75	DNA foci, inclusion bodies
LacI294-GFPi	1.32 ± 0.08	ND	11.1	Inclusion bodies
LacI312-GFPi	3110 ± 730	2.09 ± 0.33	16.3	DNA foci

Table 1. continued

LacI315-GFPi	1660 ± 98	2.59 ± 0.32	16.7	DNA foci
LacI320-GFPi	9.09 ± 0.39	7.38 ± 1.7	19.6	DNA foci
LacI351-GFPi	2000 ± 160	3.37 ± 0.33	11.1	DNA foci

[1]Repression activity = ß-gal activity CSH140 divided that of the indicated plasmid in CSH140. Cells were grown in the absence of IPTG

[2]Inducibility = Repression activity of cells grown in the absence of IPTG divided by that of cells grown in the presence of IPTG. At least three cultures were assayed.

[3]Protein levels were adjusted to reflect relative amounts by dividing each sample by the protein level of LacI99-GFP which had the lowest protein accumulation

Figures

Figure 1. Structure of TAGIT, which randomly inserts *gfp* into target genes. (A) pTAGIT-2 is an independently replicating plasmid that was constructed by ligating TAGIT-2 to the R6K-gamma origin of replication. (B) ME = mosaic ends recognized by Tn5 transposase, *loxP* = recognition sequences for Cre recombinase, *kanR* = encodes KanR in *B. subtilis* and *E. coli*. *gfp* = gene for GFP mutant 2. GFP is not fluorescent when exported via the Sec pathway, so the use of β-galactosidase, which is also only active in the cytoplasm, allows the isolation of GFP insertions into the cytoplasmic domain of membrane proteins. A single ORF extends through the leftward ME and *loxP* site into '*lacZ*, so that after transposition, β-galactosidase will be expressed only if TAGIT has inserted in the correct reading frame. Both *loxP* sites are in the same reading frame, so that after excision of the '*lacZ* and *kanR* genes by the Cre recombinase, *gfp* is in the same reading frame as was *lacZ* so that translation can continue out of *gfp* and into the 3' end of the target gene. The resulting proteins have GFP is inserted into the middle of the target protein. The TAGIT "guts" (lacking ME) can also be used to create chromosomal *gfp* insertions in operons by cloning, recombining into the operon, and then excising the *lacZ* and *kanR* genes. This is useful for membrane proteins with very short cytoplasmic domain into which to insert GFP, such as the late division proteins, which are also in operons.

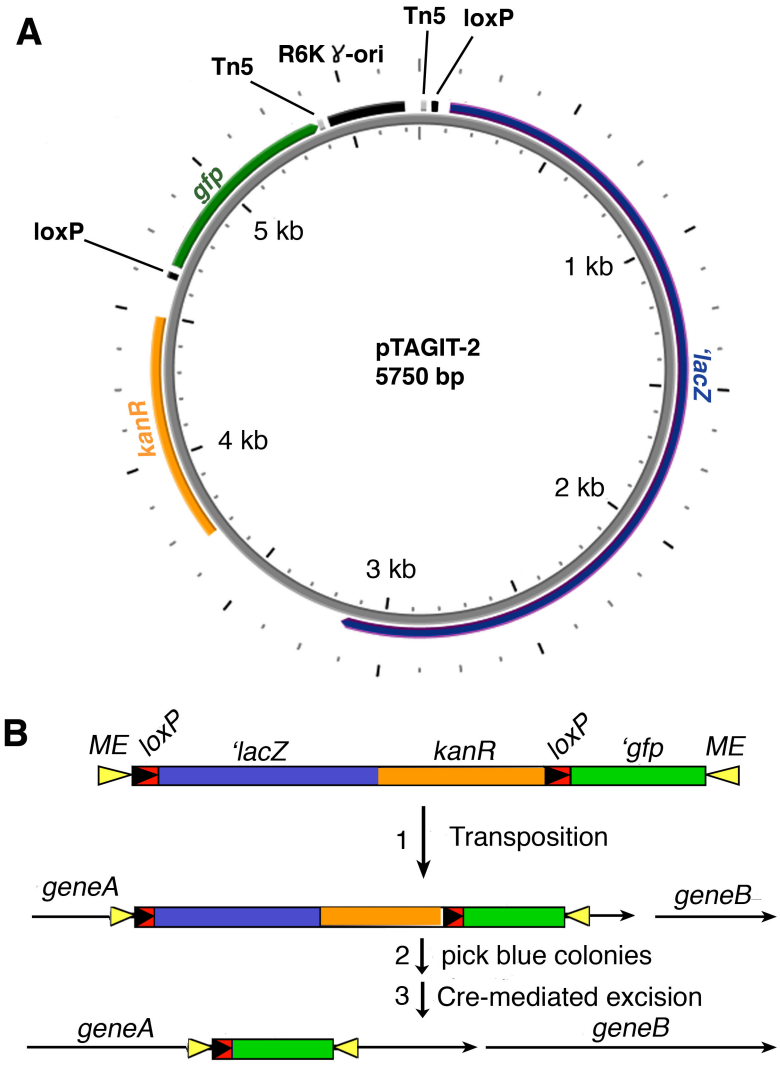
A
Tn5
loxP
Tn5
R6K γ-ori
gfp
loxP
5 kb
1 kb
pTAGIT-2
5750 bp
'lacZ
kanR
4 kb
2 kb
3 kb
B
ME
loxP
'lacZ
kanR
loxP
'gfp
ME
1
Transposition
geneA
geneB
2
pick blue colonies
3
Cre-mediated excision
geneA
geneB

Figure 2. Analysis of TAGIT-2-constructed GFP insertion proteins in the *E. coli* lactose repressor LacI. **(A)** Amino acid sequence and structural features of LacI. Red arrowheads indicate the position of non-functional GFP insertions (Repression-, Focus-). Green arrowheads indicate GFP insertions that fail to repress *lacZ*, but form foci (Repression-, Focus+) when introduced into a strain with the *lacO* array integrated near the origin of replication. Blue arrowheads indicate insertions that repress *lacZ* (Repression+, Focus+). **(B)** Expression of LacI-GFP insertions is variable and depends on the GFP insertion site. Numbers correspond to the last undisrupted *lacI* codon before TAGIT. Cells were harvested at an OD_{600} of ~0.5. Samples were then normalized and run on a 12.5% SDS-PAGE gel. Protein accumulation was determined using in-gel GFP fluorescence (top panel) and the gel was subsequently stained with Coomassie blue to reveal total protein (bottom panel).

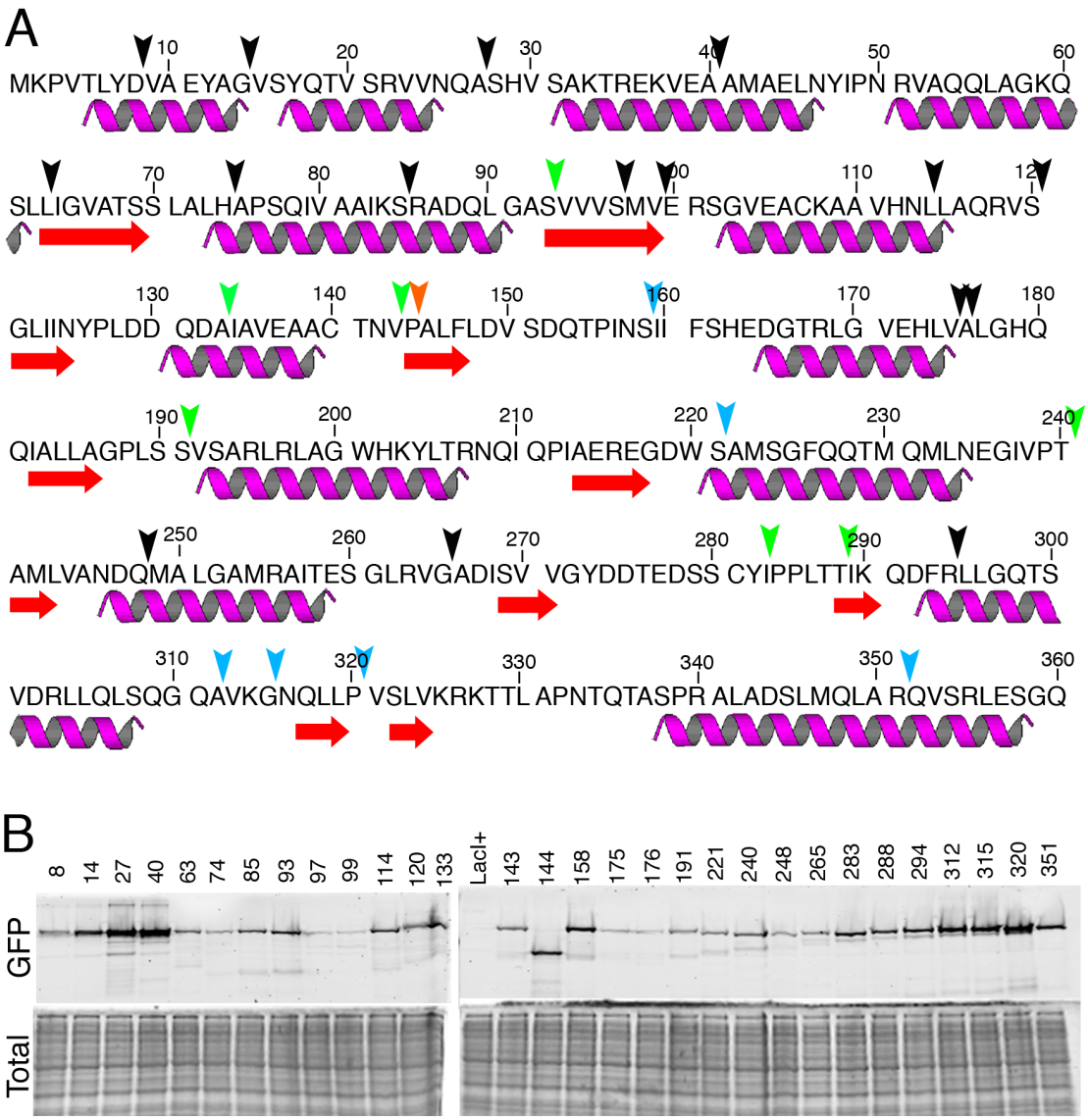
A
MKPVTLYDVA EYAGVSYQTV SRVVNQASHV SAKTREKVEA AMAELNYIPN RVAQQLAGKQ
SLLIGVATSS LALHAPSQIV AAIKSRADQL GASVVVSMVE RSGVEACKAA VHNLLAQRVS
GLIINYPLDD QDAIAVEAAC TNVPALFLDV SDQTPINSII FSHEDGTRLG VEHLVALGHQ
QIALLAGPLS SVSARLRLAG WHKYLTRNQI QPIAEREGDW SAMSGFQQTM QMLNEGIVPT
AMLVANDQMA LGAMRAITES GLRVGADISV VGYDDTEDSS CYIPPLTTIK QDFRLLGQTS
VDRLLQLSQG QAVKGNQLLP VSLVKRKTTL APNTQTASPR ALADSLMQLA RQVSRLESGQ
B
8
14
27
40
63
74
85
93
97
99
114
120
133
LacI+
143
144
158
175
176
191
221
240
248
265
283
288
294
312
315
320
351
GFP
Total

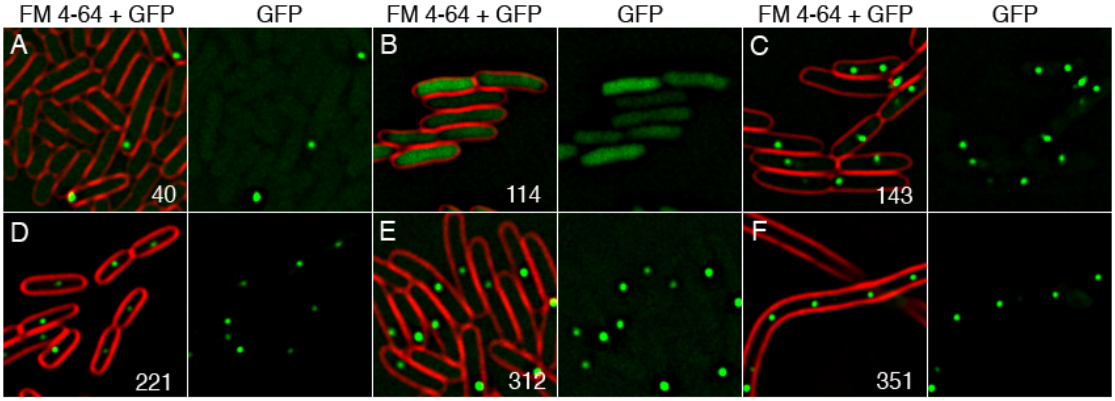

Figure 3. Binding of LacI-GFPi proteins to *lacO* arrays near the *E. coli* origin of replication in growing cells. Numbers correspond to the location of GFP insertion into LacI. (A) LacI-40-GFPi localizes in inclusion bodies. (B) LacI-114-GFPi localizes to the cytoplasm. (C) LacI-143-GFPi, (D) LacI221-GFPi, and (E) LacI-312-GFPi localize as foci. (F) LacI-351-GFPi localizes as foci in elongated cells. Scale bar, 1 μm.

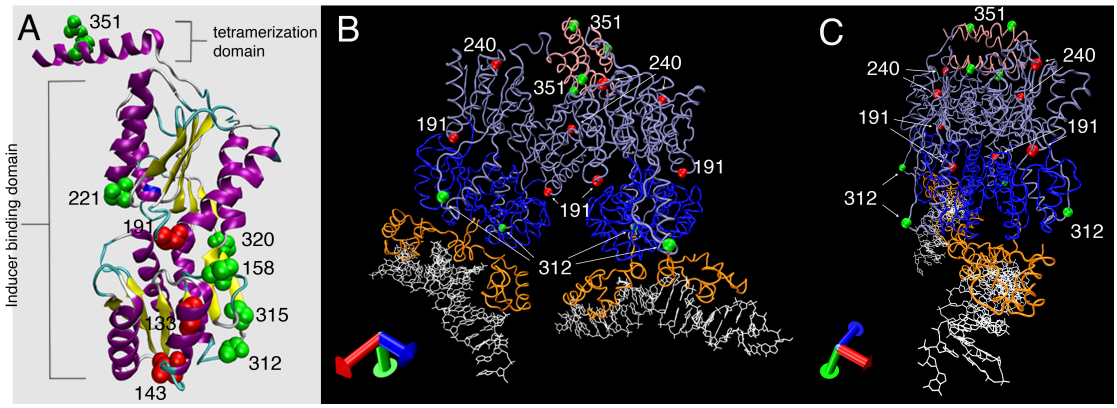

Figure 4. Cartoon of LacI-GFPi proteins mapped onto the crystal structure of LacI. (A) The monomeric structure of LacI without the DNA binding domain (PDB ID: 1LBI). All LacI-GFPi proteins that localize as foci were mapped onto a ribbon representation of the LacI crystal structure. The amino acid corresponding to the site of GFP insertion is labeled and represented as a space-filling model. Red amino acids correspond to insertion proteins that are unable to repress the *lac* operon and green amino acids correspond to insertion proteins that retain some level of repression activity. (B) Model of the LacI crystal (PDB ID: 1LBG) structure including the DNA (white), DNA binding domain (orange), N-terminal core domain (blue), C-terminal core domain (light purple), and tetramerization domain (pink). The most active GFP insertion (LacI-312-GFPi) and LacI-351-GFPi are shown as green balls and two examples of inactive GFP insertions as red balls. (C) Same as in (B) but rotated to show the projection of amino acid 312 from the surface.

Supplemental Tables

Supplemental Table 1. List of primers

EB15	cctactagtaaataacttcgtatagcatacattatacgaagttatgcgctcgggacccctatcta
EB16	acggatccataacttcgtataatgtatgctatacgaagttatcccagcgaaccatttgaggtga
EB46	tctaattcaacaagaattgggac
EB105	ttttactagtataacttcgtataatgtatgc
EB127	aaaggcgcgccggccgttattatttttgacacca
EB143	tttgaattcctgtctcttatacacatctttttgtatagttcatccatgcc
EB180	tttttgcatgcgttgtccacaaccgttaaaccttaaaagc
EB181	ttttggtaccccggccacgatgcgtc
EB231	aaatctagagccgggcctcttgcggg
EB232	aaaagcttgcgatgctgtcggaatggacg
JG10	acgaattctgtctcttatacacatctacccggggatccactagt
JG33	aagatcccaacgaaaagagag
JG119	ctatacgaagttatttactagtaccgcgattacggattcactggccg
JG120	cggccagtgaatccgtaatcgcggtactagtaaataacttcgtatag

Supplemental Figures

Supplemental Figure 1. Binding of LacI-GFP insertions to *lacO* arrays at the terminus of *E. coli*. Labels correspond to the amino acid location of GFP insertion. Scale bar, 1 μm.

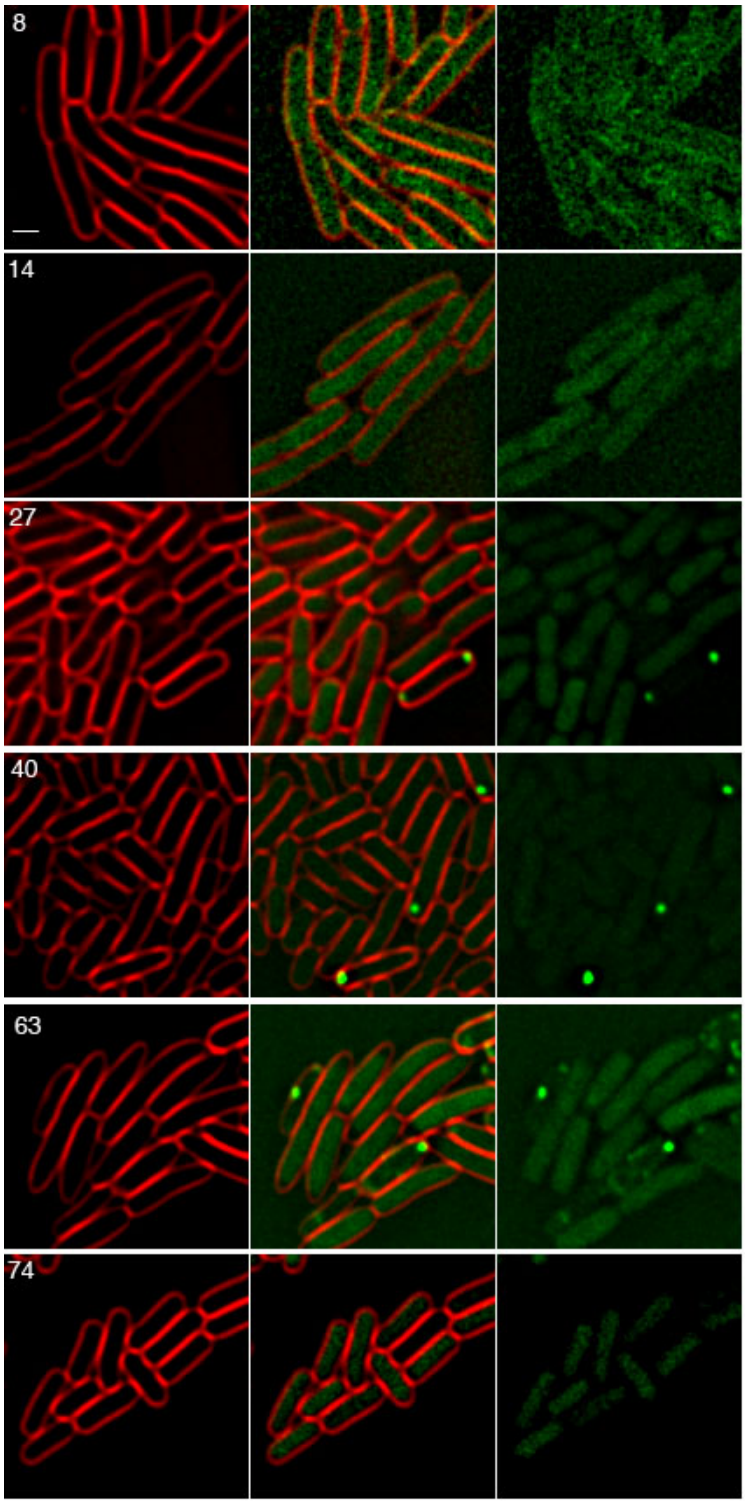
8
14
27
40
63
74

Supplemental Figure 1. continued

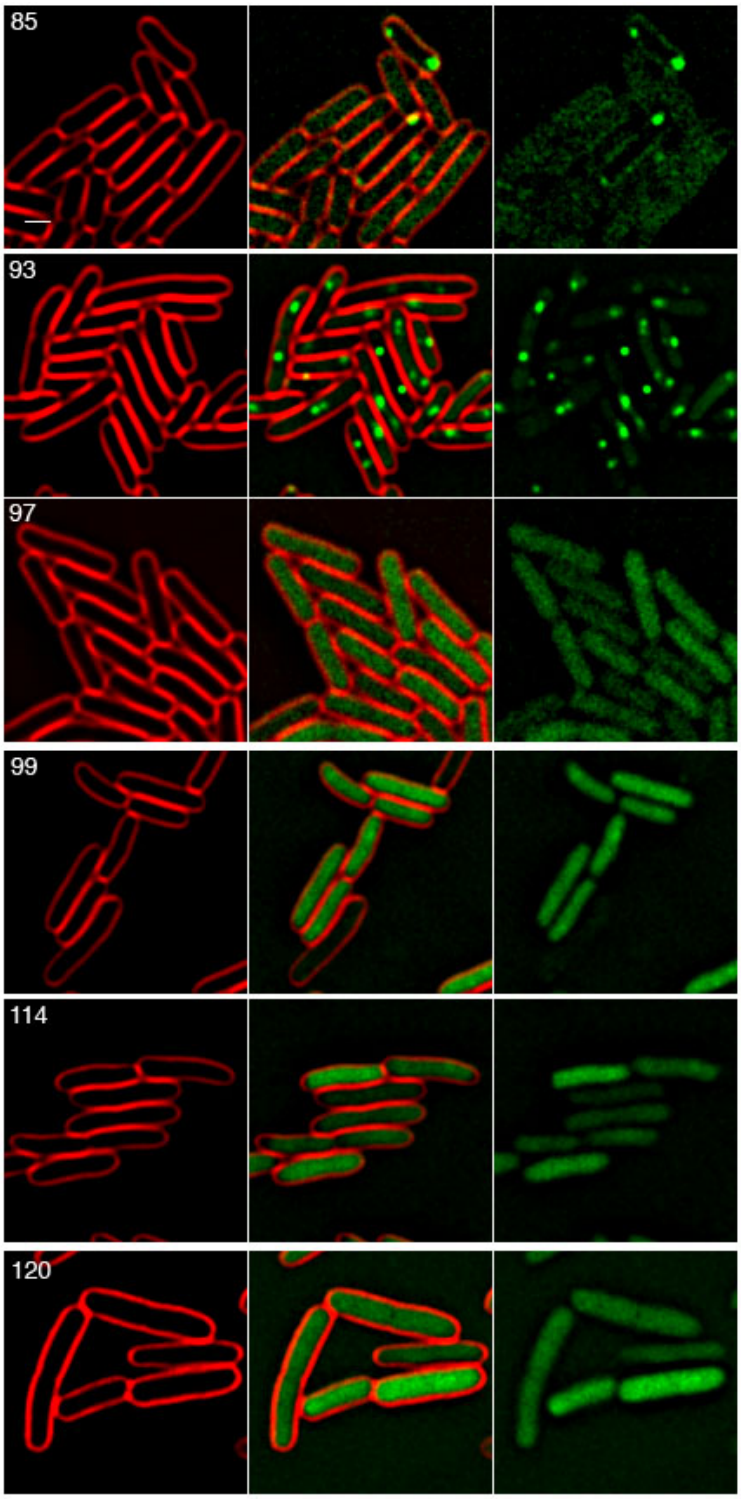

Supplemental Figure 1. continued

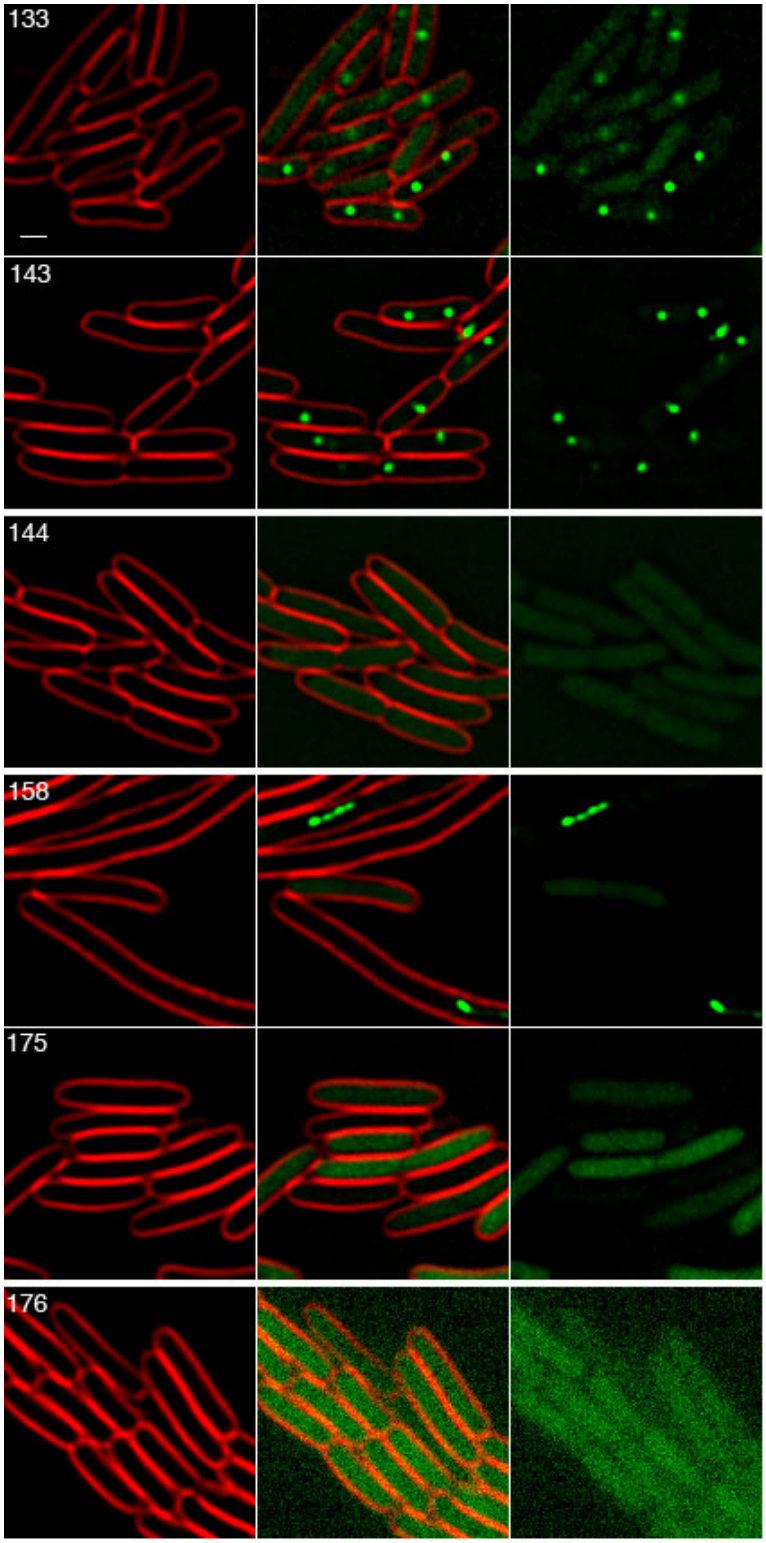

Supplemental Figure 1. continued

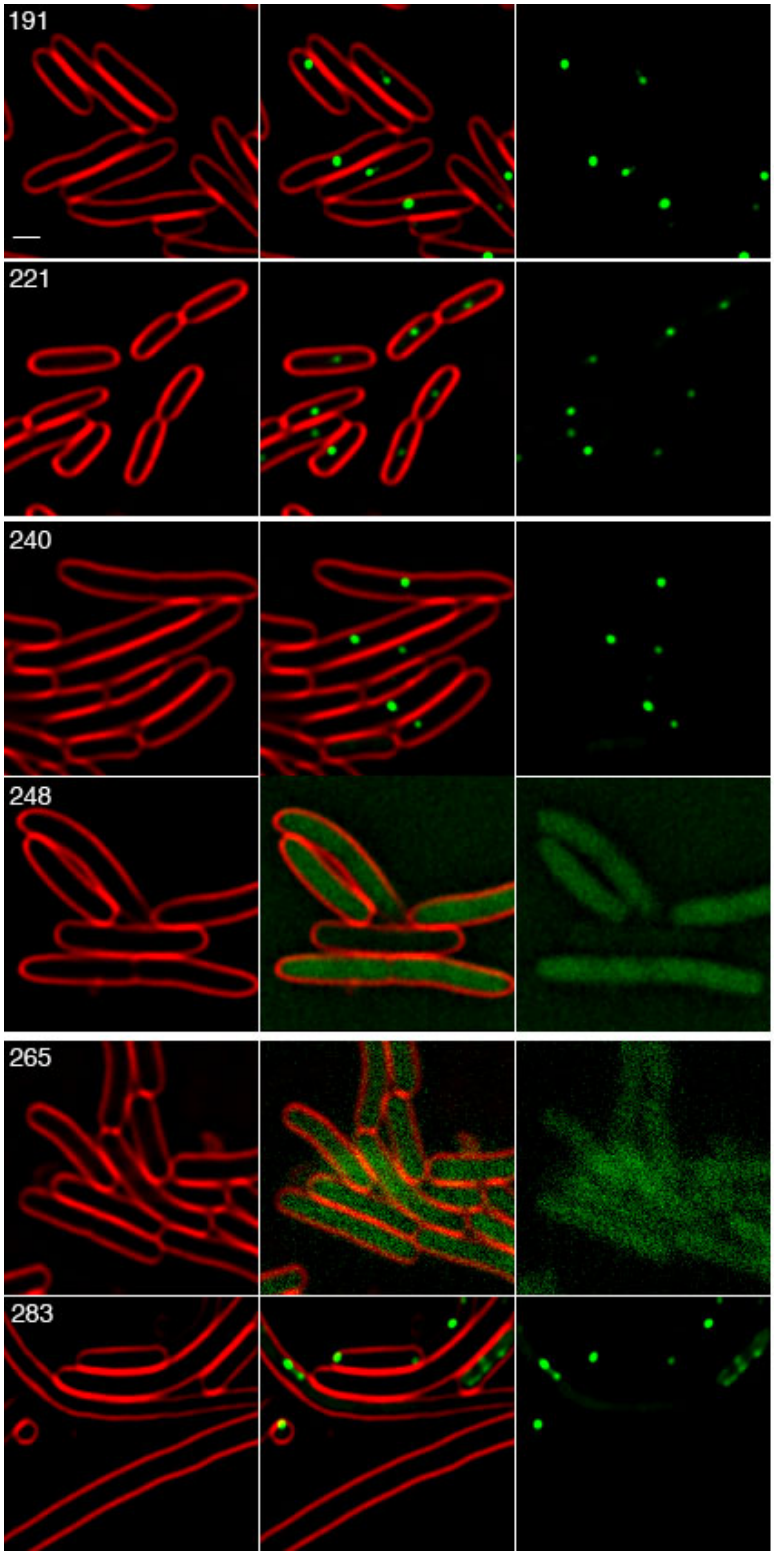

Supplemental Figure 1. continued

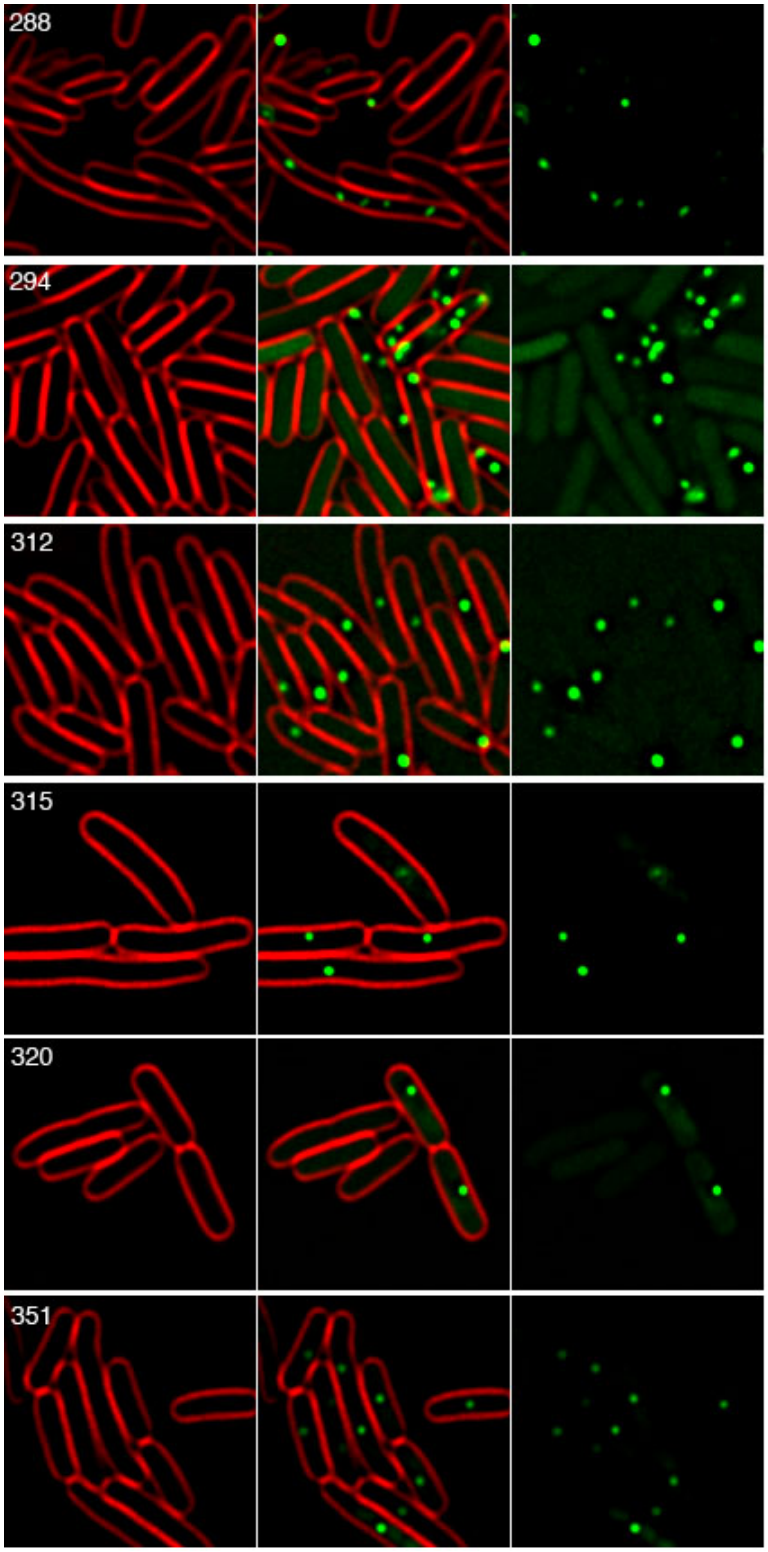

Chapter III

Bacillus subtilis MinC destabilizes FtsZ-rings at new cell poles and contributes to the timing of cell division

Abstract

Division site selection in rod shaped bacteria depends on nucleoid occlusion, which prevents division over the chromosome and MinCD, which prevent division at the poles. MinD is thought to localize MinC to the cell poles where it prevents FtsZ assembly. Timelapse microscopy demonstrates that in *B. subtilis* transient polar FtsZ rings assemble adjacent to recently completed septa and that in *minCD* strains these persist and are used for division, producing a minicell. This suggests that MinC acts when division proteins are released from newly completed septa to prevent their immediate reassembly at new cell poles. The *minCD* mutant appears to uncouple FtsZ ring assembly from cell division and thus shows a variable interdivisional time and a rapid loss of cell cycle synchrony. Functional MinC-GFP expressed from the chromosome *minCD* locus is dynamic. It is recruited to active division sites before septal biogenesis, rotates around the septum, and moves away from completed septa. Thus high concentrations of MinC are found primarily at the septum and, more transiently, at the new cell pole. DivIVA and MinD recruit MinC to division sites, rather than mediating the stable polar localization previously thought to restrict MinC activity to the pole. Together our results suggest that *B. subtilis* MinC does not inhibit

FtsZ assembly at the cell poles, but rather prevents polar FtsZ rings adjacent to new cell poles from supporting cell division.

Introduction

Division site selection in rod shaped bacteria is a highly regulated and reliable process achieved by two systems that restrict FtsZ assembly (and the subsequent assembly of a complete divisome) to midcell. One system, nucleoid occlusion (Noc), prevents FtsZ from assembling over the chromosome while the other, MinCD, prevents FtsZ assembly and division at the cell pole (Fig. 1A, reviewed by (Barak & Wilkinson, 2007; Errington et al, 2003; Margolin, 2005; Rothfield et al, 2005)). Although unrelated DNA binding proteins mediate nucleoid occlusion in *B. subtilis* and *E. coli* (Bernhardt & de Boer, 2005; Wu & Errington, 2004), the MinCD proteins are broadly conserved and encoded by many bacterial genomes (Rothfield et al, 2005). The simultaneous inactivation of the Noc and MinCD systems is lethal in both species, resulting in the assembly of multiple FtsZ structures that fail to coalesce into functional rings (Bernhardt & de Boer, 2005; Wu & Errington, 2004).

The MinCD system functions in many bacterial species and is therefore well suited for comparative studies of the spatial regulation of cell division. Indeed, disruption of *minC* or *minD* changes the position at which FtsZ assembles in both rod shaped bacteria such as *E. coli* and *B. subtilis* and in cocci such as *Neisseria gonorrhoeae* (Ramirez-Arcos et al, 2001; Szeto et al, 2001) and the cyanobacterium *Synechocystis* (Mazouni et al, 2004). Furthermore, while the absence of MinC and MinD allows assembly of additional FtsZ rings (Z-rings) at aberrant positions (Levin et al, 1998), their overexpression blocks Z-ring assembly and cell division (Bi & Lutkenhaus, 1993; Justice et al, 2000; Levin et al, 2001), suggesting that the Min

system inhibits Z-ring formation. In keeping with this hypothesis, disruption of proteins that spatially regulate MinCD activity (MinE in *E. coli* and DivIVA in *B. subtilis*) block FtsZ assembly in a MinC-dependent manner, producing filamentous cells (de Boer et al, 1989; Marston et al, 1998; Pichoff & Lutkenhaus, 2001; Zhao et al, 1995). MinC appears to be the primary division inhibitor in *E. coli* (de Boer et al, 1992; Hu et al, 1999), while MinD tethers MinC to the membrane, allowing it to be effective at physiological concentrations (de Boer et al, 1991). The biochemical mechanism by which MinC inhibits polar Z-ring formation is unclear, but in *E. coli* it appears to do so without affecting either FtsZ GTPase activity (Cordell et al, 2001; Hu et al, 1999) or the addition of FtsZ monomers to existing Z-rings (Anderson et al, 2004). Indeed recent evidence suggests that MinC inhibits lateral interactions between FtsZ-protofilaments in *E. coli* (Dajkovic et al, 2008) and *B. subtilis* (Scheffers, 2008), which might destabilize FtsZ rings and decrease their ability to recruit proteins involved in cytokinesis to potential division sites.

Understanding the spatial distribution of MinC and MinD within the cell is critical to understanding how they regulate Z-ring formation. Given the similar effects of MinC and MinD in *B. subtilis* and *E. coli*, one might expect them to display similar subcellular behavior. This is not the case. *E. coli* MinC and MinD oscillate from pole to pole with a periodicity of ~50s (Hu & Lutkenhaus, 1999; Raskin & de Boer, 1999a), while *B. subtilis* MinCD is static, localizing to the septum late in division and being retained at new cell poles by DivIVA (Marston & Errington, 1999; Marston et al, 1998). Current models of MinCD function in both species propose that these

division inhibitors have the highest time-averaged concentration at the cell poles, thereby inhibiting polar cell division while allowing division at midcell (Fig. 1A, reviewed by (Lutkenhaus, 2007; Rothfield et al, 2005; Ryan & Shapiro, 2003)). By these models, the static polar localization of *B. subtilis* MinCD could achieve the same biological function as the oscillation of *E. coli* MinCD.

We here reinvestigate the function and localization of *B. subtilis* MinC. First, we use a functional GFP insertion expressed from the native *minC* locus that maintains wild type operon structure. We find that *B. subtilis* MinC moves rapidly along the cell membrane and appears to rotate around division sites, with little accumulation at the poles. Next, we investigated FtsZ dynamics and the timing of cell division in wild type and *minCD* mutant cells using timelapse fluorescence microscopy. These experiments indicate that even in wild type cells, polar FtsZ rings often form adjacent to the recently completed septum. In the absence of MinCD, these normally transient structures are stabilized and used for cell division. We therefore propose that in *B. subtilis,* MinCD primarily acts at the new cell pole to prevent the maturation of transient FtsZ structures into active divisomes. Our data also suggest that MinCD affect the timing of cell division, because the interdivisional time is highly variable in *minCD* mutant cells.

Results

Localization of GFP insertions in MinC and MinD

We were concerned that the apparent contrast between the dynamic behavior of *E. coli* MinC and MinD and the stable polar localization of *B. subtilis* MinC and MinD might be explained by overexpression of the latter proteins from inducible promoters, because even a minor static population can mask the presence of a dynamic population of molecules using standard fluorescence microscopy. We therefore constructed and used a GFP insertion transposon (Materials and Methods) to isolate two functional *gfp* insertions into the chromosomal *minC* locus that preserve *minCD* operon structure. These fusions have *gfp* inserted after the 4th (*minC4-gfp*) or 8th (*minC8-gfp*) *minC* codon, produce <0.3% minicells and have wild type cell length (Fig. 1, Fig. S1, Table S1). Because these insertions were generated by Tn5-mediated transposition (see Materials and Methods), there is a small duplication of the coding region. Thus, after GFP, the fusion proteins encode most of MinC, starting with the 3rd (m*inC4-gfp*) or 7th (*minC8-gfp*) amino acid. We visualized these GFP insertions in growing bacteria at 30°C. Both localized in an identical manner distinct from that reported in previous publications, forming foci and rings at new and constricting septa, with little or no MinC observed at the poles (Fig. 1C, Fig. S1).

The septal localization of MinC was lost and replaced by cytoplasmic fluorescence when cells were immobilized on poly-lysine treated coverslips (Fig. S2A), indicating that proteins might be lost from division sites when slides are

prepared by this method. Indeed, FtsZ-GFP also showed increased cytoplasmic fluorescence when visualized on poly-lysine coverslips rather than agarose pads (Fig. S2B-C), and the Z-rings contained only ~20% of the fluorescence of cells growing on agarose pads (Table S3). Thus, there is a dramatic reduction in septal localization of both FtsZ and MinC when slides are prepared in a manner that does not support growth.

We also isolated many *gfp* insertions in the chromosomal *minD* locus, one of which (*minD4-gfp*) was at a location that would generate a fusion protein that is nearly identical to the previously published GFP-MinD fusion (Marston et al, 1998). Both constructs encode GFP followed by amino acids 2-268 of MinD, but *minD4-gfp* is integrated at and expressed from the native *minCD* locus rather than being integrated into an ectopic position and expressed by an inducible promoter in a *minD* background (Marston et al, 1998). Surprisingly, we found that MinD4-GFP produced elongated cells and minicells at a level similar to the *minCD* null (Table S2) and that it showed weak and inconsistent fluorescence intensity and therefore did not meet our criteria for a functional insertion. We attempted to rescue MinD4-GFP by introducing a wild type copy of *minCD* expressed from the *minCD* promoter at the *amyE* locus. This construct cannot rescue a *minCD* null for minicell production (Table S2), likely because *minCD* is also expressed from the P_{maf} promoter upstream of the *maf-radC-mreBCD* genes that are immediately upstream of *minCD* (Lee & Price, 1993). The strain containing both *minD4-gfp* and this extra copy of wild type *minCD* produced fewer minicells than either alone (Table S2) indicating that MinD4-GFP is partially functional. Unlike

MinC4-GFP, MinD4-GFP appeared to be retained at some cell poles, so it is possible that MinD is retained at the cell pole to a greater extent than MinC. However, this polar localization might be caused by overexpression or the partial functionality of MinD4-GFP. We did not further characterize this fusion.

MinC is dynamic

We used timelapse fluorescence microscopy to investigate MinC dynamics during the cell cycle. MinC localized to the division site before visible constriction, often forming a single focus at a future division site (Fig. 1E, arrowhead). MinC then assembled a ring-like structure that constricted during division and was lost from new septa with faint membrane-associated fluorescence detected throughout the cell (including the cell poles) in foci that appeared to move between timepoints. Thus MinC localizes to septa immediately before the onset of septal biogenesis and disappears from completed septa, thereby behaving as expected for a late cell division protein. MinC also appeared dynamic, leaving completed septa and moving to new division sites (Movie S1). This dynamic population of molecules was more evident using total internal reflection fluorescence (TIRF) microscopy (Fig. S3, Movies S2-3), which has decreased excitation depth and increased excitation intensity thereby allowing observation of relatively few fluorophores and rapidly moving molecules (Axelrod, 2001; Axelrod, 2003; Kusumi et al, 2005; Sako & Uyemura, 2002). This method showed that MinC moved along the cell membrane and around the pole (Fig. S3, Movies S2-3). Thus, *B. subtilis* MinC appears to show two distinct behaviors, a

stable localization to midcell and a more dynamic movement throughout the cell membrane.

The poles are a secondary localization site for MinC

The previously observed polar localization of GFP-MinC (Marston & Errington, 1999; Marston et al, 1998) could be a consequence of over-expression from the inducible xylose promoter (P_{xyl}), which could saturate septal binding sites or it could be a consequence of different slide preparation methods. We therefore compared localization of MinC4-GFP and P_{xyl}-GFP-MinC in growing cells (Fig. 2). Inducible P_{xyl}-GFP-MinC localized to division sites before and during septal biogenesis (Fig. 2B arrows) as well as to the cell poles (Fig. 2B, arrowheads). The most intense fluorescent signal was consistently observed at the midcell of dividing cells (Fig. 2B), with less intense fluorescence at the cell pole. In contrast, MinC4-GFP fluorescence was largely confined to midcell (Fig. 2A), even when a longer exposure yielded twice the maximum pixel intensity compared to the inducible fusion. Polar localization of P_{xyl}-GFP-MinC depended on expression level, because decreasing the xylose concentration from the previously used concentration of 0.5% (Fig. 2B,E) to 0.05% (Fig. 2D) reduced polar but not midcell localization, while retaining the ability of GFP-MinC to prevent minicell formation. Thus, both MinC4-GFP, which is expressed from the native promoter, and inducible P_{xyl}-GFP-MinC localize to midcell, but the inducible fusion is stably associated with the cell poles only when substantially overproduced. We also noted that MinC4-GFP is recruited to the cell poles during intermediate stages

of FtsZ depletion (Fig. S4, Movie S4). These results suggest that the poles are secondary localization sites that recruit MinC when the primary site (active division sites) is either missing or saturated by overproduced MinC.

Dynamic behavior of MinC at the septum

MinC initially assembles an asymmetric focus at the future division site (Fig 1C). We noted that MinC often remained asymmetric during constriction, with one side of the septum appearing >2X brighter than the other (Fig. 3, arrows). Timelapse epifluorescence microscopy with images collected at 1 minute time intervals showed that MinC at individual septa appeared to transition between foci and symmetric or asymmetric rings and back to foci (Fig. 3C, Movie S5, S6). In addition, the region of highest fluorescence intensity appeared to move from one side of the septum to the other (Fig. 3C, arrows and arrowhead). To quantitatively view this data, we devised a kymogram-like method that projects the GFP fluorescence at the septum through time (Fig. 3A). Briefly, the y-axis was manually aligned to each septum, the septum was cropped and plotted against time giving a two-dimensional projection of each septum through time. After projection, a uniform static ring would show two parallel lines of equal intensity, whereas an asymmetric static ring would show one brighter line (Fig. 3B). The pixel intensity data of these projections clearly showed that the maximum pixel intensity of MinC moved from one side of the septum (Fig. 3D, arrows) to the other (Fig. 3D, arrowheads) in many cells, including each of the three shown in Fig. 3C (cells 1,2,3). The apparent movement across the septum required ~4 minutes for

the cells shown in Fig. 3, and was sometimes visualized as a diagonal line in the projections (cells 2,3). In contrast, variation in FM 4-64 staining intensity was always symmetric (likely due to fluctuations in excitatory light intensity).

Thus MinC appears dynamic even at the septum, moving from one side of the septum to the other. This behavior could represent the circumferential movement of MinC foci or arcs around the septum, or it could represent the assembly and disassembly of MinC complexes on different sides of the septum. At this time, we cannot distinguish between these two possibilities. However, if MinC is rotating around the septum, then its calculated velocity around the septum is 0.25–0.34 μm/min for slightly constricted septa.

MinC localizes to the septum after the early division proteins

MinC localization is consistent with that of a late division protein, as the protein appears to arrive at midcell just prior to septal biogenesis, which is readily visualized at early stages by two spots of increased fluorescence after staining with the vital membrane stain FM 4-64 (Fig. 1E, 10 min). Indeed, quantification of MinC in growing cells revealed that it was present at midcell in 12% of pre-divisional cells (in which FM 4-64 staining showed no evidence of septal biogenesis) compared to 93% of dividing cells (Table S4). To confirm that MinC arrives after the early division proteins we colocalized MinC4-GFP with EzrA fused to CFP in growing cells (Fig. 4A, Table S5). We found that 87% of predivisional cells showed localization of EzrA but not MinC at midcell, while 13% showed MinC and EzrA at midcell. In contrast, 92% of cells that were actively dividing showed both EzrA and MinC localized at the

nascent septum. Thus, EzrA arrives at midcell prior to MinC and both proteins remain at the septum during constriction. Septal localization of MinC4-GFP was dependent on MinD and DivIVA (Fig. 4B,C), which were previously shown to be required for polar localization of MinC (Marston & Errington, 1999; Marston et al, 1998). These results indicate that MinC is a late recruit to the septum as it arrives after the early division protein EzrA, and that DivIVA localizes MinC to the septum, rather than stably sequestering it at the cell pole.

FtsZ dynamics visualized by timelapse microscopy

The results described above indicated that MinC is recruited to nascent division sites after the early division proteins and immediately before septal biogenesis, and that it leaves the new cell pole to relocalize to the midcell of the newborn daughter cells. Thus, MinC spends little time associated with the cell poles, where it must act to prevent minicell formation. We therefore hypothesized that MinC might prevent minicell formation by inhibiting the assembly of a mature divisome immediately adjacent to the most recently completed septum (or more specifically in the space between the pole and the chromosome where Noc is not inhibiting Z-ring formation). This hypothesis predicts that in *minCD* mutant cells, polar FtsZ rings would frequently assemble adjacent to the recently completed septum, and that minicells would most frequently form at these sites, rather than at the old cell pole where FtsZ polymers are not present.

To test this hypothesis and to gain further insight into FtsZ dynamics during the cell cycle, we used timelapse fluorescence microscopy to watch FtsZ-GFP relocalization in wild type and *minCD* mutant cells. We first used FtsZ-GFP, which expresses *ftsZ-gfp* as the only copy of *ftsZ* (Fig. 5A), and is somewhat temperature sensitive for growth, but at higher temperatures than used in our timelapse experiments (Levin et al, 1999). Similar fusions are routinely used for studies of FtsZ localization and dynamics. We noted two behaviors of FtsZ-GFP in this strain. First, the FtsZ ring often assembles at midcell by the collapse of a dynamic spiral-like shape into a ring (Fig. 5A, asterisk; Movie S7), as previously suggested by other studies

(Peters et al, 2007; Thanedar & Margolin, 2004). Second, when FtsZ leaves a recently completed septum (Fig. 5A, arrows), it often resulted in the transient assembly of FtsZ structures near the cell pole that fall apart and relocalize to midcell within ~10 minutes (Fig. 5A arrowheads). Similar minor populations of FtsZ are detected in some timelapse images of FtsZ-YFP (Peters et al, 2007). We suspect that these transient structures are labile and not readily visualized without timelapse microscopy, given our finding that the amount of FtsZ present even in medial rings decreases five fold in non-growing cells.

We hypothesized that the transient polar FtsZ rings we observed in wild type cells might mature into active divisomes in a *minCD* mutant. We therefore analyzed FtsZ-GFP dynamics in a *minCD* mutant (Movie S8). In a *minCD* mutant, FtsZ-GFP assembled polar FtsZ structures adjacent to the recently completed septum, but unlike wild type cells these structures persist and eventually support cell division (Fig. 5B arrowheads; Movie S8). Indeed, in FtsZ-GFP 73% of the minicells were the result of FtsZ rings that assembled adjacent to recently completed septa (here defined as those that contained FtsZ-GFP in previous timepoints) rather than at the older cell pole (here defined as those that lacked FtsZ-GFP in previous timepoints; Fig. 5B; Table S6). The remaining minicells were typically formed from long cells that assembled multiple FtsZ rings, some of which were at the cell poles (Fig. 5C arrowheads) and which could constrict nearly simultaneously to give a cell with two poles of equal age. These results suggest that MinC and MinD ensure that polar FtsZ structures visualized in wild type are transient and unable to support cell division. This view is consistent with

recent biochemical evidence that MinC does not inhibit FtsZ polymerization, but rather the lateral interactions between protofilaments that are likely necessary for septation (Dajkovic et al, 2008; Scheffers, 2008) We propose that MinCD act immediately after cell division, when the high concentration of FtsZ and other cell division proteins at the new cell pole would favor the immediate re-assembly of the cell division proteins adjacent to the new pole, a hypothesis consistent with the MinC localization data presented above.

Increasing the FtsZ/MinCD ratio causes the assembly of Z-rings near the new cell pole

It has previously been shown that overproducing FtsZ overcomes Min inhibition and produce minicells (Ward & Lutkenhaus, 1985; Weart & Levin, 2003). If MinC acts primarily at new cell poles, then under these conditions, minicells should also be assembled from FtsZ rings that assemble adjacent to recently completed septa. We therefore examined FtsZ dynamics in a strain that expresses *gfp-ftsZ* in addition to a wild type copy of *ftsZ* (denoted FtsZ-GFP/FtsZ+). This strain makes slightly shorter cells than wild type, likely because it produces more FtsZ (Table S6). The extra copy of *ftsZ* rescues the temperature sensitivity of the GFP fusion and also causes the production of approximately 7% minicells in the presence of wild type MinCD (Table S6, Movie S8). This is likely due to the increased levels of cytoplasmic FtsZ overcoming Min inhibition, as supported by our observation that overexpression of

MinCD in the FtsZ-GFP/FtsZ+ strain reduces the number of minicells from 9.9% to 2.6% (Table S6). Polar FtsZ assemblies were readily visualized in this strain (Fig. 6A, Movie S9), and 79% of the minicells were formed adjacent to a recently completed septum (again defined as those that contained FtsZ-GFP in previous timepoints), from these polar FtsZ-GFP structures.

As expected, the absence of MinCD in the FtsZ-GFP/FtsZ+ strain exacerbated this defect and caused additional polar FtsZ rings to persist and mature into active division sites, producing minicells (Fig. 6B-C arrowheads; Movie S10). Again, most minicells were assembled adjacent to the recently completed septum, but some were also assembled in long cells with multiple FtsZ rings (Fig. 6C; Table S6). These results suggest that reducing the MinC/FtsZ ratio below that needed to prevent polar cell division allows minicells to form, most adjacent to the most recently completed septum.

The minCD mutant affects the coupling between FtsZ ring assembly and cell division

In wild type cells, a single stable FtsZ ring assembles at midcell and is used for septal biogenesis in each cell cycle, so septation and FtsZ ring assembly are both temporally and spatially correlated. However, our studies of FtsZ dynamics in the *minCD* mutant revealed an uncoupling of FtsZ ring assembly and septation, so that septation no longer provided an accurate indicator of the timing of FtsZ ring assembly.

For example, multiple FtsZ rings assembled at approximately the same time often constricted at different times (Fig. 5C, arrowheads), so that an FtsZ ring assembled in the parent cell could be used in a subsequent division event in the daughter cell. Thus, an FtsZ ring could assemble and persist at a new pole until after another FtsZ ring in the cell had divided, ultimately producing a minicell at the old cell pole, but one cell cycle after the FtsZ ring was assembled. Our analysis also revealed that in the *minCD* mutant multiple cell division events could occur in rapid succession or even simultaneously producing cells that did not have a clear old and new pole. This defect made it impossible to use a simple lineage analysis to determine if minicells generally formed from FtsZ assembled adjacent to a recently completed septum. Our results suggest that the absence of MinCD affects the either the time required for Z-ring assembly or the time required for the onset of septal biogenesis, or both.

The absence of MinCD alters the timing of cell division

Timelapse observation of *minCD* mutant cells stained with the fluorescent membrane stain FM 4-64 revealed that they appeared defective in the timing of cell division (Movie S11). First, unlike the wild type (Fig. 7A), newly formed sister cells produced by a medial division rapidly became asynchronous (Fig. 7B). Second, the strain often produced abnormally long cells, even in the absence of a minicell division (Fig. 7B). These results were surprising because it has been proposed that the longer than normal cells observed in *minCD* mutants are the result of an asymmetric division that gives rise to a mini cell and a long cell. Third, individual cells often initiated multiple cell division events simultaneously (Fig. 7B, division #4), rather than having

only a single division event per cell as observed in wild type in wild type (Fig 7A). Together these data suggest that *minCD* cells have a defect in the timing of cell division in addition to an inability to prevent maturation of FtsZ-rings at the new cell pole.

To more quantitatively investigate this possibility, we used timelapse microscopy of wild type and *minCD* strains, collecting images of FM 4-64 stained membranes every three minutes at 30ºC. We noted the time at which each division event was completed (with uniform FM 4-64 staining across the cell) and the time at which septal biogenesis commenced in each daughter cell (two spots of FM 4-64 staining on each side of the cell). The difference between these times (the interdivisional time) was plotted on a histogram (Fig 7C-D). Wild type cells have a well-coordinated cell cycle during which the time between completion of division and subsequent formation of a new septum is never shorter than 20 minutes with an average of 29±6 minutes. We then repeated this using *minCD* cells and separated the midcell to midcell divisions (dark blue; 25±12 minutes) and those that form a minicell (light blue; 13±12 minutes). Neither population maintained the 20 minute minimum interdivisional time, as cells were able to initiate cell division events simultaneously (see Fig. 6B, divisions 4). There was also a population of cells that had long interdivisional times, which would result in the production of cells that are longer than wild type and capable of assembling multiple FtsZ rings.

Discussion

Most current models for MinC function indicate that this division inhibitor is restricted to the cell poles, where it inhibits FtsZ assembly (Barak & Wilkinson, 2007; Lutkenhaus, 2007; Margolin, 2006; Rothfield et al, 2005; Ryan & Shapiro, 2003). The activity of *E. coli* MinC is restricted to the cell poles by oscillation from one pole to the other (together with MinD), while *B. subtilis* MinC is thought to be stably tethered to the cell pole by DivIVA (again together with MinD). Surprisingly, several of our observations (discussed below) contradict this view and suggest a modified model for Min function.

First, functional GFP fusions to MinC expressed from the native chromosomal locus do not stably localize to the cell poles, but rather are primarily associated with sites of active cell division, to which they are recruited late in divisome assembly and prior to septation. Our data suggests that the prominent bipolar localization of MinC previously observed is due to protein over-expression, which causes MinC to localize to the cell poles as a secondary localization site that is also observed when division is blocked by FtsZ depletion. Thus, rather than being stably localized to both cell poles, MinC is only transiently associated with the new cell pole, remaining at this site for a short amount of time after constriction and then moving to midcell.

Second, *B. subtilis* MinC is dynamic, although in a manner distinct from that of *E. coli*. Specifically, we find that the net movement of *B. subtilis* MinC is from the new pole to midcell, rather than oscillating from pole to pole. *B. subtili*s MinC relocalizes from the new cell pole to midcell immediately prior to division via

membrane associated foci that move at rates of ~3 μm/min. During division, it also appears to move from one side of the invaginating septum to the other once every ~4 min (for a predicted rate of ~0.3 μm/min). Both of these latter rates of movement are slower than the measured diffusion rate of cytoplasmic or membrane proteins of similar sizes (~500 μm^2/min, ~10 μm^2/min, respectively (Elowitz et al, 1999; Mullineaux et al, 2006)), and more similar to proteins in which movement is mediated by polymerization (0.2–2 μm/min, (Perez et al, 1999; Watanabe & Mitchison, 2002; Waterman-Storer et al, 1999)), and similar to the rate of MinC oscillation in *E. coli* (Hu & Lutkenhaus, 1999; Raskin & de Boer, 1999a; Raskin & de Boer, 1999b). This suggests that MinC might be moved by a cytoskeletal protein, such as MinD, which polymerizes in a membrane and ATP-dependent manner (Hu et al, 2002; Suefuji et al, 2002) and is required for the oscillatory movement of *E. coli* MinC (Hu & Lutkenhaus, 1999; Raskin & de Boer, 1999a; Raskin & de Boer, 1999b). Thus, *B. subtilis* MinC shows two distinct dynamic behaviors, movement of smaller populations along the cell envelope that result in a net relocalization from the new pole to midcell and its apparent rotation around the septum (Fig. 8A).

Finally, we were surprised to observe that polar FtsZ rings (or ring-like structures) assemble in wild type cells adjacent to recently completed septa, as most models propose that MinC prevents the formation of these structures. This indicates that MinC does not prevent FtsZ from assembling at the poles, but rather interacts with and destabilizes polar FtsZ polymers or newly formed Z-rings before they can become active sites of cell division. Timelapse fluorescence microscopy demonstrated that in

the *minCD* mutant, 75-83% (Table S6) of minicells are produced from these polar FtsZ structures; the remaining minicells are produced in long cells that result from a defect in the initiation of cell division (discussed below).

A refined model for Min function

Our results suggest a refined model of MinCD function in *B. subtilis* (Figure 8B). First, FtsZ coalesces into a ring at midcell, recruiting the early division proteins FtsA, EzrA and ZapA, then the late cell division proteins, followed by DivIVA, and ultimately MinD and MinC (Fig. 8B, cell iii). Septal biogenesis begins and as it completes, FtsZ leaves the old division site to assemble ring-like structures adjacent to the new cell pole (cell iv-v). After septation, the affinity of MinC for the pole is reduced, and it moves away from the pole, probably together with MinD (cell v-vi). This movement from the newly completed septum effectively scans the new cell pole for FtsZ polymers that could assemble divisomes in the chromosome free space adjacent to the cell pole. We propose that MinC and MinD interact with these FtsZ polymers and either prevent them from associating with the late division proteins or directly destabilize the FtsZ assemblage, thereby allowing FtsZ to relocalize to midcell more efficiently. These possibilities are consistent with recent biochemical data demonstrating that *E. coli* and *B subtilis* MinC do not inhibit FtsZ polymerization, but rather inhibit lateral interactions between FtsZ protofilaments (Dajkovic et al, 2008; Scheffers, 2008). Such interactions are likely necessary to stabilize transient FtsZ rings and to allow their association with the late division proteins. Interestingly, *E. coli*

MinC is capable of disassociating previously assembled FtsZ networks (or bundles; (Dajkovic et al, 2008)); if this is also true of *B. subtilis* MinC, then it could directly dissociate the FtsZ rings that assemble adjacent to the new cell pole.

The mechanism by which MinC is kept inactive and unable to block cell division upon recruitment to midcell remains unclear, but we can envision two possibilities. First, the different protein-protein interactions that mediate these events could regulate MinC activity: recruitment of MinC to midcell depends on DivIVA and the late cell division proteins (Edwards & Errington, 1997; Marston et al, 1998), whereas MinC is capable of directly inhibiting FtsZ bundling both *in vitro* and *in vivo* (Dajkovic et al, 2008; de Boer et al, 1992; Marston et al, 1998; Scheffers, 2008). It is therefore possible that DivIVA and/or the late division proteins inhibit MinC activity. Second, it is possible that MinC interacts with transient FtsZ assemblages before the late division proteins, and that it cannot disrupt the activity of the complete divisomes to which it is recruited at midcell. Additional experiments are required to discriminate between these models, but our studies clearly demonstrate that in *B. subtilis*, MinC activity is not restricted to the poles by localization, but rather is regulated by an unknown mechanism.

The absence of MinC and MinD causes a cell cycle timing defect

The *B. subtilis minCD* mutant also has a striking defect in the timing of cell division. Whereas wild type *B. subtilis* shows well-synchronized chains of daughter cells and regular interdivisional times, *minCD* daughter cells (even those produced by medial division) are not synchronized and the strain shows highly variable

interdivisional times. We find that it is the longer interdivisional times, rather than the production of minicells, that produces the long cells that are characteristic of the *minCD* strain, because long cells are often produced either before or without a minicell division. Such longer cells are capable of assembling multiple FtsZ rings that constrict nearly simultaneously, resulting in very short interdivisional times and often producing a polar minicell. Similar observations have been made regarding the timing of cell division in *E. coli minCD* mutants (Akerlund et al, 1992), suggesting that the role of the Min system in controlling the timing of cell division is conserved. One possible model for this timing defect is that in the absence of MinC, FtsZ polymers, perhaps together with other division proteins, accumulate at the new cell pole as well as the midcell thus splitting these proteins between two sites instead of a single midcell site as in wild type. This might cause the cell to grow longer until both sites accumulate enough FtsZ and other proteins to support cell division, resulting in an extended latent period between assembly of the FtsZ ring and the onset of constriction. This model is in keeping with the observation that *minCD* mutant cells often make two concurrent or nearly concurrent divisions (Fig. 7; (Akerlund et al, 1992)).

The rotation of MinC at active division sites suggests it might associate with another septal component that rotates. Indeed, timelapse microscopy indicates that FtsZ itself is highly dynamic within the cell and appears to rotate around midcell before coalescing into a more stable ring (Fig. 5, Movies S5-6). It is possible that this rotation persists during division, and that we are unable to observe it in our timelapse experiments because the Z-ring is relatively uniform. Previous photobleaching

experiments have indicated that the Z-ring is dynamic and exchanging subunits from a non-localized pool (Stricker et al, 2002). It is therefore possible that rotation is a general characteristic of the divisome, rather than a unique property of MinC.

Materials and Methods

Strains and reagents

Strains are derived from PY79 (Youngman et al, 1984) except PAL1213 and PL642 (which are 0168 derivatives), using standard methods (Hoch, 1991). The methods used to construct the *minD* deletion (JAG79), EzrA-CFP (JAG151), *amyE::*P_{xyl}*-gfp-minCD* (PAL1213), and FtsZ-GFP/FtsZ (AD3007) are described in supplemental information.

Isolation of GFP insertions in minCD

We wanted to localize functional GFP fusions to MinC and MinD expressed at native levels, to minimize potential artifacts. We therefore constructed the GFP insertion transposon TAGIT (to be described in detail elsewhere, J.A.G, E.C.B, Ida P. Tuwatananurak, James Jung, and K.P., in preparation) to mediate the random insertion of *GFP* into the chromosomal *minCD* locus, without disrupting normal transcriptional regulation or operon structure. Briefly, TAGIT is a Tn5-based transposon into which we cloned *'lacZ* without translational initiation sites to allow identification of in frame insertions in an expressed target gene, a *kanR* gene to allow selection for insertions in both *E. coli* and *B. subtilis*, and *gfp* without translational initiation sites. We flanked '*lacZ* and *kanR* with *loxP* sites to allow Cre-mediated excision of *lacZ* and *kanR*. TAGIT generates insertions of the GFP protein into the middle of a target protein, similar to Alkaline Phosphatase "sandwich" fusions that generate bi-functional fusion proteins (Ehrmann et al, 1990). As described below, we integrated TAGIT insertions

into *B. subtilis* chromosome at *minCD* and expressed Cre *in vivo* to excise *lacZ* and *kanR* from the in-frame and expressed fusions.

We used *in vitro* transposition (Goryshin et al, 1998) to insert TAGIT into pJAG1, a TOPO plasmid (pCR2.1-topo, Invitrogen) containing a 3.2 kb fragment encoding *minCD* genes plus ~600 nucleotides upstream and downstream amplified with primers JG3 and JG4 (Supplemental Materials). To allow selection for TAGIT insertions, the *kanR* gene in the pCR2.1 vector was inactivated by digesting the plasmid with NarI, which cuts twice within the gene. After *in vitro* transposition, the resulting pool was transformed into XL-10 Gold competent cells (Stratagene), and the plasmid DNA isolated and transformed into wild type *B. subtilis* strain EBS42 (*amyE::*P_{spoIIQ}*-cre*). The transformation was plated on LB containing 10 μg/ml kanamycin to select for integration of the plasmid into the chromosome and 10 μg/ml X-Gal to screen for insertions in which TAGIT had inserted into the same reading frame as *minCD,* allowing expression of β-galactosidase. Strain EBS42 expresses the Cre recombinase from the sporulation specific *spoIIQ* promoter, so to excise the *lacZ* and *kanR* genes we sporulated the cells in DSM for 24 hrs, heated the culture for 20 min at 80°C to kill vegetative cells. The cells were plated on LB and patched to LB kanamycin to identify Kan^S colonies in which *lacZ* and *kanR* had been excised to leave *GFP* in the same reading frame as upstream and downstream coding regions. PCR was used to ensure that the plasmids had integrated by the desired double recombination event (replacing *minCD* with *minCD::TAGIT* from the plasmid) rather

than a single recombination event (duplicating *minCD* and integrating the entire plasmid into the chromosome).

We initially used fluorescence microscopy of FM 4-64 stained cells to screen for functional GFP insertions, but noted that at 42°C on DSM plates the *minCD* null strain made irregular star-shaped colonies with projecting tendrils, while the wild type strain made smooth edged colonies. This allowed us to more rapidly screen for functional GFP insertions. In total ~500 colonies with in frame GFP insertions were screened for *minCD* function by this assay and 100 by microscopy. Only two functional insertion sites (*minC4-GFP* and *minC8-GFP*) were isolated. To assess the randomness of TAGIT transposition, 100 randomly selected insertions were sequenced; these were distributed throughout the gene (Figure S5), although the only functional insertions were at the N-terminus of MinC. In other experiments, we have used TAGIT to isolate functional GFP insertions in the middle of LacI (J.A.G, E.C.B, Ida P. Tuwatananurak, James Jung, and K.P., in preparation), suggesting that the failure to isolate functional GFP sandwich fusions in these studies is specific to MinC.

Timelapse Microscopy

Timelapse microscopy used 1.2% agarose pads (Becker & Pogliano, 2007) prepared as follows. FM 4-64 (Molecular Probes) was added to a final concentration of 0.5 μg/ml in a 1.2% solution of molten agar/media (CH or LB diluted 1:5 in water) and added to the well of a culture slide and covered with a glass slide. To induce P_{xyl}-

GFP-MinC, xylose was added to the indicated concentration. After cooling, the slide was removed and two air pockets were cut out of the agar leaving a 3 to 5 mm agar bridge in the center of the well. Cells were grown overnight on the appropriate solid media at 30ºC and applied to the agar bridge and covered by a glass cover slip. To prevent drying during the experiment, 50% glycerol was applied to the region of contact between the slide and the coverslip. The slide was then allowed to equilibrate in an environmentally controlled chamber at 30ºC (Precision Control Weather Station) for at least 30 minutes prior to visualization. Exposure times were minimized to reduce phototoxicity. These slides supported growth at nearly the same rate as in liquid (a doubling time of ~50 minutes on slides vs. ~40 minutes in liquid). Images were acquired using an Applied Precision Spectris microscope and deconvolved using softWoRx v3.3.6 software (Applied Precision). Figures were assembled with Photoshop v7.0 software (Adobe).

Total Internal Reflection Fluorescence (TIRF) Microscopy

TIRF experiments were performed using the same microscope and a 488 nm argon laser installed in a TIRF module supplied by Applied Precision and a Plan Apochromat 100X 1.40 NA objective. GFP was visualized with using FITC excitation and emission filters and 0.3 second pulses at 35% power. FM 4-64 was imaged once using the 488 nm laser (with 0.1 second pulses at 35% power) to excite and the rhodamine emission filter (control experiments demonstrated that no FM 4-64 fluorescence was visualized with the GFP emission filter). Summation and maximum

intensity projections were constructed using the Quick Projection tool (softWoRx 3.3.6).

Quantitative image analysis: 2-D, 3-D, and kymogram-like plots

3-D and 2-D pixel intensity plots were created using the Data Inspector tool in the softWoRx v3.3.6 software (with the heat intensity setting), with plots exported to Photoshop. To create kymogram-like plots of EBS499, the septum was cropped and rotated to align with the y-axis using the Resample 2D function. The Volume Viewer function normally creates 3D projections of 2D images by using several Z-sections of one sample. This function was utilized to project 2D images through time by converting time points into Z-sections in the file header. Care was taken to align (Align Image Tool) and crop (Resample 2D tool) each septum to the smallest area possible to faithfully represent the movement of GFP molecules through time. If images could not be aligned for any reason (focal plane and X/Y drift, rapid movement of cells due to growth, etc.) they were not used to create kymogram-like projections.

Quantification of Interdivisional Time

Cells were grown according to timelapse microscopy methods and images were taken every three minutes. The interdivisional time was defined as the amount of time that elapsed between the completion of division in the parent cell and beginning

of constriction in each daughter cell. The interdivisional time for each daughter cell/parent cell pair was recorded and plotted in a histogram using 20 bins (giving each timepoint its own bin; 3 minute timepoints for 60 minutes). The histogram was created using Matlab and edited in Adobe Photoshop.

Acknowledgments

We thank Eric Stewart for advice on timelapse fluorescence microscopy, William Reznikoff for Tn5 transposase, Richard Losick and Petra Levin for strains, and Alan Derman for constructing the FtsZ-GFP/FtsZ+ fusion. This research was supported by the National Science Foundation (NSF0135955), the National Institute of Health (GM57045) and by the University of California at San Diego.

This chapter was published on December 15th, 2008, in Genes and Development. I would like to thank Eric Becker and Kit Pogliano for their permission to use this manuscript in my dissertation. The dissertation author was the primary author and researcher.

Tables

Table 1. Strains used in this study

Strain	Genotype	Reference or source
PY79	wild type	(Youngman et al, 1984)
PB302	*minCD::cat, trpC2*	(Lee & Price, 1993)
FG94	*divIVA::spec, amyE::P_{xyl}-divIVAΩcat*	R. Losick
MDS642	*minCD::cat::tet*	lab stock
MDS651	*amyE::P_{maf}-minCDΩcat*	lab stock
MDS652	*amyE::P_{minCD}-minCDΩcat*	lab stock
PAL1213	*amyE::P_{xyl}-gfp-minCDΩcat, trp, phe*	P. Levin
PL642	*ftsZ-gfp^{Ts}Ωcat, trp, phe*	P. Levin
AD3007	*ftsAZ::ftsAZ-gfpΩerm*	this study
EBS483	*minC4-gfp, ftsZ::P_{spac}-ftsZΩphleo, sacA::P_{spoIIR}-creΩspec*	this study
EBS499	*minC4-gfp, sacA::tet*	this study
EBS42	*sacA::P_{spoIIR}-creΩspec*	(Becker et al, 2006)
JAG15	*minC8-gfp, sacA::P_{spoIIR}-creΩspec*	this study
JAG32	*minC4-gfp, sacA::P_{spoIIR}-creΩspec*	this study
JAG67	*minC4-gfp, sacA::tet, divIVA::spec*	this study
JAG79	*minC4-gfp, sacA::tet, 110ind::loxP-kan-loxP*	this study
JAG114	*minD4-gfp, sacA::P_{spoIIR}-creΩspec*	this study
JAG118	*minD4-gfp, sacA::P_{spoIIR}-creΩspec, amyE::P_{maf}-minCDΩcat*	this study

Table 1. continued

JAG120	*minD4-gfp, sacA::*P_{spoIIR}*-creΩspec, amyE::*P_{minCD}*-minCDΩcat*	this study
JAG135	*ftsAZ::ftsAZ-gfpΩerm, minCD::cat*	this study
JAG151	*ezrA-cfpΩerm*	this study
JAG189	*minCD::cat::tet, amyE::*P_{xyl}*-gfp-minCDΩcat*	this study
JAG226	*ezrA-cfpΩerm, minC4-gfp-Ωcat,*	this study
JAG252	*minCD::cat::tet, ftsZ-gfp*^{Ts}*Ωcat*	this study
JAG431	*amyE::*P_{xyl}*-gfp-minCD, ftsAZ::ftsAZ-gfpΩerm*	this study
JAG437	*minD4-loxP-'lacZ-kan-loxP*	this study
JAG439	*amyE::*P_{minCD}*-minCDΩcat, minCD::cat::tet*	this study
JAG441	*amyE::*P_{maf}*-minCDΩcat, minCD::cat::tet*	this study

Figures

Figure 1. Localization of MinC4-GFP (EBS499) and MinD4-GFP (JAG118). (A) the current model for the spatial regulation of cell division in *B. subtilis* and *E. coli,* indicates that the DNA binding protein Noc blocks division over the chromosome, while MinC (green) has the highest time averaged concentration at the poles, thereby blocking polar cell division. In *E. coli* the increased concentration of MinCD at the poles is achieved by its oscillation from one cell pole to the other, while in *B. subtilis* MinCD were previously thought to localize to the cell poles. (B) Our studies find MinC to have the highest concentration at midcell, with a few molecules moving rapidly along the cell envelope. Thus, MinC has a high concentration only at the most recent cell pole (right pole), and only before it relocalizes to midcell. (C) Epifluorescence microscopy of MinC4-GFP (EBS499) and (D) MinD4-GFP (JAG118) in growing *B. subtilis* cells. The non-functional MinD4-GFP fusion here complemented by *amyE::*P_{minCD}*-minCD*, which does not express sufficient MinC or MinD to fully complement the *minCD* null mutation for minicell production (supplemental data), but does complement MinD4-GFP, suggesting that MinD4-GFP retains some function. (E) Timelapse microscopy showing the localization of MinC4-GFP throughout the cell cycle. FM 4-64 and GFP images were collected every 10 minutes. Movie S1 shows MinC4-GFP. Scale bars, 1 μm.

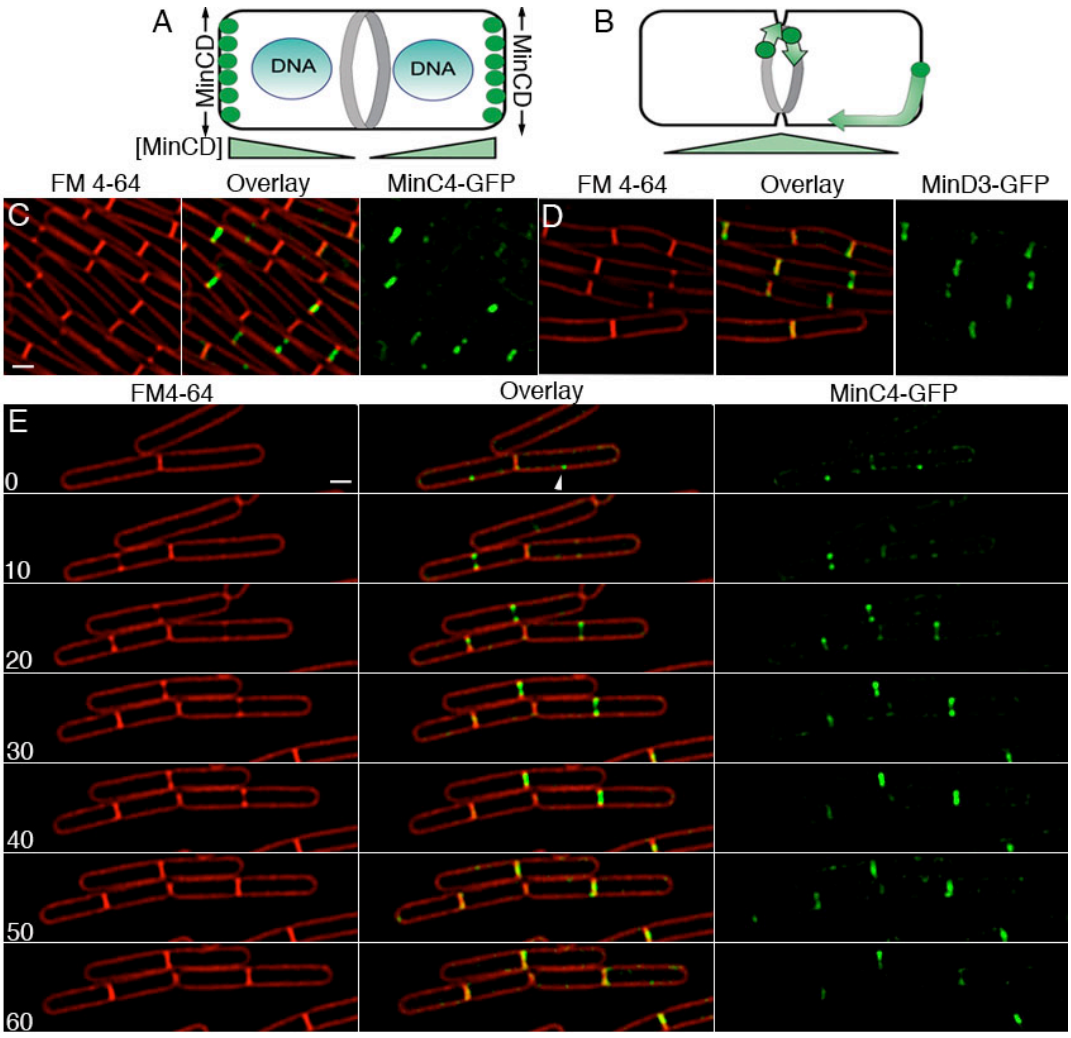
A
MinCD
DNA
DNA
MinCD
[MinCD]
B
FM 4-64
Overlay
MinC4-GFP
FM 4-64
Overlay
MinD3-GFP
C
D
FM4-64
Overlay
MinC4-GFP
E
0
10
20
30
40
50
60

Figure 2. Quantitative comparison of MinC4-GFP and inducible GFP-MinC (*P_{xyl}-GFP-minC*) localization. Arrowheads indicate the cell poles; arrows indicate the midcell position. The pixel intensities are shown as a heat intensity plot with red being the highest, blue the lowest with colors corresponding to the scale on the right for each image. (A) MinC4-GFP (EBS499) with a 5 second exposure, which results in a 2x higher maximum pixel intensity than P_{xyl}-GFP-MinC. The highest fluorescence intensity is at midcell, with low levels of fluorescence elsewhere along the membrane including the cell pole. No polar caps of MinC are observed. (B) P_{xyl}GFP-MinC (PAL1213) grown with 0.5% xylose and imaged with a 1 second GFP exposure. The protein localizes both to septa and to midcell. (C-E) P_{xyl}-GFP-MinC was expressed at various levels by titrating the xylose concentration from (C) 0.02%, a concentration that does not produce sufficient protein to block minicell formation, to (D) 0.05% and (E) 0.5%, both of which produce sufficient protein to prevent minicell formation. Decreasing the xylose concentration to 0.05% decreases polar GFP-MinC localization while maintaining midcell localization. Scale bars, 1 μm.

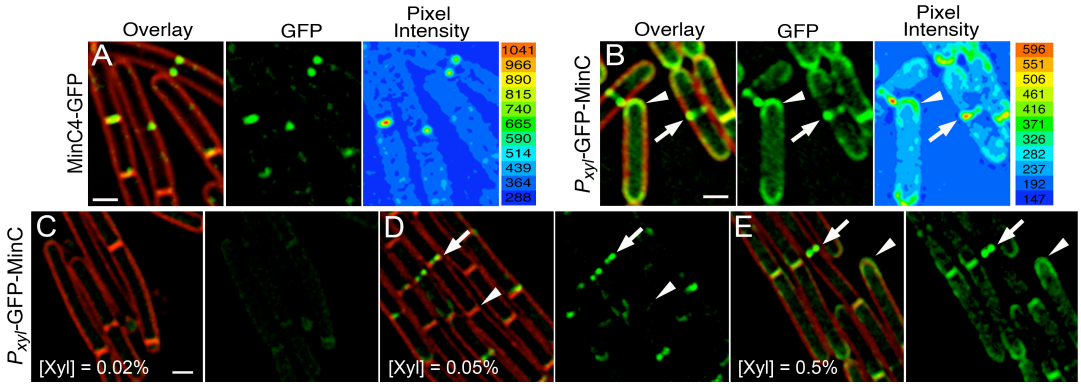
Overlay
GFP
Pixel Intensity
MinC4-GFP
A
1041
966
890
815
740
665
590
514
439
364
288
Overlay
GFP
Pixel Intensity
P_{xyl}-GFP-MinC
B
596
551
506
461
416
371
326
282
237
192
147
P_{xyl}-GFP-MinC
C
[Xyl] = 0.02%
D
[Xyl] = 0.05%
E
[Xyl] = 0.5%

Figure 3. Movement of MinC4-GFP at division sites visualized by epifluorescence microscopy. To quantify changes in the appearance of MinC4-GFP at septa over time, we employed a kymogram-like method to follow individual septa through time, together with an analysis of the pixel intensities over time. (A) Briefly, the septa were rotated to align the septa with the Y-axis, cropped, stacked and the Y-axis projected through time. (B) An example of the expected kymograms for symmetric rings (top), for an asymmetric assembly (middle) and for an asymmetric assembly that rotates about the septum (bottom). (C) Timelapse microscopy of MinC4-GFP (EBS499) at three adjacent division sites (numbers 1-3). Images were taken at approximately 1 minute intervals; the time in seconds is shown on the right. MinC appeared to translocate from one side of the septa (arrows) to the other (arrowhead). See movies S5-6 for more examples. (D) Kymograms of each septum (labeled 1-3) showing GFP (right) and FM 4-64 fluorescence (left) and the corresponding 3D-pixel intensity plots. The number in the upper right indicates the septum in C; the arrows and arrowheads also correspond to those in C for each cell. The FM 4-64 intensity fluctuates evenly across the septum, in contrast to the GFP intensity, in which one side can gain or lose intensity. Scale bar, 1 μm. Time indicated in seconds.

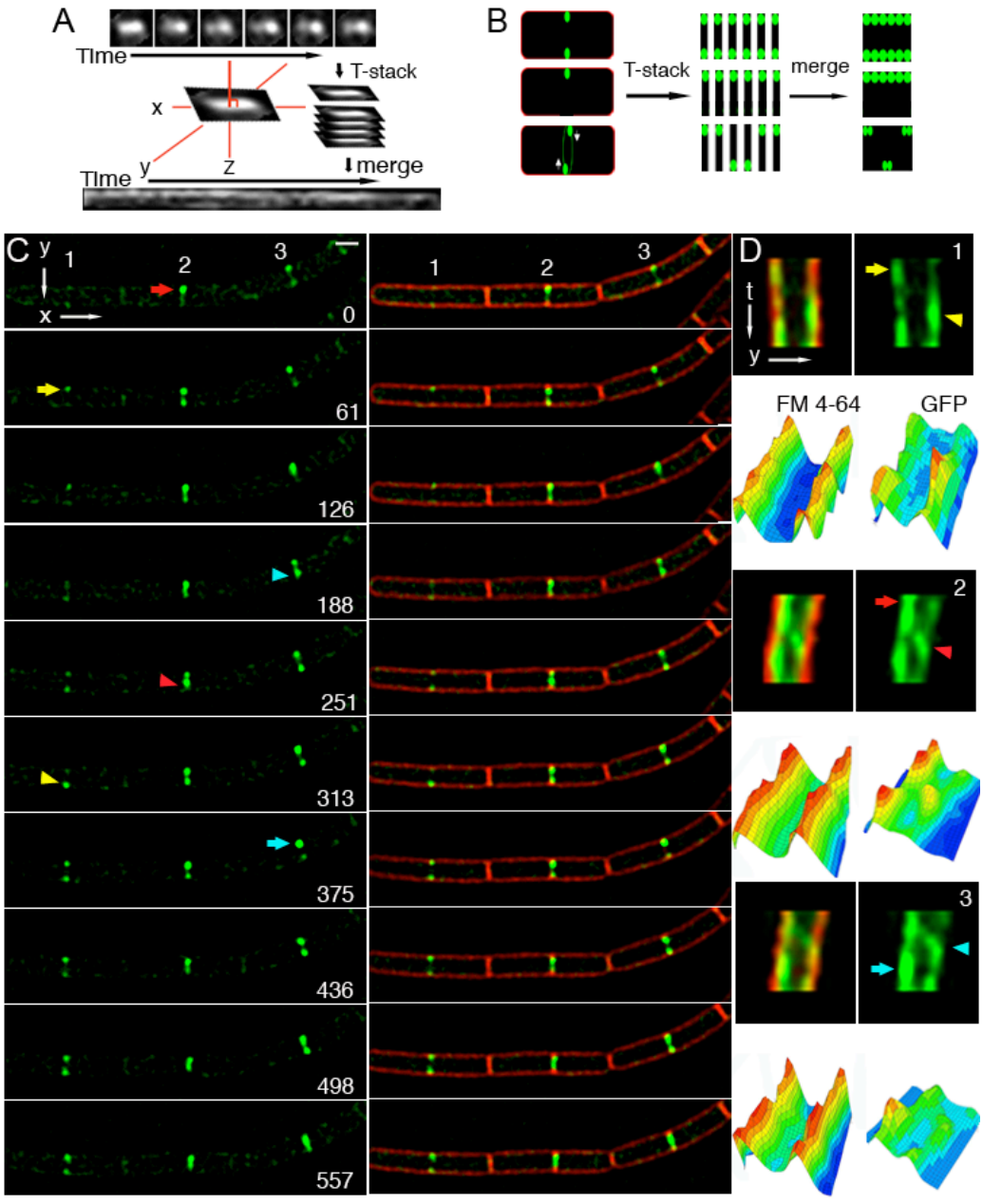
A
Time
T-stack
x
y
z
merge
Time
B
T-stack
merge
C
y
x
1
2
3
0
61
126
188
251
313
375
436
498
557
D
t
y
1
2
3
FM 4-64
GFP

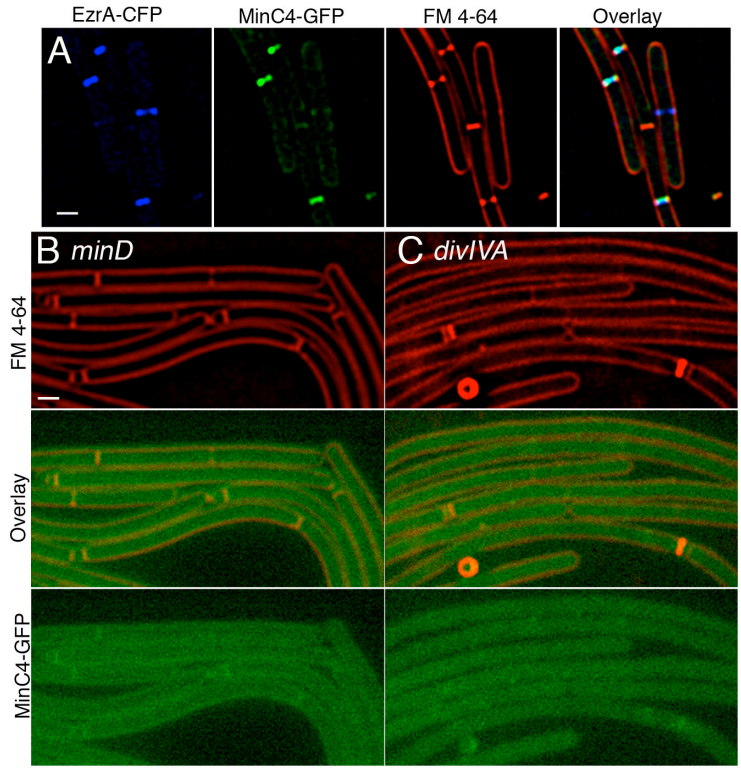

Figure 4. MinC localizes to division sites late in division in a manner dependent on DivIVA and MinD. (A) Colocalization of EzrA-CFP (blue) and MinC4-GFP (green) with FM 4-64n stained membranes (red) in strain JAG226. (B) MinC4-GFP fails to localize in the absence of MinD (JAG79*)* (C) or DivIVA (JAG67) and shows low fluorescence that is barely above background. Thus, DivIVA and MinD appear to be required for septal localization of MinC, rather than for retention at the cell pole. Scale bars, 1 μm.

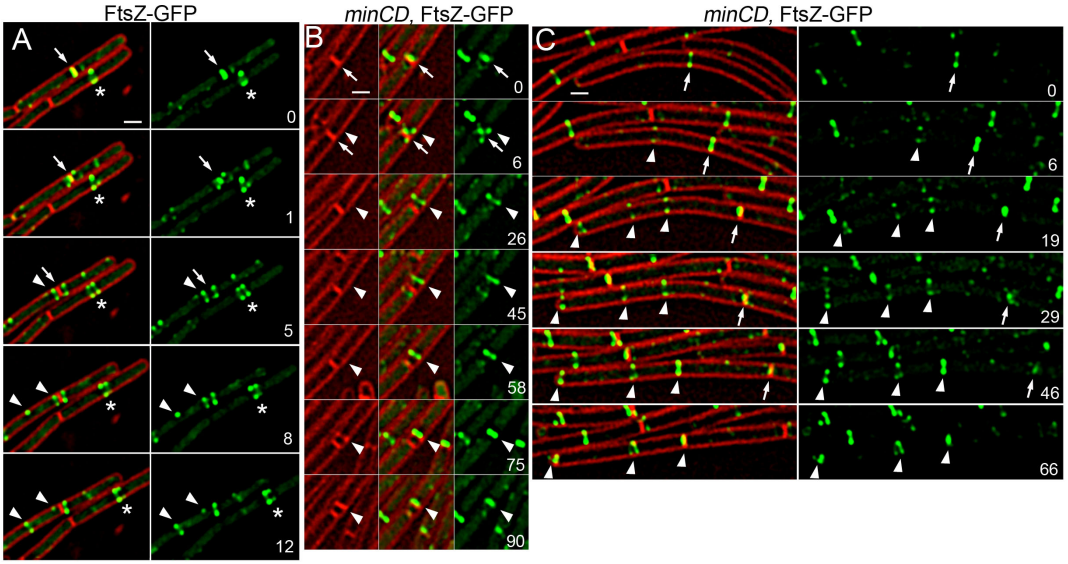

Figure 5. Comparison of FtsZ-GFP dynamics in wild type and *minCD* cells. Images of FtsZ-GFP (green) and FM 4-64 (red) were collected every 1-3 minutes for several cell division events. Times were selected for display that best showed the illustrated behavior; additional timepoints and examples of wild type and *minCD* mutant cells can be found in supplemental movies S7-S8). Time is indicated in minutes in the right panel of each set. (A) Relocalization of FtsZ-GFP (JAG212) from a completed septum (arrows), showing the transient assembly of an FtsZ-ring adjacent to the new pole (arrowheads) that disappears while an FtsZ ring assembles at midcell (arrowheads). The assembly of an FtsZ ring at midcell often entails stabilization of a dynamic structure into a single, brighter ring (asterisk). (B) In the *minCD* strain JAG252, FtsZ-GFP assembles structures (arrowhead) adjacent to the recently completed septum (arrow); these ultimately constrict to generate a minicell. This pathway accounts for 75% of all minicells. (C) The remaining minicells are produced in long cells that assemble several FtsZ rings. The arrow indicates the first FtsZ ring to assemble, arrowheads subsequent rings. The leftmost ring constricts to generate a minicell. Scale bars, 1 μm.

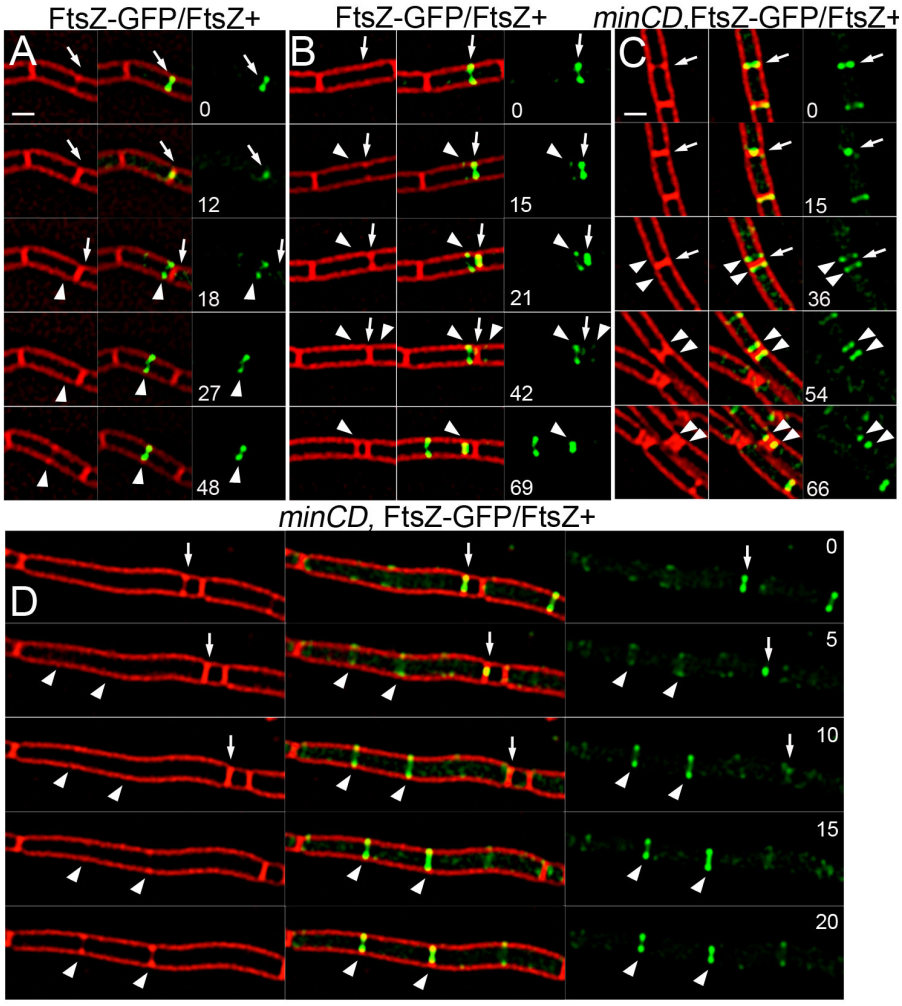

Figure 6. FtsZ dynamics in strains co-expressing FtsZ-GFP and FtsZ. Images of FtsZ-GFP (green) and FM 4-64 (red) were collected every 3 minutes for several cell division events. (A) Relocalization of FtsZ-GFP/FtsZ+ (AD3007) from a completed septum (arrow) to a transient polar site and to midcell (arrowhead). (B) Relocalization of FtsZ-GFP/FtsZ+ (AD3007) from completed septum (arrow) to a polar site that constricts to form a minicell (arrowhead). (C) In the *minCD* strain JAG135, FtsZ-GFP/FtsZ+ assembles polar FtsZ rings (arrowheads) adjacent to completed septa (arrow), which constrict to form minicells. This strain also forms long cells (D) that assemble multiple FtsZ-rings that can constrict nearly simultaneously (arrowheads). Scale bars, 1 μm.

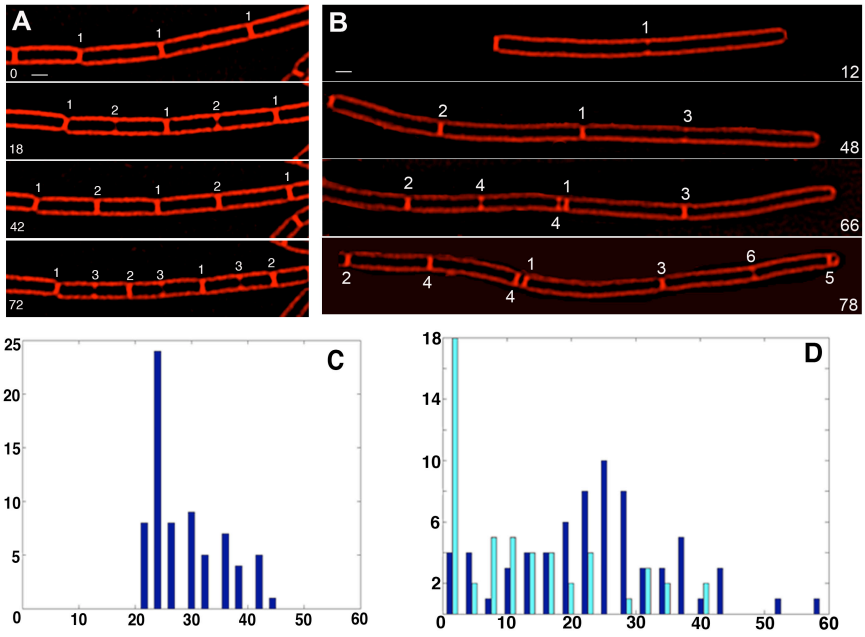

Figure 7. Comparison of interdivisional time in wild type and *minCD* cells. Timelapse microscopy of FM 4-64 stained cells was performed with images collected every 6 minutes. Numbers above septa indicate the order they were formed. Identical numbers in the same timepoint denote septa that formed simultaneously. (A) The wild type strain PY79 shows well-synchronized daughter cells. (B) The *minCD* strain MDS642 shows asynchronous division in the daughter cells (divisions 2, 3), and simultaneous divisions (divisions 4). Scale bar, 1 μm. (C-D) The time between the completion of one septum and the start of the next (described in materials and methods) was plotted for (C) PY79 and (D) MDS642. Dark blue lines denote midcell to midcell interdivisional time and light blue lines denote that for any division involving a minicell.

Figure 8. Summary of MinC dynamics in *B. subtilis* and a proposed role for MinC in relocalization of FtsZ from new cell poles (A) MinC (red) localizes to septa before septal biogenesis, rotating around sites of active cell division (top cell) and constricting as septal biogenesis completes (middle cell). After septation is complete, it leaves the new pole and moves to midcell. (B) Model for the role of MinC (yellow) in relocalization of FtsZ (green filaments) during the cell cycle. Chromosomes are shown in cyan. Cells 1-2 show the formation of an FtsZ ring at midcell from short FtsZ protofilaments (green filaments; (Li et al, 2007; Osawa et al, 2008)), cells 3-4 the onset of septal biogenesis and the recruitment of MinC (yellow) to the active divisome (solid green ring). As septation completes (cells 4-5), FtsZ is released from the new cell pole and accumulates in ring-like structures near the cell pole that MinC either disrupts prevents from recruiting the late division proteins. (C) In the absence of MinC, these normally transient structures persist and are used for cell division.

A Summary of MinC dynamics

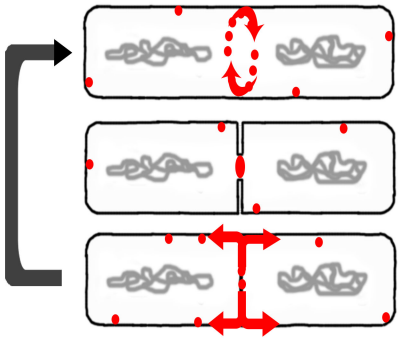

B wildtype

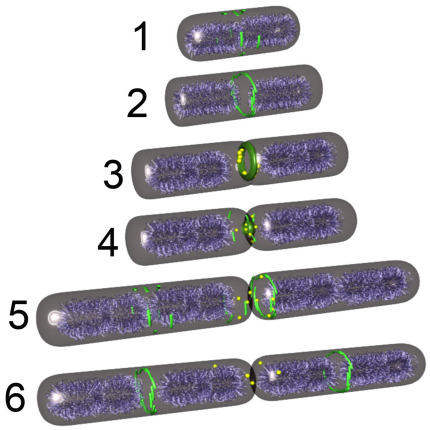

C *minCD*

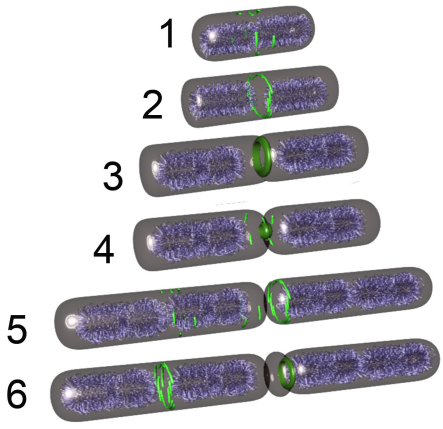

Supplemental Methods

Description of the MinC and MinD GFP insertions

The fusion used in most of these studies (MinC4-GFP) contains GFP and flanking recombination sites inserted into the 4th codon of *minC*, and includes two duplicated amino acids flanking the insert (T_3K_4) that were generated by transposition, an N-terminal linker encoded by restriction and recombination sites and one amino acid on each side of GFP that is encoded by the junction between *minC* and the transposon. The protein sequence for MinC4-GFP is:

$M_1K_2T_3K_4$<u>N</u>CLLYTSITSYNVCYTKLWAAA(SKGE//LYK)KMCIRD<u>R</u>T_3K_4 K_5Q_6…MinC

Amino acids with numbers are MinC, the underlined amino acids are created by junction of the insertion element and *minC*, the amino acids in parenthesis are GFP, while the remaining amino acids are encoded by DNA sequences including restriction and recombination sites. A second functional fusion was isolated that contains GFP inserted into the 8th codon of *minC*. The sequence of this insertion (MinC8-GFP) is:

$M_1K_2T_3K_4T_5K_6K_7Q_8$<u>N</u>CLLYTSITSYNVCYTKLWAAA(SKGE//LYK)KMCI RD<u>R</u>K_7Q_8 …MinC.

A partially functional fusion was isolated that contains GFP inserted into the 4th codon of *minD*. The sequence of this insertion is: $M_1G_2E_3A_4$CLLYTSTRGSTSITSYNVCYTKLWAAA(SKGE//LYK)KMCIRD<u>R</u>G_2E_3 A_4...MinD.

Construction of MinD knockout

The *minD* strain was constructed using plasmid pJG32, a derivative of pEB71 (which contains a kanamycin resistance cassette flanked by *loxP* sites (Becker et al, 2006). The 5' region of *minD* was amplified using PY79 chromosomal DNA with primers JG34 (5'-catatgtattcggcattcagtctttg-3') and JG35 (5'-actagtctcacccaattcacattcctc-3') and cloned into SpeI/NdeI of pEB71 to create pJG24. Then the 3' region was amplified with primers JG36 (5'-ctcgagcaagatcttaatgtgatagaatc-3') and JG37 (5'-cagctgtgcacatggatctttaagataagg-3') and cloned into PvuII/XhoI of pJG24 to create pJG32. The plasmid was integrated into the chromosomal *minD* locus by a double recombination event to replace *minD* with the *kanR* cassette. PCR amplification used Pfu DNA polymerase (Stratagene) with oligonucleotides from Integrated DNA Technologies. Restriction endonucleases and T4 DNA ligase were acquired from New England Biolabs and cloning was performed in *E. coli* Top10 from Invitrogen.

Construction of EzrA-CFP

Strain JAG151 contains a fusion to CFP to the *B. subtilis ezrA* gene that is integrated at the chromosomal *ezrA* locus. JAG151 was created by integrating pJAG60 into PY79. This was accomplished by the following method. pJAG34 was created using primers JG75 and JG76 to mutagenize pMUTIN-CFP to insert an NheI site at the beginning of CFP. A 1 kb fragment of EzrA was then amplified from PY79 chromosomal DNA using PCR with primers JG89 (5'-

gctagccatttccaggcggctagcggatatgtcagctttgatttttttcaactg-3') and JG90 (5'-cggccggtgccgaagctgttagctgact-3') and cloned into pCR2.1-topo to give pJAG56. pJAG56 was then sequentially digested with BamHI then NheI. The approximately 1 kb band was then digested with EagI. This fragment was ligated to pJAG35 digested with NheI and EagI to give pJAG60. pJAG60 codes for a *cfp* fusion to *ezrA* with the intervening four amino acid linker SRLE, as in (Levin et al, 1999). pJAG60 was then integrated by single recombination into PY79 by transformation and selection for resistance to erythromycin at 2 mg/ml to yield JAG151. Primers were purchased from IDT, restriction endonucleases and T4 DNA ligase were acquired from New England Biolabs and cloning was performed in *E. coli* Top10 from Invitrogen and XL-10 Gold from Stratagene.

Construction of AD3007

Strain AD3007 contains a fusion of gfp+ to the *B. subtilis ftsZ* gene that is integrated at the chromosomal *ftsAZ* locus. The integrant was generated from plasmid pAID3001, which was constructed by amplifying genomic DNA from *B. subtilis strain* PY79 with the primers 5'-gagggtaccagcgctatcgatcggccggactggtgctcggaatag-3' and 5'-ctttgctagccatttccaggcggctgccgcgtttattacgg-3', and ligating the resulting amplicon to the vector pMUTIN-GFP+ after restriction of amplicon and vector with EagI and NheI. The resulting plasmid encodes a GFP fusion to the C-terminus of FtsZ with the intervening four amino acid linker SRLE, as in (Levin et al, 1999). The 3024

bp chromosomal insert begins at base pair 1595252 in the published *B. subtilis* 168 sequence and contains in addition to the entire *ftsZ* gene, the upstream *ftsA* gene, and upstream of that, about half of the *sbp* gene. The structure of pAID3001 was confirmed by restriction endonuclease digestion, and the plasmid was integrated by a single recombinational event into the PY79 chromosome by transformation and selection for resistance to erythromycin at 2 mg/ml. The integrant contains two copies of *ftsA*, one copy of *ftsZ*, and one copy of *ftsZ-gfp*.

Construction of PAL1213

Strain PAL1213 contains a xylose inducible copy of GFP-MinC and MinD that is integrated at the *amyE* locus. The integrant was generated from plasmid pPL123, which was constructed by amplifying genomic DNA from *B. subtilis* 168 with primers GFP-MinC (5'-gatcgcggccgcaagaccaaaaagcagcaatatg-3') and GFP-MinD (5'-gatcggatcccacattaagatcttactccg-3') and ligating the resulting amplicon to pEA18 after digesting the vector and amplicon with NotI and BamHI. The resulting plasmid contains GFP fused to the N-terminus of *minC* followed by *minD*.

Quantification of MinC velocity

The rate of MinC movement was calculated by assuming that it travelled in a circle with a radius of approximately 0.45 μm, which equals half the measured width of FM 4-64 stained cells. The circumference of that circle was then divided by the

approximate time it took to travel completely around the circle, to give rates of 0.25–0.34 μm/min. The rate of MinC foci in TIRF experiments was calculated by summing the distances that the spot moved between each time point using the measure distance function. That distance was then divided by the total time it took the foci to travel that distance to give rates of 2-3 μm/min.

Quantification of the percent FtsZ in the ring in pads versus poly-lysine treated coverslips

Images were analyzed using softWoRx 3.3.6. Three z-sections including the medial focal plane and flanking optical sections 0.2 microns apart were merged from deconvolved images, summing the pixel intensities so that most of the Z-ring was included in the calculation. Pixel intensity data and areas were determined using the edit polygon function, by drawing polygons around the selected area in the merged image. Data was exported to Excel, where all calculations were performed (Table S2).

Quantification of the percent minicells produced adjacent to recently completed septa

To quantify the number of minicells that assemble from Z-rings that form at the old pole versus the new pole we performed timelapse microscopy of cells with FtsZ-GFP, because the *minCD* mutant partially uncouples FtsZ ring assembly from cell division. A Z-ring at the new pole was defined as a Z-ring that assembled adjacent

to the most recently completed septum in a cell. Most often these Z-rings formed shortly after division was complete when FtsZ could be seen moving away from the completed septum in the previous timepoints. However in the *minCD* mutant polar FtsZ rings could persist and be used for division even after another cell division had occurred in the cell because the time required for FtsZ ring assembly and the onset of septal biogenesis appeared variable. Such division events would appear to produce a minicell near an old cell pole, but the polar FtsZ ring assembled in the previous cell cycle. The timing defect in a *minCD* strain often caused multiple divisions to occur in rapid succession or even simultaneously in one cell. In this case a Z-ring at the new pole was defined as a Z-ring where FtsZ could be observed moving from one completed septum in the timepoints preceding the assembly of the polar Z-ring.

Supplemental Tables

Supplemental Table 1. Quantification of cell length and minicells in *minC-GFP* strains

	PY79 (LB)	EBS499 (LB) *minC4-GFP*	JAG189 (LB) P_{xyl}-*GFP-minC*	JAG189 (1/5 LB) P_{xyl}-*GFP-minC*
Cell length (μm) Excluding Mini-cells	3.6 ± 0.9	3.8 ± 0.9	7.8 ± 3.0	6.8 ± 2.2
% minicells	None detected n = 250	0.2 n = 480	30.2 n = 341	12.0 n = 313
Mini-cells and cell lengths were quantified after growth on 1.2% agarose pads with 0.5 μg/ml of FM 4-64 and the indicated medium for >60 minutes.				

Supplemental Table 2. Quantification of cell length and minicells in *minD* strains

	JAG114	JAG118	JAG120	JAG437	JAG439	JAG441
Cell length (μm), excluding minicells	5.1 ± 1.7	3.7 ± 1.1	4.2 ± 1.9	5.2 ± 2.2	5.2 ± 1.8	3.1 ± 1.1
%	13.9	4.3	7.2	14.8	8.4	8.2
minicells	n = 216	n = 141	n = 221	n = 115	n = 119	n = 170

Mini-cells and cell lengths were quantified after growth on 1.2% agarose pads with 0.5 μg/ml of FM 4-64 and 1/5 LB.

JAG114 = *minD4-gfp*; JAG118 = *minD4-gfp, P_{maf}-minCD*; JAG120 = *minD4-GFP, P_{minCD}-minCD*; JAG437 = *minD::kan*; JAG439 = *P_{minCD}-minCD, minCD;* JAG441 = *P_{maf}-minCD, minCD*

Supplemental Table 3. Quantification of FtsZ-GFP localization in cells imaged on agarose pads versus glass slides/poly-lysine treated cover slips.

A. Cells imaged on agarose pads

	Total CF[1]	Z-ring CF[A]	% FtsZ in Z-ring[B]	Cyto FtsZ[C]	Cyto Area (μm^2)	Ring Area (μm^2)	Cyto FtsZ/ μm^{2D}	$\frac{Ring/\mu m^2}{Cyto/\mu m^{2E}}$
1	2.18E+06	6.59E+05	30.21%	1.52E+06	5.13	0.42	2.97E+05	5.29
2	2.24E+06	8.38E+05	37.37%	1.40E+06	4.79	0.48	2.93E+05	5.95
3	1.83E+06	8.19E+05	44.89%	1.01E+06	4.60	0.48	2.19E+05	7.81
4	1.27E+06	4.03E+05	31.77%	8.66E+05	4.08	0.43	2.12E+05	4.42
5	2.79E+06	7.73E+05	27.67%	2.02E+06	5.82	0.48	3.47E+05	4.64
6	2.21E+06	8.28E+05	37.37%	1.39E+06	4.36	0.45	3.18E+05	5.78
7	2.46E+06	8.64E+05	35.15%	1.59E+06	5.70	0.52	2.80E+05	5.94
8	1.77E+06	4.88E+05	27.59%	1.28E+06	5.13	0.51	2.50E+05	3.83
9	1.26E+06	4.77E+05	37.82%	7.84E+05	4.54	0.59	1.73E+05	4.68
10	1.31E+06	5.12E+05	39.24%	7.93E+05	3.92	0.54	2.02E+05	4.69
11	2.29E+06	7.36E+05	32.20%	1.55E+06	5.66	0.48	2.74E+05	5.60
12	1.95E+06	4.97E+05	25.45%	1.45E+06	6.96	0.36	2.09E+05	6.60
13	8.13E+05	4.89E+05	60.09%	3.25E+05	2.18	0.43	1.49E+05	7.63
14	9.35E+05	4.99E+05	53.39%	4.36E+05	2.16	0.42	2.02E+05	5.89
15	1.94E+06	7.97E+05	41.07%	1.14E+06	4.93	0.48	2.32E+05	7.16
16	1.24E+06	4.06E+05	32.74%	8.35E+05	3.77	0.42	2.21E+05	4.37
17	1.38E+06	2.66E+05	19.23%	1.12E+06	5.50	0.30	2.03E+05	4.37
18	9.89E+05	3.30E+05	33.39%	6.59E+05	4.74	0.52	1.39E+05	4.57
19	1.56E+06	6.88E+05	44.03%	8.75E+05	5.45	0.68	1.61E+05	6.30
20	1.34E+06	6.13E+05	45.59%	7.31E+05	4.82	0.56	1.52E+05	7.21
21	1.71E+06	5.01E+05	29.26%	1.21E+06	6.30	0.54	1.92E+05	4.82
22	1.41E+06	4.88E+05	34.68%	9.19E+05	4.20	0.46	2.19E+05	4.85
23	1.70E+06	5.11E+05	30.10%	1.19E+06	6.65	0.48	1.78E+05	5.97
24	1.07E+06	4.43E+05	41.43%	6.26E+05	4.36	0.56	1.44E+05	5.51
25	2.26E+06	7.57E+05	33.56%	1.50E+06	4.93	0.43	3.04E+05	5.79
26	1.12E+06	4.87E+05	43.41%	6.35E+05	3.03	0.38	2.10E+05	6.12
27	1.31E+06	5.91E+05	44.95%	7.24E+05	2.42	0.47	2.99E+05	4.20
28	1.05E+06	4.86E+05	46.49%	5.60E+05	2.41	0.43	2.32E+05	4.87
29	1.40E+06	5.76E+05	41.12%	8.25E+05	5.02	0.43	1.64E+05	8.15
30	2.22E+06	8.23E+05	37.15%	1.39E+06	5.10	0.50	2.73E+05	6.03
31	1.87E+06	6.70E+05	35.87%	1.20E+06	4.58	0.43	2.62E+05	5.96
32	1.02E+06	4.26E+05	41.70%	5.95E+05	2.84	0.32	2.10E+05	6.35
AVG	1.62E+06	5.86E+05	37.37%	1.04E+06	4.57	0.47	2.26E+05	5.67
STDEV	5.16E+05	1.64E+05	8.31%	3.99E+05	1.24	0.08	5.58E+04	1.12

B. cells imaged on poly-lysine coverslips and slides

	Total CF[A]	Z-ring CF[A]	% FtsZ in Z-ring[B]	Cyto FtsZ[C]	Cyto Area (μm^2)	Ring Area (μm^2)	Cyto FtsZ/ μm^{2D}	$\frac{Ring/\mu m^2}{Cyto/\mu m^{2E}}$
1	1.48E+06	1.01E+05	6.83%	1.38E+06	5.91	0.3	2.34E+05	1.44
2	1.32E+06	1.39E+05	10.54%	1.18E+06	4.37	0.32	2.70E+05	1.61
3	1.69E+06	1.33E+05	7.87%	1.56E+06	6.82	0.36	2.29E+05	1.62
4	1.52E+06	1.58E+05	10.37%	1.36E+06	5.18	0.38	2.63E+05	1.58
5	1.86E+06	1.28E+05	6.92%	1.73E+06	6.12	0.27	2.82E+05	1.69
6	1.42E+06	1.29E+05	9.08%	1.29E+06	4.95	0.41	2.62E+05	1.21
7	1.67E+06	1.07E+05	6.41%	1.57E+06	7.1	0.35	2.21E+05	1.39

Supplemental Table 3. continued.

8	1.44E+06	9.44E+04	6.56%	1.35E+06	5.79	0.27	2.33E+05	1.50
9	1.34E+06	1.08E+05	8.04%	1.23E+06	5.47	0.25	2.25E+05	1.91
10	8.98E+05	8.24E+04	9.18%	8.15E+05	4.82	0.25	1.69E+05	1.95
11	1.26E+06	1.13E+05	9.00%	1.14E+06	6.39	0.32	1.79E+05	1.97
12	1.62E+06	1.27E+05	7.82%	1.49E+06	5.77	0.31	2.59E+05	1.58
13	1.07E+06	1.26E+05	11.76%	9.46E+05	4.85	0.33	1.95E+05	1.96
14	1.63E+06	1.50E+05	9.18%	1.48E+06	6.39	0.27	2.32E+05	2.39
15	1.57E+06	1.54E+05	9.82%	1.42E+06	6.15	0.3	2.30E+05	1.97
16	1.81E+06	1.12E+05	6.21%	1.69E+06	7.02	0.3	2.41E+05	1.86
17	1.20E+06	1.05E+05	8.69%	1.10E+06	5.64	0.3	1.95E+05	1.49
AVG	1.46E+06	1.22E+05	8.49%	1.34E+06	5.81	0.31	2.30E+05	1.71
STDEV	2.57E+05	2.14E+04	1.61%	2.49E+05	0.80	0.04	3.19E+04	0.29

[A]CF = corrected fluorescence. CF was calculated by subtracting the background fluorescence using the using the "edit polygon" function of Delta Vision software to define regions and calculate the total fluorescence and volume of the shapes defined. The average background (from a cell free region) was calculated in fluorescence/μm^2. The Total CF was calculated by summing the fluorescence in a cell, then subtracting the background fluorescence/μm^2 multiplied by the area of the cell. Example - Total CF = Total Fluorescence – [(Background/μm^2)x(cell area/μm^2)]. The corrected fluorescence of the FtsZ ring was similarly calculated from the region of the cell containing an FtsZ ring.

[B]Using CF for the cell and the Z-ring, the percentage of FtsZ in the Z-ring was calculated by (Z-ring CF)/(Total CF) x 100.

[C]Cytoplasmic FtsZ = (Total CF) – (Z-ring CF)

[D]The total cytoplasmic FtsZ will increase as the cells get longer, although the concentration of FtsZ should not change. We therefore calculated cytoplasmic FtsZ-GFP intensity per square micron – (Cytoplasmic FtsZ)/(Cytoplasmic area). Although not listed in the above table, the exact same calculation was made for the Z-ring.

[E]Using the calculations of pixel intensity per square micron described above, a ratio of the Z-ring intensity versus the cytoplasmic intensity was calculated – (Z-ring/area)/(Cyto/area). This calculation is not affected by cell length variability and gives a more accurate reflection of the amount of FtsZ in the Z-ring relative to the cytoplasm.

Supplemental Table 4. Quantification of MinC4-GFP localization to midcell in pre-divisional and dividing cells

	Predivisional cells (n = 242)	Dividing cells (n = 30)
MinC	12.4%	93.3%
No MinC	87.6%	6.7%

MinC4-GFP was visualized in growing cells on 1.2% agarose pads with 20% LB and 0.5 μg/ml of FM 4-64 at 30ºC. Dividing cells are those with an incomplete septum in which FM 4-64 staining does not fully traverse the cell. Predivisional cells showed no evidence of septal biogenesis.

Supplemental Table 5. Quantification of MinC4-GFP and EzrA-CFP colocalization to midcell

	Pre-divisional cells (n = 86)	Dividing cells (n=37)
EzrA only	87.2%	8.1
EzrA and MinC	12.8	91.9

MinC4-GFP and EzrA-CFP were visualized in growing cells on 1.2% agarose pads with 20% LB and 0.5 μg/ml of FM 4-64 at 30ºC, and scored for the presence or absence of MinC and EzrA. Dividing cells are those with an incomplete septum in which FM 4-64 staining does not fully traverse the cell.

Supplemental Table 6. Quantification of cell lengths and minicells in FtsZ-GFP fusions[A]

	JAG212 FtsZ-GFP	JAG252 FtsZ-GFP *minCD*	AD3007 FtsZ-GFP/Z+	JAG135 FtsZ-GFP/Z+, *minCD*	JAG431[B] FtsZ-GFP/Z+, P_{xyl}-*minCD*	JAG431 FtsZ-GFP/Z+, P_{xyl}-*minCD* 0.5% xyl
Cell length (μm) Excluding minicells	8.7 ± 3.5 n = 89	4.1 ± 1.1 n = 126	3.5 ± 1.6 n = 158	3.4 + 1.1 n = 127	NA[C]	NA
% minicells	ND[D] n = 120	9.4 n = 139	7.0 n = 187	45 n = 224	9.9 n = 384	2.6 n = 383
% minicells from Z-rings at new poles[E]	NA	73 n = 15	79 n = 15	83 n = 29	NA	NA

[A]Minicells and cell lengths were quantified after growth on 1.2% agarose pads with 20% LB and 0.5 μg/ml of FM 4-64 for >60 minutes.
[B]This strain expresses wild type *minCD* and also a second copy of *minCD* that can be overexpressed from the xylose promoter.
[C]NA = Not assessed
[D]ND = none detected
[E]Here defined as minicells that formed from FtsZ that assembled adjacent to a recently completed septum (in which FtsZ that was present in previous timepoints). These FtsZ rings sometimes assembled in the parent cell but persisted and were ultimately used for division in the daughter cell.

Supplemental Figures

Supplemental Figure 1. Localization of MinC4-GFP, MinC8-GFP and MinD4-GFP. (A) EBS499 (MinC4-GFP) was grown on CH plates and transferred to CH agarose pads at 30ºC. One minicell was found among several fields containing 480 cells (see Table S1). **(B)** JAG12 (MinC8-GFP) was grown on CH plates and transferred to CH agarose pads at 30ºC. **(C)** JAG118 (MinD4-GFP, *amyE::*P_{maf}*-minCD*) was grown on 10% LB 1.2% agarose pad at 30ºC without FM 4-64 to reduce background fluorescence and prevent aberrant GFP signal from FM 4-64 caused by overlapping excitation and emission spectra between GFP and FM 4-64. Scale bar, 5 μm.

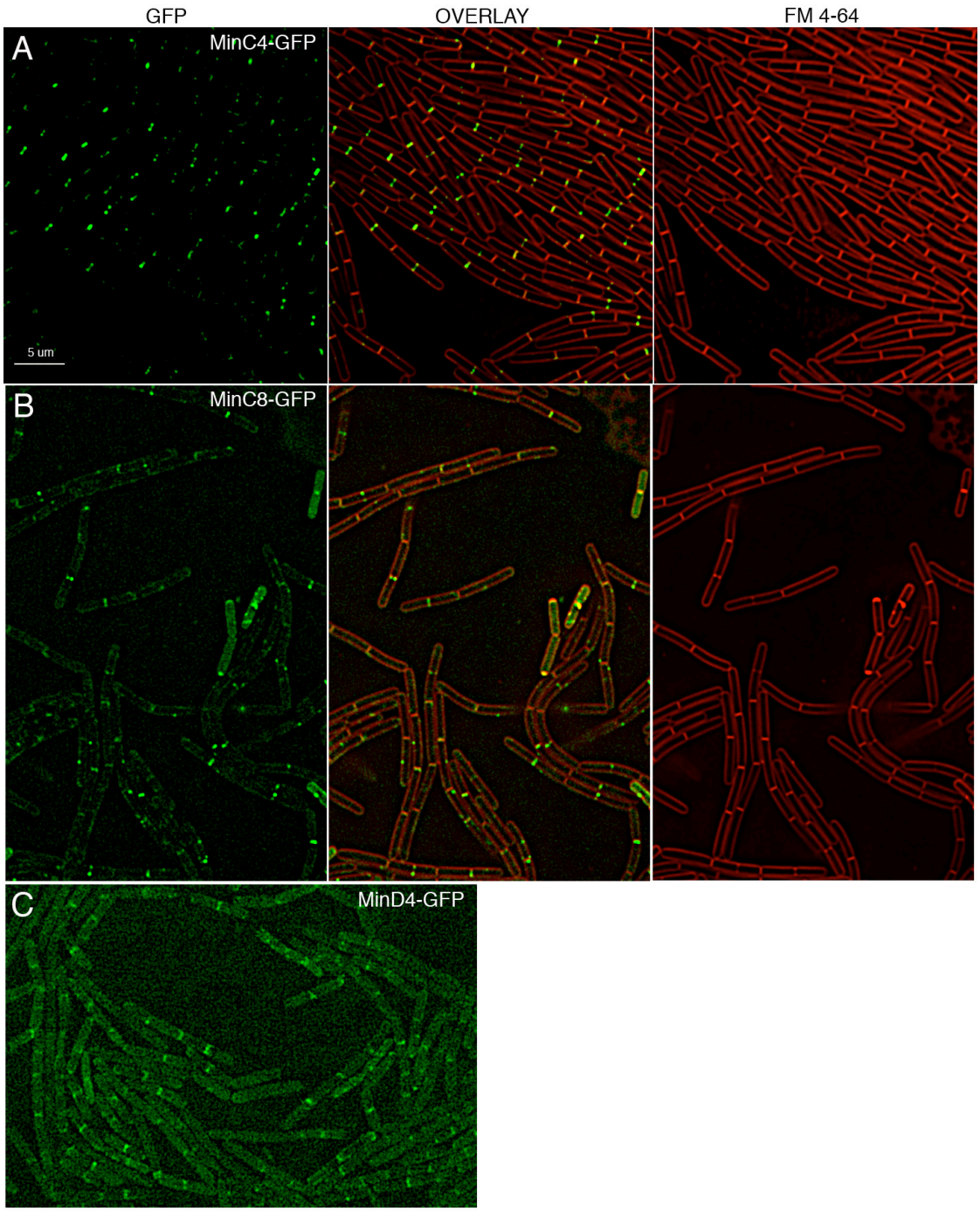
GFP
OVERLAY
FM 4-64
A
MinC4-GFP
5 um
B
MinC8-GFP
C
MinD4-GFP

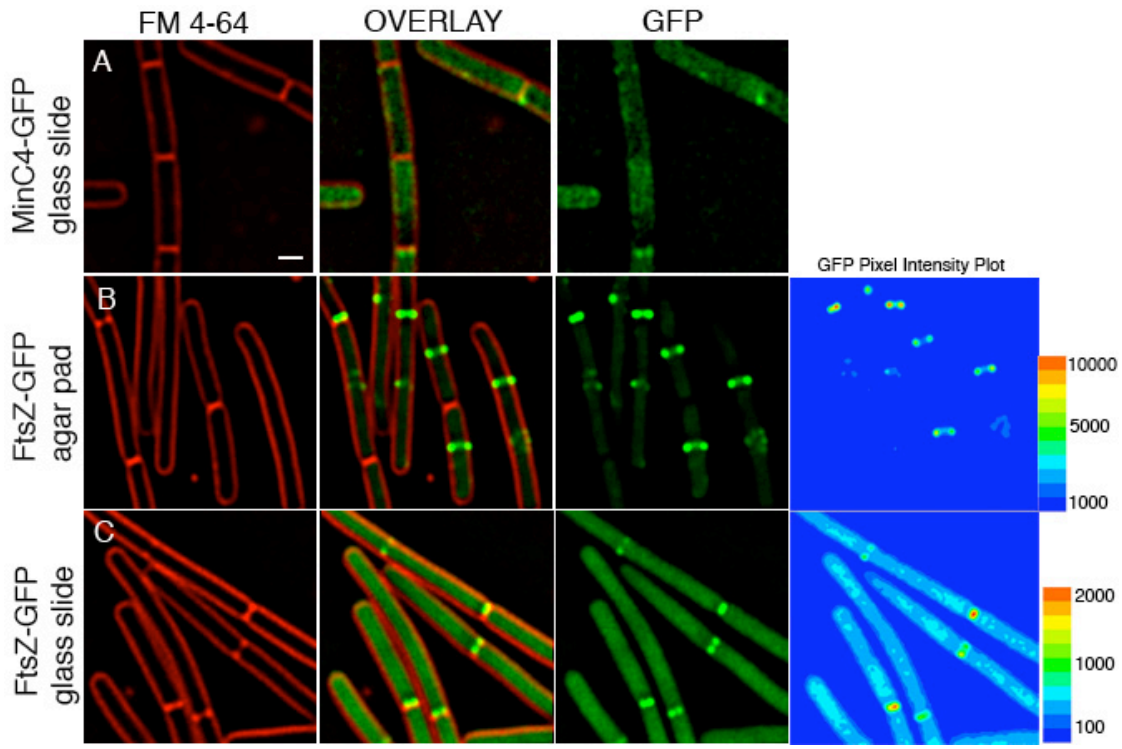

Supplemental Figure 2. MinC4-GFP and FtsZ-GFP are lost from midcell when imaged on a glass slide using a poly-lysine treated coverslip rather than on an agarose pad. (A) EBS499 (MinC4-GFP) imaged on a poly-lysine treated coverslip and slide, rather than on an agarose pad that supports growth. (B) JAG212 (FtsZ-GFP) was grown on LB plates and transferred to an LB agarose pad at 30ºC. Quantification revealed that 37±8% of FtsZ-GFP was present in the medial FtsZ ring (Table S2a). (C) JAG212 (FtsZ-GFP) was grown in liquid LB, concentrated 10 fold, and placed on a glass slide using a poly L-lysine treated coverslip. Quantification revealed that 8.5±1.6% of FtsZ-GFP was present in the medial ring (Table S2b). Scale bar, 1 μm.

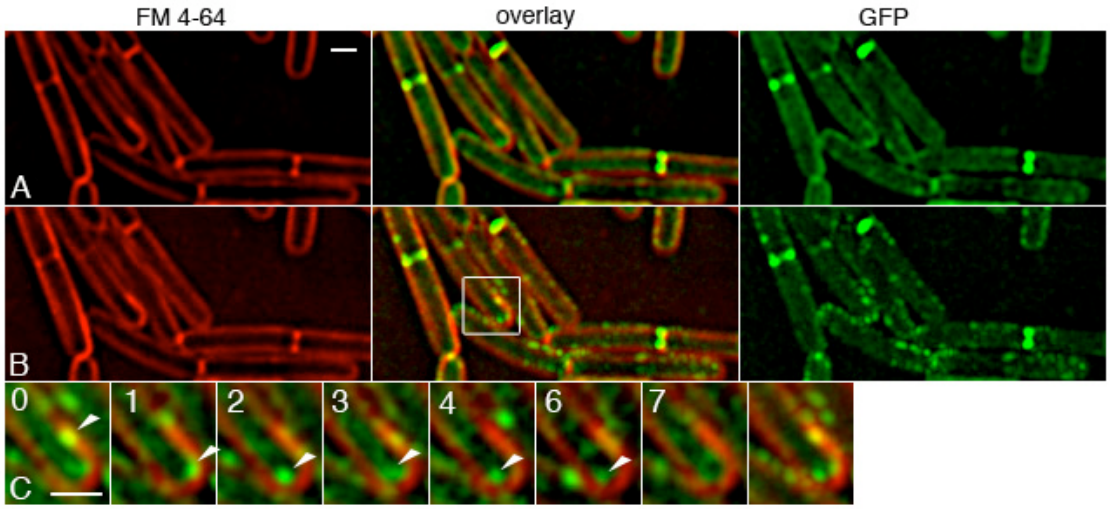

Supplemental Figure 3. Localization of MinC4-GFP using Total Internal Reflection Fluorescence (TIRF) Microscopy. EBS499 was applied to agarose pads and 0.3s TIRF images collected every 4s for a total of ~50s (see movies S2-3). Panels show two methods by which the images were collapsed. (A) Summation of the pixel intensities throughout the experiment, which highlights locations at which MinC spends the most time. (B) Maximum pixel intensity projection, which highlights transient Min foci. (C) Seven consecutive TIRF images ~4s apart that follow MinC4-GFP foci observed in the maximum intensity projection. In this example, one bright focus appears to move towards and then around the cell pole, although we cannot be absolutely certain that the same focus is observed in all of the images. Scale bars, 1 μm. See movies S2-3.

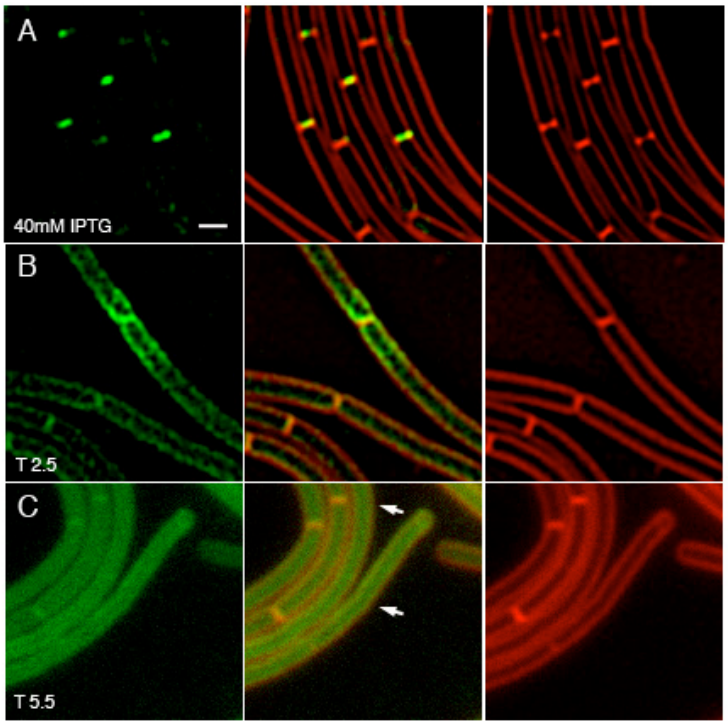

Supplemental Figure 4. MinC localizes to the poles at intermediate stages of FtsZ depletion. EBS483 (*P*$_{spac}$*ftsZ, minC4-gfp*) was grown overnight with 40 mM IPTG and then placed on 20% LB 1.2% agarose pads either (A) containing 40 mM IPTG or (B-C) lacking IPTG. Cells were grown at 30ºC for (B) 2.5 or (C) 5.5 hours. Scale bar, 1 μm.

Supplemental Movie Legends

Supplemental Movie 1. MinC4-GFP during the cell cycle. Epifluorescence images were acquired with 2-4 second exposures at 10 minute time intervals for a total of 90 minutes. Scale bar, 5 μm.

Supplemental Movies 2 and 3. TIRF movies of MinC4-GFP. TIRF images of GFP were acquired with 0.3 second exposures (35% laser power) every 4 seconds for a total of 50 seconds. A single FM 4-64 image was collected at the beginning of the experiment and overlaid with the GFP images for reference. Scale bar, 5 μm.

Supplemental Movie 4. Dynamic localization of MinC4-GFP to the poles during FtsZ depletion. Epifluorescence images were acquired every 15 seconds for a total time of 15 min. Scale bar, 5 μm.

Supplemental Movie 5. Epifluorescence movies showing MinC4-GFP apparently rotating around septa. Images were acquired every minute with 1-2 second exposures for a total of ~10 minutes. Scale bar, 5 μm.

Supplemental Movie 6. Epifluorescence movies showing MinC4-GFP apparently rotating around septa. Images were acquired every minute with 1-2 second exposures for a total of ~10 minutes. Scale bar, 5 μm.

Supplemental Movie 7. Epifluorescence movie of JAG212 (FtsZ-GFP). GFP and FM 4-64 images were acquired every minute for 90 min. Scale bar, 5 μm.

Supplemental Movie 8. Epifluorescence movie of JAG252 (*minCD*, FtsZ-GFP). GFP and FM 4-64 images were acquired every minute for 90 min. Scale bar, 5 μm.

Supplemental Movie 9. Epifluorescence movie of AD3007 (FtsZ-GFP/FtsZ+). GFP and FM 4-64 images were acquired every three minutes for approximately two hours. Scale bar, 5 μm.

Supplemental Movie 10. Epifluorescence movie of JAG135 (*minCD*, FtsZ-GFP/FtsZ+). GFP and FM 4-64 images were acquired every three minutes for approximately 2 hrs. Scale bar, 5 μm.

Supplemental Movie 11. Epifluorescence movie of MD642 (*minCD*). Sytox Green and FM 4-64 images were acquired every three minutes for approximately 100 minutes. Scale bar, 5 μm.

Chapter IV

In vivo analysis of FtsZ dynamics in growing *Bacillus subtilis* cells

Abstract

The tubulin-related protein FtsZ plays a critical role in bacterial cell division. FtsZ assembles into a ring-like structure at midcell known as the Z-ring, which serves as a scaffold that recruits proteins that are required for cell division into a complex known as the divisome and likely provides a constrictive force during cytokinesis. The movement of FtsZ to midcell and subsequent assembly into the Z-ring has been proposed to occur via an extended helical structure. We have examined the *in vivo* localization pattern of FtsZ-GFP in *Bacillus subtilis* using timelapse epifluorescence microscopy, total internal reflection microscopy (TIRFM), and three-dimensional structured illumination microscopy (3D-SIM) in growing cells. We show that FtsZ assembles into short protofilaments and that these protofilaments are highly dynamic. Furthermore, Z-ring assembly occurs via multiple FtsZ protofilaments that move to the midcell by an unknown mechanism that ultimately coalesce into a ring like structure.

Introduction

The tubulin-related protein FtsZ is conserved in nearly all bacteria and is essential for cell division. In the first step of cell division, FtsZ assembles into a ring like structure known as the Z-ring (Bi & Lutkenhaus, 1991) that serves as a scaffold for recruiting the 'early' and 'late' division proteins to the divisome. The divisome includes proteins that are involved in septal biogenesis, cytokinesis, and cell cycle regulation (reviewed by (Dajkovic & Lutkenhaus, 2006; Errington et al, 2003; Goehring & Beckwith, 2005)). Following the completion of cytokinesis, the divisome disassembles by an unknown mechanism so that it may reassemble at the future division site.

FtsZ monomers assemble in a head-to-tail fashion to form short polymers called protofilaments (Lowe & Amos, 1999; Lowe & Amos, 2000). Polymerization of FtsZ into protofilaments is dependent on GTP binding (Mukherjee & Lutkenhaus, 1994), which is mediated by the GTP binding pocket that is formed by the cleft between two FtsZ monomers within a protofilament (Lowe & Amos, 1999). Protofilaments further assemble into sheets and bundles under certain conditions *in vitro* (Kuchibhatla et al, 2009; Lowe & Amos, 2000; Yu & Margolin, 1997). It has been proposed that bundling and higher order assembly of FtsZ is mediated by lateral interactions between FtsZ protofilaments (Popp et al, 2009).

The cells ability to spatially and temporally regulate FtsZ polymerization is essential to proper division. This is accomplished in part by three systems that negatively regulate FtsZ assembly. The first prevents FtsZ from assembling over the

chromosome, in a process known as nucleoid occlusion that occurs in *Bacillus subtilis* (Wu & Errington, 2004) and *Escherichia coli* (Bernhardt & de Boer, 2005). Nucleoid occlusion depends on the NocA DNA-binding protein, which acts by a biochemically-undefined mechanism (Wu & Errington, 2004). The second is EzrA, which prevents the assembly of additional Z-rings in the cell (Levin et al, 1999); biochemical studies suggest that EzrA inhibits FtsZ polymerization (Chung et al, 2007; Haeusser et al, 2004; Singh et al, 2007). The third system involves the widely conserved MinCD proteins, which spatially regulate cell division in a variety of organisms (Lutkenhaus, 2007; Mazouni et al, 2004; Ramirez-Arcos et al, 2001; Rothfield et al, 2005; Szeto et al, 2001), and whose absence produces anucleate minicells. Recent biochemical data indicate that MinC inhibits the lateral interactions between FtsZ-protofilaments in *E. coli* (Dajkovic et al, 2008) and *B. subtilis* (Scheffers, 2008), which might destabilize Z-rings or compromise interactions between the Z-ring and the late division proteins. Consistent with this latter hypothesis is my observation that *B. subtilis* MinC prevents transient FtsZ rings that assemble near the new cell poles from persisting and maturing into active divisomes (Chapter 3, (Gregory et al, 2008)).

Several proteins have been identified as positive regulators of FtsZ assembly that act by tethering FtsZ to the membrane or by promoting FtsZ bundling. FtsZ is a soluble protein and therefore requires the accessory proteins FtsA and ZipA, which interacts directly with FtsZ to anchor it to the membrane and are essential for divisome assembly in *E. coli* (Liu et al, 1999; Pichoff & Lutkenhaus, 2002; Pichoff & Lutkenhaus, 2005). *B. subtilis* FtsZ appears to be anchored to the membrane through

the overlapping function of FtsA, YlmF, ZapA, and EzrA, although only the absence of FtsA decreases the efficiency of Z-ring assembly (Beall & Lutkenhaus, 1992; Gueiros-Filho & Losick, 2002; Ishikawa et al, 2006; Jensen et al, 2005), suggesting that it performs a more critical role in FtsZ assembly. *E. coli* ZipA, ZapA, and YgfE and *B. subtilis* SepF and ZapA promote bundling of FtsZ protofilaments *in vitro* (Gueiros-Filho & Losick, 2002; Hale et al, 2000; Singh et al, 2008; Small et al, 2007). The exact mechanism for FtsZ bundling is unclear, but it appears that these proteins directly bind to FtsZ to either stabilize or act as crosslinking agent between FtsZ protofilaments.

The combined action of the FtsZ-regulating proteins produces a net movement of FtsZ from completed septa to the nascent division site and allows recruitment of the late division proteins to the Z-ring at midcell. The mechanism for the movement of FtsZ is largely unknown. One possible mechanism is via a helical FtsZ intermediate that has been proposed to extend out from the completed septum to the new division site at midcell. Helical structures have been observed using fluorescence microscopy techniques in vegetative cells (Peters et al, 2007; Shih et al, 2003) as well as those undergoing the initial stage of sporulation in which polar Z-rings are assembled (Ben-Yehuda & Losick, 2002). It remains unclear how these helical structures form and move throughout the cell. FtsZ could also move by the treadmilling of short protofilaments, a process by which a polymer moves by addition of subunits to one end of the polymer and loss of subunits from the other. This mechanism has recently been demonstrated for the bacterial tubulin TubZ, which is involved in plasmid

segregation (Larsen et al, 2007). Given the limited resolution of fluorescence microscopy, it is possible that the extended spirals previously reported do not represent a contiguous extended FtsZ spiral, but rather a collection of protofilaments anchored to the cell envelope.

The limited resolution of fluorescence microscopy has also been a barrier to determining the ultrastructure of the Z-ring, which could provide insight into the mechanism of constriction. The Z-ring appears to be a contiguous structure when visualized by fluorescence microscopy, suggesting that constriction could be mediated by a eukaryotic-like sliding filament model, but a protein that is analogous to the motor protein responsible for the movement of the filaments has yet to be indentified. Alternatively, the depolymerization of FtsZ protofilaments could provide the constrictive force (Waterman-Storer et al, 1995). Recently, cryoelectron tomography of Z-rings in *Caulobacter crescentus* suggests that the Z-ring may be a collection of short separate FtsZ protofilaments rather than a contiguous structure (Li et al, 2007). This model proposes that each protofilament provides a constrictive force that is generated by a conformational switch between straight and bent protofilaments that results in the iterative pinching of the membrane (Ghosh & Sain, 2008). All of these mechanisms rely on FtsZ protofilaments being anchored to the cell membrane, which would allow a sliding, depolymerizing, or bending protofilament to pull the membrane.

Here we present a detailed study of FtsZ-GFP dynamics and ultrastructure in living *B. subtilis* cells using timelapse epifluorescence microscopy, total internal

reflection microscopy (TIRFM), and structured light microscopy (SIM). These methods allowed us to visualize a variety of novel FtsZ structures, including ~300 nm protofilaments that move along the cell membrane in TIRFM, and partially assembled FtsZ rings that SIM suggests to be discontinuous and often branched. Our data suggest that FtsZ moves throughout the cell as protofilaments that coalesce at midcell.

Results

Timelapse microscopy of FtsZ-GFP

We used timelapse epifluorescence microscopy to investigate FtsZ dynamics during the cell cycle in strain AD3007 (Gregory et al, 2008), which contains a wild type copy of *ftsZ* in addition to *ftsZ-gfp*. We first performed timelapse experiments to observe FtsZ movement during the entire cell cycle. Under the conditions used in our timelapse experiments the doubling time was approximately 60 to 70 minutes (see Materials and Methods). In these experiments, FtsZ forms a stable ring that persists during much of the cell cycle, followed by cytokinesis, and finally relocalization to the nascent division site (Fig. 1). In some cells a transient ring-like structure assembled adjacent to the recently completed septum before ultimately relocalizing to the nascent division site (Fig 1; arrowhead). We also observed FtsZ foci (Fig. 1; asterisks) outside of the Z-ring that appeared to localize to the cell membrane. The signal for these foci was dim compared to the Z-ring, which made interpretation of the foci difficult. Unfortunately, increasing the exposure time in these experiments results in arrest of cell growth, presumably due to phototoxicity.

We decided to perform shorter timelapse experiments with increased temporal resolution and exposure times to better observe the FtsZ foci outside of the Z-ring. Previous studies suggest that FtsZ relocalizes from the completed septum to the nascent division site via an extended helical structure (Ben-Yehuda & Losick, 2002; Shih et al, 2003). To determine if the FtsZ foci we observed are part of these helical

structures, we examined cells in which FtsZ was moving from a completed septum to a stable Z-ring in newborn daughter cells (Z-ring transition). These shorter timelapse experiments revealed FtsZ foci that are associated with the cell membrane, which often change position with time. Figure 2A shows three newborn cells without a medial Z-ring shortly after constriction. In these cells, we observed multiple dynamic membrane associated foci. Overlaying the GFP images from all three timepoints illustrates the amount of movement that occurred over a one minute interval (Fig 2A; time overlay). Figure 2B shows two newborn cells with slightly different FtsZ localization. The cell on the left appears to have several dynamic FtsZ foci whereas the cell on the right formed a ring like structure near the new cell pole (arrowhead) and the midcell. The polar Z-ring persisted for a few minutes, but ultimately disassembled leaving a single medial Z-ring. The dynamic nature of FtsZ in these timelapse experiments is inconsistent with previous reports of an extended helical FtsZ structure. To further investigate this discrepancy we reconstructed three-dimensional images of cells without a medial Z-ring.

3D reconstruction of FtsZ-GFP using structured illumination microscopy

Conventional fluorescence microscopy cannot differentiate between foci that are independent of one another and a continuous helix wherein each of the foci are part of a connected filament. This is due to limited spatial resolution, which will make discontinuous structures appear continuous, and a relative overemphasis of polymers that are perpendicular to the imaging plane rather than those on the cell surface. The

latter is evident when a Z-ring appears as two opposing foci at midcell connected by a much fainter horizontal ring. We were therefore unsure whether the FtsZ foci we observed during Z-ring transitions using timelapse microscopy were due to rapidly moving foci or protofilaments or to an inherently dynamic or unstable helical structure.

We collected stacks of optical sections of growing *B. subtilis* cells containing FtsZ-GFP using the Applied Precision OMX™ microscope to determine if the foci we observed are part of a helical structure or are independent filaments (Fig 3). The OMX™ microscope achieves a ~100nm spatial resolution, or two-fold better resolution than that of conventional light microscopes, by using 3D-structured illumination (SI) microscopy (see materials and methods). Using 3D-SI microscopy we expected to detect extended helical FtsZ structures in cells undergoing Z-ring transition as well as potential discontinuities in the Z-ring itself.

We first performed a 3D-reconstruction of a cell that contained a medial Z-ring and rotated it 180 degrees around the Y-axis (Fig. 3A). The Z-ring appears to be completely assembled and of nearly uniform intensity. Then we reconstructed a cell that was undergoing a Z-ring transition (Fig. 3B). This cell contains FtsZ near the completed septum and also at the nascent division site suggesting that FtsZ is relocalizing to midcell and should contain an extended helical structure. Instead there were several protofilaments emanating from the completed septum and two resolvable polymers (Fig. 3B; arrowheads) at the midcell that can be seen by rotating the midcell about the Y-axis and the X-axis. These two putative protofilaments at midcell

appeared to be ~0.5 um and 1 um in length and did not appear to be connected to one another. Clearly cells can contain several FtsZ polymers of variable length that are not necessarily connected into a contiguous helix.

We also observed a cell that contained four resolvable FtsZ protofilaments of between 200-500 nm in length on one side of the cell (Fig. 3C; arrowheads). From these data we conclude that FtsZ does not move from the completed septum to midcell via an extended helical structure, but rather by the movement of short protofilaments of FtsZ. We postulated that the previously observed helical structures were the result FtsZ protofilaments that were moving in a helical pattern due to the constraints of movement that are imposed by membrane anchored polymer moving within a cylindrical cell. To further examine the FtsZ microdynamics with greater temporal resolution we used TIRFM (Total Internal Reflection Fluorescence Microscopy). We define microdynamics as the movement of FtsZ before and after Z-ring assembly to distinguish it from the dynamics of the Z-ring demonstrated by FRAP experiments.

Movement of FtsZ protofilaments by TIRFM

We used Total Internal Reflection Microscopy (TIRFM) in an attempt to visualize minor populations of FtsZ moving along the membrane. TIRFM has an increased signal to noise ratio compared to epifluorescence thus allowing for increased temporal resolution and the ability to detect smaller numbers of molecules. Furthermore, TIRFM has a limited excitation depth making it well suited for

observing the top of the cell that is closest to the cover slip rather than a medial focal plane that is generally seen with epifluorescence microscopy (Axelrod, 2001; Axelrod, 2003). Together, these two features make TIRFM ideal for visualizing dynamic protofilaments that move across the cell, perhaps in a helical pattern. Alternatively, if the FtsZ-GFP foci we observed are part of an extended helix, then the arcs of the helix should be clearly evident in the TIRFM images.

We first performed a direct comparison between epifluorescence and TIRF in the same cells (Fig. 4A-B). In cells that contained a medial Z-ring, we observed two adjacent foci using epifluorescence and a solid band using TIRFM, indicating that TIRFM was visualizing of the top of the Z-ring. Several cells also showed dynamic foci and arcs away from the ring that could only be visualized with TIRFM. To visualize the movement of FtsZ in these experiments we overlaid three separate timepoints using green (0 seconds), blue (20 seconds), and red (40 seconds). The white indicates stable FtsZ localization during the timecourse whereas individual colors correspond to transient FtsZ. These data suggest that FtsZ assembles foci in the cells that are highly dynamic. These foci might represent protofilaments, which are 120-240 nm in length and would therefore appear as diffraction limited spots.

Figure 4C is the first image of timelapse using TIRFM overlaid with the medial focal plane showing the cell membranes imaged with deconvolution fluorescence microscopy. The cell indicated by an arrowhead appears to be assembling an FtsZ ring midcell. As shown in the timelapse series in Fig. 4D, in this cell FtsZ-GFP foci moved rapidly about the cell, occasionally traversing the short axis

of the cell. The FtsZ at midcell appears to go back and forth from one or more foci to an arc over a two minute interval. This suggests that at early stages in Z-ring assembly, a dynamic population of FtsZ protofilaments move around midcell.

Timelapse of Z-ring assembly and disassembly

The movement of FtsZ during Z-ring transition suggests that the Z-ring is not formed from bidirectional polymerization at midcell, nor is it assembled from an extended helical structure. We hypothesized that Z-rings might form from dynamic FtsZ protofilaments that coalesce at midcell. To test this hypothesis we observed Z-ring formation in growing cells using timelapse microscopy. In figure 5A, FtsZ in the cell on the right (arrow) starts as a single foci and then appears as multiple foci or arcs that move about the midcell in subsequent timepoints. This series of events is typical of cells that are assembling a Z-ring although the amount of time required to assemble a Z-ring appears to be quite variable. The cell on the left (Fig. 5A; asterisks) undergoes a similar pattern of FtsZ localization, but fails to assemble a ring in during the course of the timelapse experiment. From these data, in conjunction with the movement seen by TIRFM, we conclude that there are multiple dynamic FtsZ protofilaments at midcell immediately prior to Z-ring assembly.

FtsZ protofilaments also appear in the later stages of cytokinesis. The Z-ring constricts to a single focus at the end of cell division and at some later stage FtsZ foci and arcs begin to appear on the membrane (Fig 5B; arrowheads). These foci persist

and begin to move away from the completed septa following cytokinesis. These data suggest that the protofilaments in the FtsZ ring fall apart at some late stage of cytokinesis or that polymerization of FtsZ protofilaments occurs simultaneously with Z-ring constriction.

Discussion

The first observable step in bacterial cell division is the formation of the Z-ring at midcell. The Z-ring serves as a scaffold for the recruitment of additional proteins that are required for division. Several papers have proposed that the Z-ring assembles via an extended helical structure that emanates from the old division to the nascent division site (or possibly the length of the cell) after the completion of cytokinesis (Ben-Yehuda & Losick, 2002; Peters et al, 2007; Thanedar & Margolin, 2004). We here analyzed the movement of FtsZ in growing cells using timelapse epifluorescence microscopy, TIRFM, and structured illumination microscopy (SIM). We found that FtsZ foci rapidly move about the cell membrane, eventually accumulating at midcell, and finally coalescing into a ring at the nascent division site. Importantly, we did not observe any helical structures that extended from the old division site to the new division site, indicating that they are either highly unstable or do not assemble.

Timelapse microscopy of FtsZ-GFP in growing cells revealed highly dynamic foci that are associated with the cell membrane in cells that lack a medial Z-ring. At any given timepoint, many of these foci are often offset to suggest the presence of a helical structure. The dynamic nature of these foci, however, is inconsistent with an extended helix and more indicative of individual FtsZ protofilaments. Dynamic foci could be the result of a dynamic helix, but this seems unlikely given that the number of foci on each side is highly variable and changes rapidly.

We postulate that the foci we sometimes observed using epifluorescence correspond to highly dynamic foci we observed using TIRFM. There is no apparent

path that FtsZ follows, but we suspect that movement along the long axis of the cell is accomplished by moving in a helical pattern. This is likely the reason that previous studies have observed extended helical structures. FtsZ polymerization does not require accessory proteins *in vitro* therefore it is likely that the movement is independent of other cytoskeletal proteins, but we cannot rule out the possibility that they are moving along another cytoskeletal protein such as MreB or Mbl (Carballido-Lopez & Formstone, 2007).

Visualizing FtsZ-GFP using structured illumination revealed individual FtsZ protofilaments rather than an extended helical structure in cells that are in the process of assembling a central FtsZ ring. These protofilaments appear to be no longer than one half of the cell circumference. This suggests that FtsZ protofilaments are too unstable to form longer helices and that they might move by treadmilling. If FtsZ does move by a treadmilling mechanism then the length of FtsZ protofilaments would be governed by the rate of polymerization and depolymerization at the plus and minus end respectively. The FtsZ protofilaments we observed were always associated with the cell membrane. FtsA and possibly ZapA, EzrA, and YlmF are responsible for anchoring FtsZ to the membrane. Since these proteins are not required for polymerization *in vitro*, it is likely that they raise the local concentration of FtsZ at the membrane to reach the critical concentration necessary for polymerization. FtsZ protofilaments often emanated from division sites that had either completed cytokinesis or were nearly completed. It is unclear whether these protofilaments were

already assembled as part of the Z-ring or if they are newly polymerized protofilaments.

Timelapse epifluorescence and SI microscopy suggest that there are multiple FtsZ protofilaments at midcell prior to the assembly of the Z-ring. These protofilaments then assemble into a Z-ring, possibly through bundling interactions that are mediated by ZapA and the lateral interactions between protofilaments. This view of the FtsZ ring as a collection of protofilaments is consistent with recent cryoelectron tomography visualization of the FtsZ ring in *C. crescentus*, which demonstrates that the Z-ring is a collection of short individual protofilaments.

These studies suggest a novel assembly pathway for Z-rings whereby individual FtsZ protofilaments move to the midcell, possibly by treadmilling, and then coalesce into a nearly uniform ring at midcell. The number of protofilaments in the Z-ring is unknown. There is likely an equilibrium between FtsZ protofilaments and FtsZ monomers that is determined by the critical concentration for FtsZ assembly *in vivo*. Our results also suggest that the Z-ring is a collection of FtsZ protofilaments that are bundled together, however, the organization of these bundles is unclear. Several different structures, including sheets and bundles (Erickson et al, 1996; Lowe & Amos, 1999), have been observed in vitro, but the biological relevant structure has yet to be determined.

Finally, how is the movement of FtsZ regulated to ensure that sufficient FtsZ protofilaments are present at midcell to assemble the Z-ring? It is possible that nucleation of FtsZ protofilaments is favored at midcell, but we prefer the hypothesis

that the movement of FtsZ protofilaments is random, but that they prevented from moving away from midcell by the nucleoid after sufficient chromosome segregation. Further studies are required to identify the mechanisms by which FtsZ protofilaments moved to the midcell.

Materials and Methods

Strains and reagents

Strains are derived from PY79 (Youngman et al, 1984). Strain AD3007 and JAG212 are described in (Gregory et al, 2008).

Timelapse microscopy

Timelapse microscopy used 1.2% agarose pads (Becker & Pogliano, 2007) prepared as follows. FM 4-64 (Molecular Probes) was added to a final concentration of 0.5 μg/ml in a 1.2% solution of molten agar/media (LB diluted 1:5 in water) and added to the well of a culture slide and covered with a glass slide. After cooling, the slide was removed and two air pockets were cut out of the agar leaving a 3 to 5 mm agar bridge in the center of the well. Cells were grown overnight on the appropriate solid media at 30ºC and applied to the agar bridge and covered by a glass cover slip. To prevent drying during the experiment, 50% glycerol was applied to the region of contact between the slide and the coverslip. The slide was then allowed to equilibrate in an environmentally controlled chamber at 30ºC (Precision Control Weather Station) for at least 30 minutes prior to visualization. Exposure times were minimized to reduce phototoxicity. Images were acquired using an Applied Precision Spectris microscope and deconvolved using softWoRx v3.3.6 software (Applied Precision). Figures were assembled with Photoshop v7.0 software (Adobe).

Total Internal Reflection Fluorescence Microscopy

TIRF experiments were performed using the same microscope and a 488 nm argon laser installed in a TIRF module supplied by Applied Precision and a 100X 1.65 NA objective, sapphire coverslips (Olympus), and 1.78 refractive index oil (Cargille Labs). GFP was visualized with using FITC excitation and emission filters and 0.3 second pulses at 35% power. FM 4-64 was imaged using conventional epifluorescence microscopy as in timelapse microscopy. Cells were prepared in an identical manner to timelapse microscopy.

Structured Illumination Microscopy

Cells were prepared as in timelapse microscopy and imaged with the Deltavision OMX microscope (Applied Precision, Issaquah, WA). The OMX microscope achieves 100 nm resolution by applying three-dimensional structured illumination technology (3D-SIM; (Schermelleh et al, 2008)). The OMX also provides increased spatial resolution by using faster and more sensitive cameras as well as true multicolor simultaneous imaging. The cameras were constructed by applied precision and use monochrome 20Mhz camera with Sony ICX285 ER progressive scan CCD. Excitation was achieved using monochromatic lasers with standard filter sets.

Figures

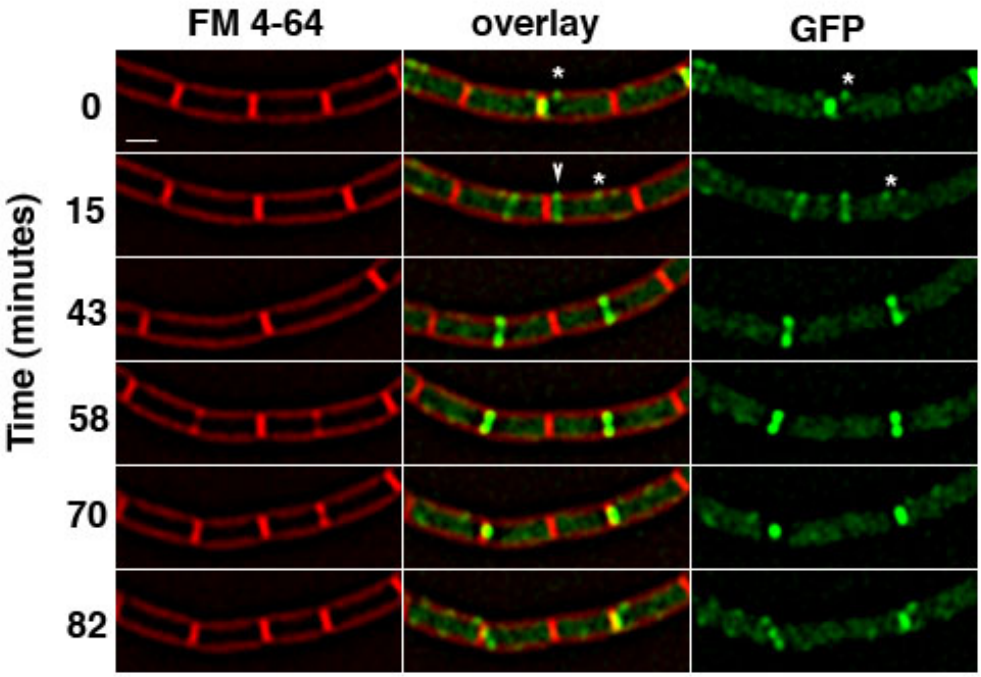

Figure 1. Timelapse microscopy showing the relocalization of FtsZ-GFP from completed septa to a nascent division site followed by cytokinesis. Images of FtsZ-GFP (green) and FM 4-64 (red) were collected every minute for several division events. FtsZ can be seen as a focus at midcell as well as smaller membrane associated foci (asterisks). FtsZ leaves the completed septum and assembles into a polar Z-ring (arrowhead), which ultimately disassembles. FtsZ relocalizes to midcell and ultimately constricts into a foci. Scale bar 1 μm.

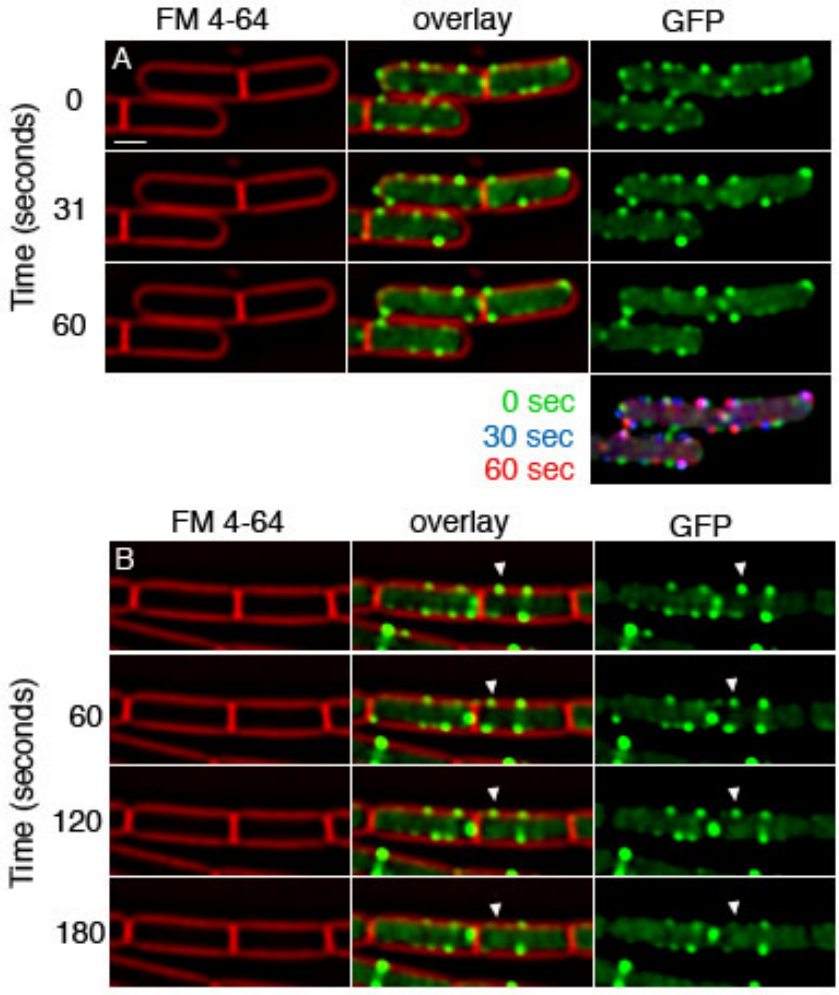

Figure 2. Movement of FtsZ-GFP foci visualized by epifluorescence microscopy. To observe the changes in FtsZ localization over a shorter timescale, we utilized timelapse microscopy with increased temporal resolution and increased excitation. Images of FtsZ-GFP (green) and FM 4-64 (red) were acquired every 30 seconds. (A) Multiple foci of FtsZ are observed at different subcellular locations in each timepoint. Images from the 0 (green) and 30 (blue) and 60 (red) second timepoints were overlaid to emphasize the movement of foci between timepoints. (B) FtsZ assembles into a transient polar Z-ring in the cell on the right (arrowhead). Several FtsZ foci are observed in the left cell that appear to change location in each timepoint. Scale bar 1 μm.

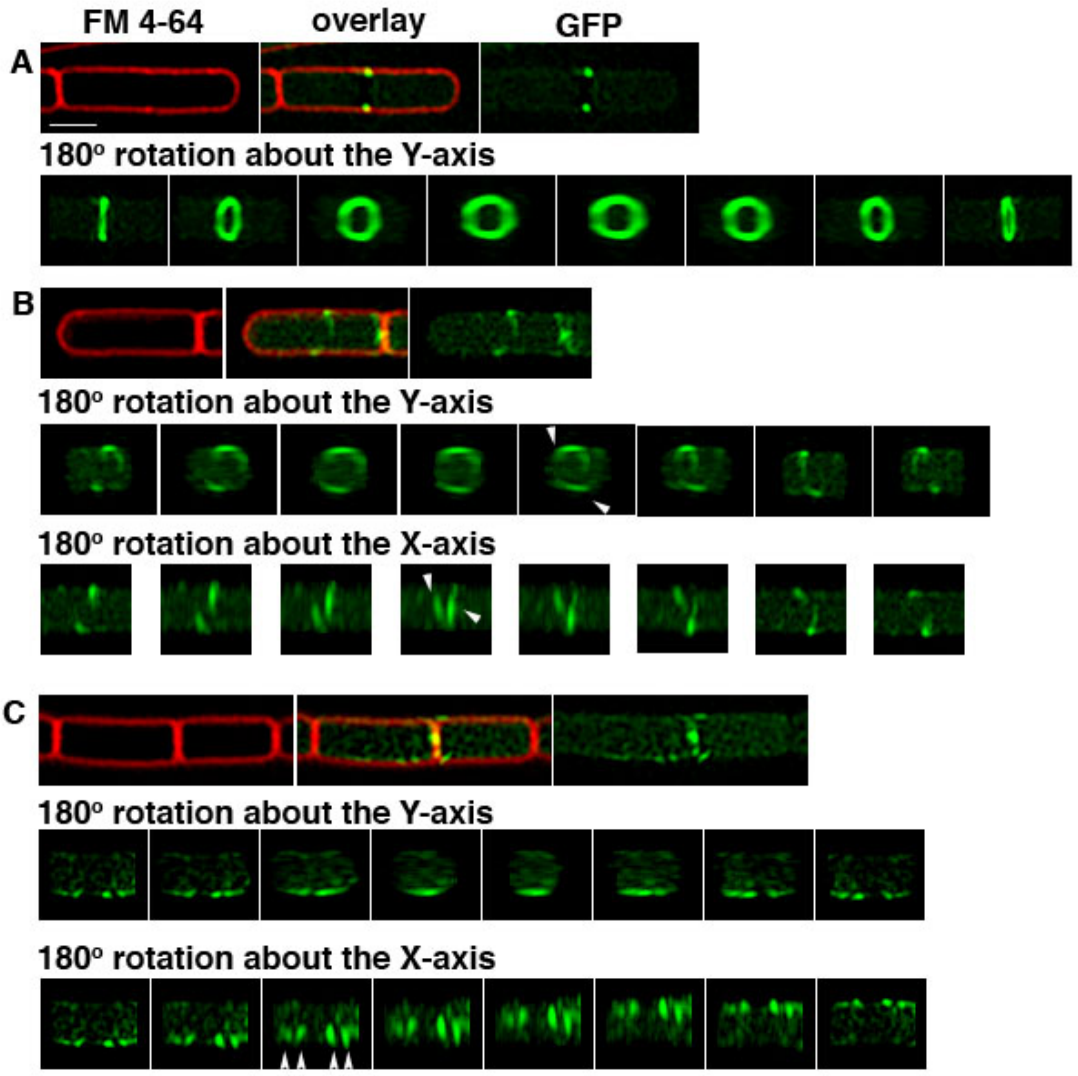

Figure 3. Three-dimensional reconstruction of FtsZ-GFP in growing cells using SIM (Structured Illumination Microscopy). Images of FtsZ-GFP (green) and FM 4-64 (red) were acquired using the OMX™ microscope. Panels show the rotation of the 3D image in space. (A) Reconstruction of a Z-ring at midcell. The ring was rotated 180° about the Y-axis to show the entire Z-ring. (B) Reconstruction of FtsZ-GFP undergoing a transition from the completed septum to the nascent division site. Rotating the GFP image from the midcell 180° about the X and Y-axis revealed two resolvable FtsZ protofilaments. (C) FtsZ-GFP during the final stages of cytokinesis reveals membrane associated FtsZ-GFP foci. Rotating the GFP image 180° about the X- and Y-axis reveals four resolvable FtsZ protofilaments on one side of the cell.

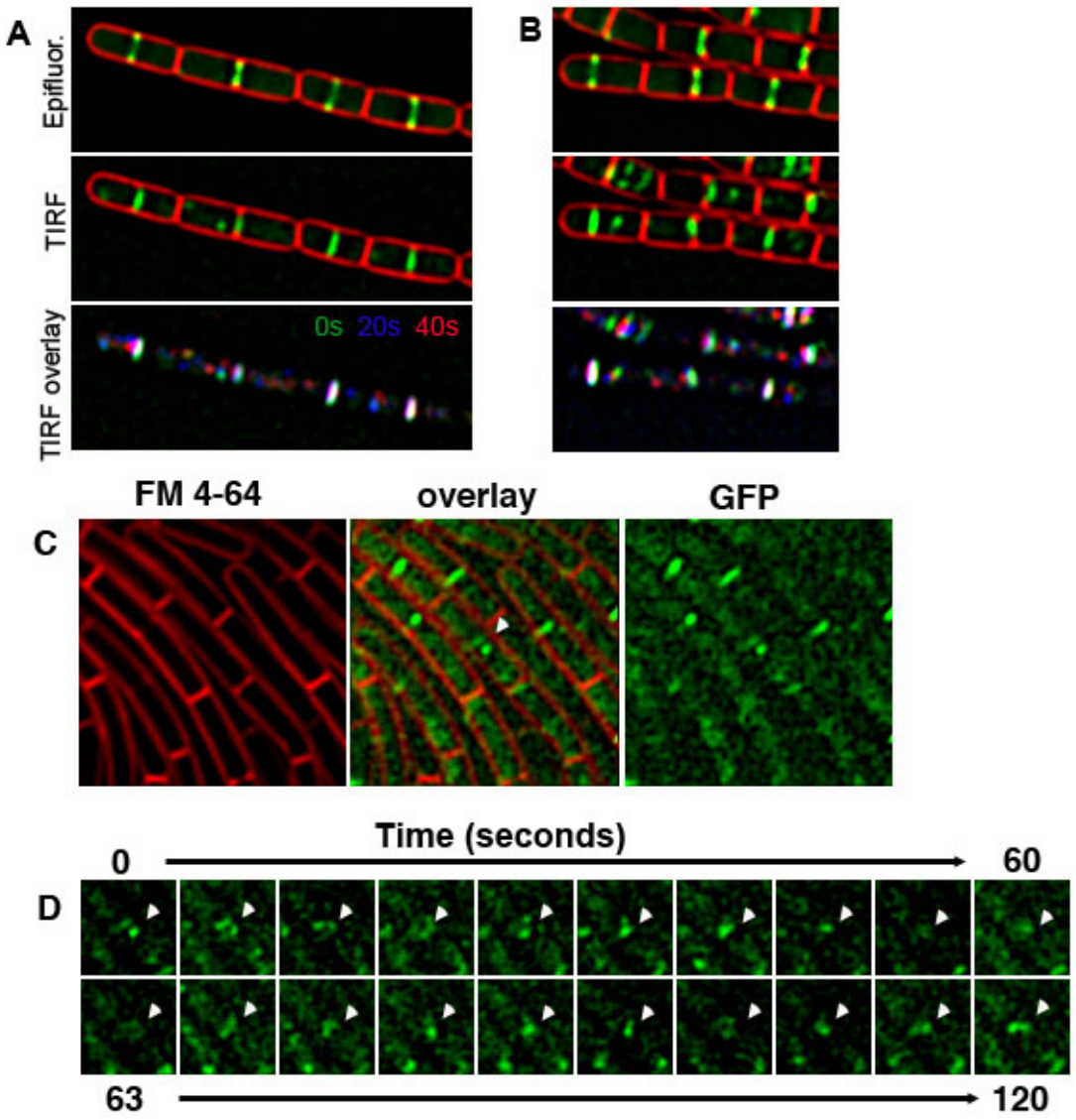

Figure 4. Comparison of the localization of FtsZ-GFP using Total Internal Reflection Fluorescence (TIRF) microscopy and epifluorescence microscopy and timelapse using TIRF microscopy. (A) and (B) are mages of FtsZ-GFP (green) and FM 4-64 (red) were acquired in identical cells for direct comparison. Epifluorescence shows two adjacent dots indicating a ring whereas TIRF reveals the top of the Z-ring. The 0 (green), 20 (blue), and 40 (red) second timepoints from the timelapse using TIRF were overlaid to emphasize the movement of FtsZ foci. (C) The first timepoint of a timelapse showing FtsZ-GFP (green) imaged by TIRF and FM 4-64 (red) imaged by epifluorescence. The panels below (D) are evenly spaced timepoints (approximately 6 seconds apart) of the area indicated by the arrowhead in (C) of FtsZ-GFP imaged by TIRFM.

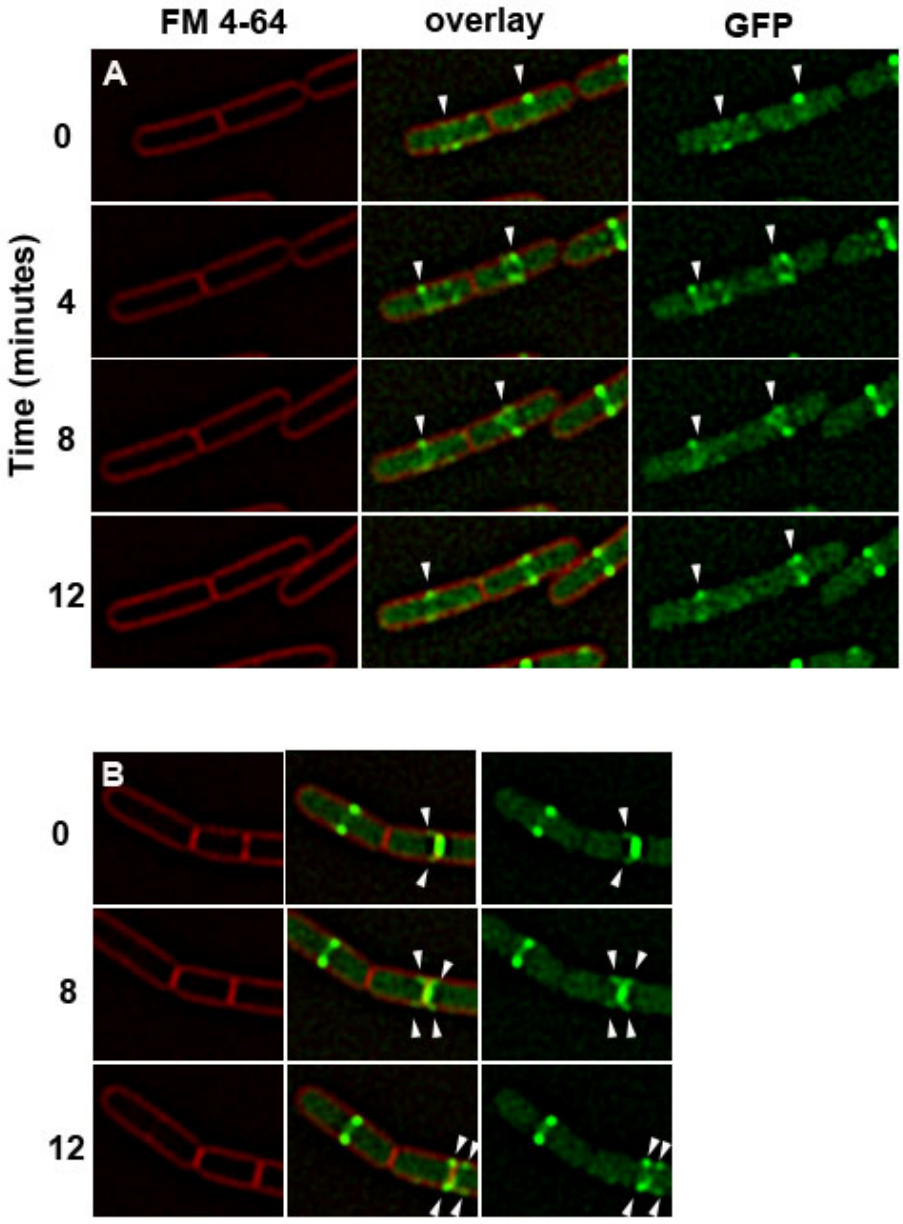

Figure 5. FtsZ foci emanate from the completed septum in the later stages of cytokinesis and are visible at midcell prior to Z-ring formation. Images of FtsZ-GFP (green) and FM 4-64 (red) were acquired every minute under timelapse conditions. (A) FtsZ-GFP foci (arrowheads) can be seen at midcell prior to the assembly of a complete Z-ring. (B) FtsZ-GFP can been seen as faint lines that emanate from the constricting Z-ring (arrowheads) and form membrane associated foci after cytokinesis is complete.

Chapter V

Conclusions and perspectives

My studies on MinC and FtsZ have led to a new model for MinCD function in *B. subtilis*. Previous models of division site selection proposed that DivIVA anchored MinCD to the cell poles where it inhibited FtsZ polymerization. I found that MinC is highly dynamic and predominantly localizes to active division sites. Following cytokinesis, MinC is released from the division site where it acts to destabilize Z-rings that immediately reassemble adjacent to the new cell pole. Timelapse microscopy of FtsZ-GFP suggests that these polar Z-rings and midcell Z-rings are assembled from short FtsZ protofilaments that emanate from the completed septum. In the absence of MinCD, these Z-rings progress into a divisome that ultimately constricts giving rise to an anucleate minicell.

Towards understanding the mechanism of MinCD

There are numerous proteins that affect FtsZ dynamics, but surprisingly little is known about the mechanism by which they affect FtsZ assembly. My studies of FtsZ-GFP demonstrate that transient FtsZ ring-like structures assemble near the new cell pole shortly after cytokinesis, and these Z-rings become competent for division in the absence of MinCD (Gregory et al, 2008). This suggests that the primary role of MinC *in vivo* is not to prevent FtsZ polymerization as previously thought, but rather to

perturb bundling of FtsZ protofilaments. A key question that needs to be addressed is the mechanism by which MinC destabilizes FtsZ bundles *in vivo*.

There are two distinct biochemical activities that could account for the destabilization of polar Z-rings by MinC. First, MinC might perturb the lateral interactions between FtsZ protofilaments, which directly promotes the disassembly of Z-rings. In support of this hypothesis, MinC is sufficient to destabilize FtsZ scaffolds and reduces bundling of FtsZ protofilaments *in vitro* (Dajkovic et al, 2008) (Scheffers, 2008). Importantly, the effect of MinC is concentration dependent and is most effective at MinC to FtsZ ratios of one to one in *E. coli* and closer to two to one in *B. subtilis*, which are higher than the physiological ratios of MinC to FtsZ. The stoichiometry of the interaction between MinC and FtsZ *in vivo* remains unknown. Second, MinC my act indirectly to destabilize FtsZ bundles by disrupting the interactions between FtsZ and other stabilizing proteins such as ZapA or FtsA. It has been proposed that *E. coli* MinC prevents the recruitment of FtsA to the Z-ring, which arrests the development of the divisome therefore rendering the Z-ring incapable of constriction (Justice et al, 2000). In support of this hypothesis, Shen et al recently demonstrated that *E. coli* MinC competes with FtsA for binding to the C-terminal end of FtsZ (Shen & Lutkenhaus, 2009). Thus MinC appears to act through both direct and indirect methods. MinC directly interacts with FtsZ, which might itself destabilize FtsZ bundles, and it can displace FtsA in *E. coli*, which is required for cell division.

The activity of MinC must be temporally and spatially regulated to ensure that it does not interfere with appropriate Z-ring assembly. Surprisingly, the highest

concentration of MinC in *B. subtilis* cells is found at division sites, but MinC does not destabilize Z-rings at the midcell. Furthermore, there is no established role for MinC during cytokinesis. In *B. subtilis*, DivIVA may render MinCD inactive when it is localized to the divisome, therefore it is not until MinCD is released from the completed septum that it can act on bundles of FtsZ. This implies that the predominant subcellular localization of MinC is not where it is biologically active. How then do we determine when a protein is active? The difference for MinC may be the presence or absence of DivIVA, but the implications of this on other FtsZ regulatory proteins is unclear.

FtsZ dynamics

My studies demonstrate that FtsZ is highly dynamic and moves about the cell in the form of short protofilaments. These protofilaments coalesce at midcell to form the Z-ring and emanate from completed septa following cytokinesis (Chapter IV). This model of FtsZ movement contrasts previous models that suggest that FtsZ polymerizes into extended helical structures during relocalization from the completed septum to the nascent division site. I suspect that the helical FtsZ structures that were previously observed were an artifact caused by the helical pattern of movement in which FtsZ is confined; the cell is essentially a cylinder.

The number of FtsZ protofilaments in the cell is likely influenced by the equilibrium between FtsZ monomers and protofilaments, which is controlled in part,

by the critical concentration for FtsZ polymerization and the ultrastructure of FtsZ protofilaments *in vivo*. Essential to our understanding of cell division will be the characterization of the equilibrium between FtsZ monomers, FtsZ protofilaments, and the bundles of FtsZ protofilaments that comprise the Z-ring. What causes FtsZ bundles to favor assembly at midcell and then disassembly during constriction? My studies have demonstrated that FtsZ protofilaments can immediately reassemble into a ring-like structure at the new cell pole immediately after constriction (Chapter III). Is this due to a high concentration of FtsZ protofilaments at the cell pole immediately after cytokinesis or the presence of accessory proteins such as ZapA that promote bundling? It is possible that there is a critical concentration of FtsZ protofilaments that, once met, results in Z-ring assembly?

The assembly of Z-rings from FtsZ protofilament precursors provides some insight into the ultrastructure of the Z-ring itself. At present, the only high resolution images of FtsZ are from Caulobacter crescentus (Li et al, 2007). Interestingly, the FtsZ protofilaments observed at midcell were not part of a contiguous ring, suggesting the Z-ring may not be a ring at all. My studies of FtsZ in *B. subtilis* using three-dimensional structure illumination microscopy (3D-SIM), which affords a 100 nm resolution, revealed a contiguous and nearly uniform Z-ring (Chapter IV). These conflicting results could be due to a difference between species, insufficient resolution in my studies of *B. subtilis* FtsZ, or fixation artifacts due to cryoEM imaging. Resolving this dilemma will narrow the possibilities for the mechanism of constriction

because a sliding filament model is not consistent with a discontinuous Z-ring. It might also reveal the organization of other proteins within the divisome.

References

Abanes-De Mello A, Sun YL, Aung S, Pogliano K (2002) A cytoskeleton-like role for the bacterial cell wall during engulfment of the *Bacillus subtilis* forespore. *Genes Dev* **16**(24)**:** 3253-3264

Abremski K, Hoess R (1984) Bacteriophage P1 site-specific recombination. Purification and properties of the Cre recombinase protein. *J Biol Chem* **259**(3)**:** 1509-1514

Abremski K, Wierzbicki A, Frommer B, Hoess RH (1986) Bacteriophage P1 Cre-loxP site-specific recombination. Site-specific DNA topoisomerase activity of the Cre recombination protein. *J Biol Chem* **261**(1)**:** 391-396

Addinall SG, Cao C, Lutkenhaus J (1997) FtsN, a late recruit to the septum in Escherichia coli. *Mol Microbiol* **25**(2)**:** 303-309

Addinall SG, Johnson KA, Dafforn T, Smith C, Rodger A, Gomez RP, Sloan K, Blewett A, Scott DJ, Roper DI (2005) Expression, purification and crystallization of the cell-division protein YgfE from Escherichia coli. *Acta Crystallogr Sect F Struct Biol Cryst Commun* **61**(Pt 3)**:** 305-307

Akerlund T, Bernander R, Nordstrom K (1992) Cell division in Escherichia coli minB mutants. *Mol Microbiol* **6**(15)**:** 2073-2083

Akhmanova A, Stehbens SJ, Yap AS (2009) Touch, grasp, deliver and control: functional cross-talk between microtubules and cell adhesions. *Traffic* **10**(3)**:** 268-274

Anderson DE, Gueiros-Filho FJ, Erickson HP (2004) Assembly dynamics of FtsZ rings in Bacillus subtilis and Escherichia coli and effects of FtsZ-regulating proteins. *J Bacteriol* **186**(17)**:** 5775-5781

Arigoni F, Pogliano K, Webb CD, Stragier P, Losick R (1995) Localization of protein implicated in establishment of cell type to sites of asymmetric division. *Science* **270**(5236)**:** 637-640

Asato Y (2006) Perspectives in the coordinate regulation of cell cycle events in Synechococcus. *Curr Issues Mol Biol* **8**(2)**:** 91-95

Aung S, Shum J, Abanes-De Mello A, Broder DH, Fredlund-Gutierrez J, Chiba S, Pogliano K (2007) Dual localization pathways for the engulfment proteins during *Bacillus subtilis* sporulation. *Mol Microbiol* **65:** 1534-1546

Ausebel FM BR, Kingston RE, Moore DD, Seidman JG, Struhl K. (1992) *Current protocols in molecular biology*, New York, New York: Wiley.

Axelrod D (2001) Total internal reflection fluorescence microscopy in cell biology. *Traffic* **2**(11)**:** 764-774

Axelrod D (2003) Total internal reflection fluorescence microscopy in cell biology. *Methods Enzymol* **361:** 1-33

Barak I, Wilkinson AJ (2007) Division site recognition in Escherichia coli and Bacillus subtilis. *FEMS Microbiol Rev* **31**(3)**:** 311-326

Barr FA, Gruneberg U (2007) Cytokinesis: placing and making the final cut. *Cell* **131**(5)**:** 847-860

Bates M, Huang B, Dempsey GT, Zhuang X (2007) Multicolor super-resolution imaging with photo-switchable fluorescent probes. *Science* **317**(5845)**:** 1749-1753

Beall B, Lutkenhaus J (1992) Impaired cell division and sporulation of a Bacillus subtilis strain with the ftsA gene deleted. *J Bacteriol* **174**(7)**:** 2398-2403

Becker E, Herrera FG, Gunderson F, Derman AI, Dance AL, Sims J, Larsen R, Pogliano J (2006) DNA segregation by the bacterial actin AlfA during *Bacillus subtilis* growth and development. *EMBO J **25***(24)**:** 5919-5931

Becker EC, Pogliano K (2007) Cell-specific SpoIIIE assembly and DNA translocation polarity are dictated by chromosome orientation. *Mol Microbiol* **66:** 1066-1079

Beghin A, Galmarini CM, Dumontet C (2007) Tubulin folding pathways: implication in the regulation of microtubule dynamics. *Curr Cancer Drug Targets* **7**(8)**:** 697-703

Ben-Yehuda S, Losick R (2002) Asymmetric cell division in B. subtilis involves a spiral-like intermediate of the cytokinetic protein FtsZ. *Cell* **109**(2)**:** 257-266

Bernhardt TG, de Boer PA (2005) SlmA, a nucleoid-associated, FtsZ binding protein required for blocking septal ring assembly over Chromosomes in E. coli. *Mol Cell* **18**(5)**:** 555-564

Betzig E, Patterson GH, Sougrat R, Lindwasser OW, Olenych S, Bonifacino JS, Davidson MW, Lippincott-Schwartz J, Hess HF (2006) Imaging intracellular fluorescent proteins at nanometer resolution. *Science* **313**(5793)**:** 1642-1645

Bhalla N, Dernburg AF (2008) Prelude to a division. *Annu Rev Cell Dev Biol* **24:** 397-424

Bi E, Lutkenhaus J (1993) Cell division inhibitors SulA and MinCD prevent formation of the FtsZ ring. *J Bacteriol* **175**(4)**:** 1118-1125

Bi EF, Lutkenhaus J (1991) FtsZ ring structure associated with division in Escherichia coli. *Nature* **354**(6349)**:** 161-164

Bramhill D (1997) Bacterial cell division. *Annu Rev Cell Dev Biol* **13:** 395-424

Bramkamp M, Emmins R, Weston L, Donovan C, Daniel RA, Errington J (2008) A novel component of the division-site selection system of Bacillus subtilis and a new mode of action for the division inhibitor MinCD. *Mol Microbiol* **70**(6)**:** 1556-1569

Bramkamp M, Weston L, Daniel RA, Errington J (2006) Regulated intramembrane proteolysis of FtsL protein and the control of cell division in Bacillus subtilis. *Mol Microbiol* **62**(2)**:** 580-591

Briegel A, Dias DP, Li Z, Jensen RB, Frangakis AS, Jensen GJ (2006) Multiple large filament bundles observed in Caulobacter crescentus by electron cryotomography. *Mol Microbiol* **62**(1)**:** 5-14

Broder DH, Pogliano K (2006) Forespore engulfment mediated by a ratchet-like mechanism. *Cell* **126:** 917-928

Buddelmeijer N, Beckwith J (2002) Assembly of cell division proteins at the E. coli cell center. *Curr Opin Microbiol* **5**(6)**:** 553-557

Buddelmeijer N, Beckwith J (2004) A complex of the Escherichia coli cell division proteins FtsL, FtsB and FtsQ forms independently of its localization to the septal region. *Mol Microbiol* **52**(5)**:** 1315-1327

Butala M, Zgur-Bertok D, Busby SJ (2009) The bacterial LexA transcriptional repressor. *Cell Mol Life Sci* **66**(1)**:** 82-93

Caplan MR, Erickson HP (2003) Apparent cooperative assembly of the bacterial cell division protein FtsZ demonstrated by isothermal titration calorimetry. *J Biol Chem* **278**(16)**:** 13784-13788

Carballido-Lopez R, Formstone A (2007) Shape determination in Bacillus subtilis. *Curr Opin Microbiol* **10**(6)**:** 611-616

Caspar DL (1980) Movement and self-control in protein assemblies. Quasi-equivalence revisited. *Biophys J* **32**(1)**:** 103-138

Chalfie M, Tu Y, Euskirchen G, Ward WW, Prasher DC (1994) Green fluorescent protein as a marker for gene expression. *Science* **263**(5148)**:** 802-805

Charette MF, Henderson GW, Doane LL, Markovitz A (1984) DNA-stimulated ATPase activity on the lon (CapR) protein. *J Bacteriol* **158**(1)**:** 195-201

Chen Y, Bjornson K, Redick SD, Erickson HP (2005) A rapid fluorescence assay for FtsZ assembly indicates cooperative assembly with a dimer nucleus. *Biophys J* **88**(1)**:** 505-514

Chung KM, Hsu HH, Yeh HY, Chang BY (2007) Mechanism of regulation of prokaryotic tubulin-like GTPase FtsZ by membrane protein EzrA. *J Biol Chem* **282**(20)**:** 14891-14897

Claessen D, Emmins R, Hamoen LW, Daniel RA, Errington J, Edwards DH (2008) Control of the cell elongation-division cycle by shuttling of PBP1 protein in Bacillus subtilis. *Mol Microbiol* **68**(4)**:** 1029-1046

Corbin BD, Geissler B, Sadasivam M, Margolin W (2004) Z-ring-independent interaction between a subdomain of FtsA and late septation proteins as revealed by a polar recruitment assay. *J Bacteriol* **186**(22)**:** 7736-7744

Cordell SC, Anderson RE, Lowe J (2001) Crystal structure of the bacterial cell division inhibitor MinC. *Embo J* **20**(10)**:** 2454-2461

Cordell SC, Lowe J (2001) Crystal structure of the bacterial cell division regulator MinD. *FEBS Lett* **492**(1-2)**:** 160-165

Cormack BP, Valdivia RH, Falkow S (1996) FACS-optimized mutants of the green fluorescent protein (GFP). *Gene* **173**(1 Spec No)**:** 33-38

D'Ari R, George J, Huisman O (1979) Suppression of tif-mediated induction of SOS functions in Escherichia coli by an altered dnaB protein. *J Bacteriol* **140**(2)**:** 381-387

Dajkovic A, Lan G, Sun SX, Wirtz D, Lutkenhaus J (2008) MinC spatially controls bacterial cytokinesis by antagonizing the scaffolding function of FtsZ. *Curr Biol* **18**(4)**:** 235-244

Dajkovic A, Lutkenhaus J (2006) Z ring as executor of bacterial cell division. *J Mol Microbiol Biotechnol* **11**(3-5)**:** 140-151

Daniel RA, Errington J (2000) Intrinsic instability of the essential cell division protein FtsL of Bacillus subtilis and a role for DivIB protein in FtsL turnover. *Mol Microbiol* **36**(2)**:** 278-289

Daniel RA, Harry EJ, Errington J (2000) Role of penicillin-binding protein PBP 2B in assembly and functioning of the division machinery of Bacillus subtilis. *Mol Microbiol* **35**(2)**:** 299-311

Datsenko KA, Wanner BL (2000) One-step inactivation of chromosomal genes in Escherichia coli K-12 using PCR products. *Proc Natl Acad Sci U S A* **97**(12)**:** 6640-6645

de Boer PA (1993) Chromosome segregation and cytokinesis in bacteria. *Curr Opin Cell Biol* **5**(2)**:** 232-237

de Boer PA, Crossley RE, Hand AR, Rothfield LI (1991) The MinD protein is a membrane ATPase required for the correct placement of the Escherichia coli division site. *Embo J* **10**(13)**:** 4371-4380

de Boer PA, Crossley RE, Rothfield LI (1989) A division inhibitor and a topological specificity factor coded for by the minicell locus determine proper placement of the division septum in E. coli. *Cell* **56**(4)**:** 641-649

de Boer PA, Crossley RE, Rothfield LI (1992) Roles of MinC and MinD in the site-specific septation block mediated by the MinCDE system of Escherichia coli. *J Bacteriol* **174**(1)**:** 63-70

Dennis JJ, Zylstra GJ (1998) Plasposons: modular self-cloning minitransposon derivatives for rapid genetic analysis of gram-negative bacterial genomes. *Appl Environ Microbiol* **64**(7)**:** 2710-2715

Desai A, Mitchison TJ (1997) Microtubule polymerization dynamics. *Annu Rev Cell Dev Biol* **13:** 83-117

Di Lallo G, Fagioli M, Barionovi D, Ghelardini P, Paolozzi L (2003) Use of a two-hybrid assay to study the assembly of a complex multicomponent protein machinery: bacterial septosome differentiation. *Microbiology* **149**(Pt 12)**:** 3353-3359

Drew D, Lerch M, Kunji E, Slotboom DJ, de Gier JW (2006) Optimization of membrane protein overexpression and purification using GFP fusions. *Nat Methods* **3**(4)**:** 303-313

Dye NA, Shapiro L (2007) The push and pull of the bacterial cytoskeleton. *Trends Cell Biol* **17**(5)**:** 239-245

Ebersbach G, Galli E, Moller-Jensen J, Lowe J, Gerdes K (2008) Novel coiled-coil cell division factor ZapB stimulates Z ring assembly and cell division. *Mol Microbiol* **68**(3)**:** 720-735

Edwards DH, Errington J (1997) The Bacillus subtilis DivIVA protein targets to the division septum and controls the site specificity of cell division. *Mol Microbiol* **24**(5)**:** 905-915

Ehrmann M, Boyd D, Beckwith J (1990) Genetic analysis of membrane protein topology by a sandwich gene fusion approach. *Proc Natl Acad Sci U S A* **87**(19)**:** 7574-7578

Elowitz MB, Surette MG, Wolf PE, Stock JB, Leibler S (1999) Protein mobility in the cytoplasm of Escherichia coli. *J Bacteriol* **181**(1)**:** 197-203

Erickson HP (2007) Evolution of the cytoskeleton. *Bioessays* **29**(7)**:** 668-677

Erickson HP, Taylor DW, Taylor KA, Bramhill D (1996) Bacterial cell division protein FtsZ assembles into protofilament sheets and minirings, structural homologs of tubulin polymers. *Proc Natl Acad Sci U S A* **93**(1)**:** 519-523

Errington J, Daniel RA, Scheffers DJ (2003) Cytokinesis in bacteria. *Microbiol Mol Biol Rev* **67**(1)**:** 52-65

Fernandez S, Ayora S, Alonso JC (2000) Bacillus subtilis homologous recombination: genes and products. *Res Microbiol* **151**(6)**:** 481-486

Gamba P, Veening JW, Saunders NJ, Hamoen LW, Daniel RA (2009) Two-step assembly dynamics of the Bacillus subtilis divisome. *J Bacteriol*

Gayda RC, Markovitz A (1978) Altered bacteriophage lambda expression in cell division mutants capR(lon) of Escherichia coli K-12. *Mol Gen Genet* **159**(1)**:** 1-11

Gayda RC, Yamamoto LT, Markovitz A (1976) Second-site mutations in capR (lon) strains of Escherichia coli K-12 that prevent radiation sensitivity and allow bacteriophage lambda to lysogenize. *J Bacteriol* **127**(3)**:** 1208-1216

Ghosh B, Sain A (2008) Origin of contractile force during cell division of bacteria. *Phys Rev Lett* **101**(17)**:** 178101

Goehring NW, Beckwith J (2005) Diverse paths to midcell: assembly of the bacterial cell division machinery. *Curr Biol* **15**(13)**:** R514-526

Goehring NW, Gonzalez MD, Beckwith J (2006) Premature targeting of cell division proteins to midcell reveals hierarchies of protein interactions involved in divisome assembly. *Mol Microbiol* **61**(1)**:** 33-45

Goldberg AL, Moerschell RP, Chung CH, Maurizi MR (1994) ATP-dependent protease La (lon) from Escherichia coli. *Methods Enzymol* **244:** 350-375

Gonzalez JM, Velez M, Jimenez M, Alfonso C, Schuck P, Mingorance J, Vicente M, Minton AP, Rivas G (2005) Cooperative behavior of Escherichia coli cell-division protein FtsZ assembly involves the preferential cyclization of long single-stranded fibrils. *Proc Natl Acad Sci U S A* **102**(6)**:** 1895-1900

Goranov AI, Katz L, Breier AM, Burge CB, Grossman AD (2005) A transcriptional response to replication status mediated by the conserved bacterial replication protein DnaA. *Proc Natl Acad Sci U S A* **102**(36)**:** 12932-12937

Goryshin IY, Miller JA, Kil YV, Lanzov VA, Reznikoff WS (1998) Tn5/IS50 target recognition. *Proc Natl Acad Sci U S A* **95**(18)**:** 10716-10721

Gottesman S, Halpern E, Trisler P (1981) Role of sulA and sulB in filamentation by lon mutants of Escherichia coli K-12. *J Bacteriol* **148**(1)**:** 265-273

Gottesman S, Zipser D (1978) Deg phenotype of Escherichia coli lon mutants. *J Bacteriol* **133**(2)**:** 844-851

Graumann PL (2007) Cytoskeletal elements in bacteria. *Annu Rev Microbiol* **61:** 589-618

Gregory JA, Becker EC, Pogliano K (2008) Bacillus subtilis MinC destabilizes FtsZ-rings at new cell poles and contributes to the timing of cell division. *Genes Dev* **22**(24)**:** 3475-3488

Grenga L, Luzi G, Paolozzi L, Ghelardini P (2008) The Escherichia coli FtsK functional domains involved in its interaction with its divisome protein partners. *FEMS Microbiol Lett* **287**(2)**:** 163-167

Gudas LJ, Pardee AB (1975) Model for regulation of Escherichia coli DNA repair functions. *Proc Natl Acad Sci U S A* **72**(6)**:** 2330-2334

Gueiros-Filho FJ, Losick R (2002) A widely conserved bacterial cell division protein that promotes assembly of the tubulin-like protein FtsZ. *Genes Dev* **16**(19)**:** 2544-2556

Haeusser DP, Garza AC, Buscher AZ, Levin PA (2007) The division inhibitor EzrA contains a seven-residue patch required for maintaining the dynamic nature of the medial FtsZ ring. *J Bacteriol* **189**(24)**:** 9001-9010

Haeusser DP, Lee AH, Weart RB, Levin PA (2009) ClpX inhibits FtsZ assembly in a manner that does not require its ATP hydrolysis-dependent chaperone activity. *J Bacteriol* **191**(6)**:** 1986-1991

Haeusser DP, Levin PA (2008) The great divide: coordinating cell cycle events during bacterial growth and division. *Curr Opin Microbiol* **11**(2)**:** 94-99

Haeusser DP, Schwartz RL, Smith AM, Oates ME, Levin PA (2004) EzrA prevents aberrant cell division by modulating assembly of the cytoskeletal protein FtsZ. *Mol Microbiol* **52**(3)**:** 801-814

Hale CA, de Boer PA (1999) Recruitment of ZipA to the septal ring of Escherichia coli is dependent on FtsZ and independent of FtsA. *J Bacteriol* **181**(1)**:** 167-176

Hale CA, Rhee AC, de Boer PA (2000) ZipA-induced bundling of FtsZ polymers mediated by an interaction between C-terminal domains. *J Bacteriol* **182**(18)**:** 5153-5166

Hamoen LW, Meile JC, de Jong W, Noirot P, Errington J (2006) SepF, a novel FtsZ-interacting protein required for a late step in cell division. *Mol Microbiol* **59**(3)**:** 989-999

Hanahan D (1983) Studies on transformation of Escherichia coli with plasmids. *J Mol Biol* **166**(4)**:** 557-580

Harry E, Monahan L, Thompson L (2006) Bacterial cell division: the mechanism and its precison. *Int Rev Cytol* **253:** 27-94

Harry EJ, Wake RG (1997) The membrane-bound cell division protein DivIB is localized to the division site in Bacillus subtilis. *Mol Microbiol* **25**(2)**:** 275-283

Hayashi I, Oyama T, Morikawa K (2001) Structural and functional studies of MinD ATPase: implications for the molecular recognition of the bacterial cell division apparatus. *EMBO J* **20**(8)**:** 1819-1828

Heintzmann R, Ficz G (2006) Breaking the resolution limit in light microscopy. *Brief Funct Genomic Proteomic* **5**(4)**:** 289-301

Heintzmann R, Ficz G (2007) Breaking the resolution limit in light microscopy. *Methods Cell Biol* **81:** 561-580

Henrici AT (1925) On Cytomorphosis in Bacteria. *Science* **61**(1591)**:** 644-647

Henrici AT (1928) Morphologic Variation and Rate of Growth of Bacteria. *London: Bailliere, Tindall, and Cox*

Henrici AT (1933) Studies of Freshwater Bacteria: I. A Direct Microscopic Technique. *J Bacteriol* **25**(3)**:** 277-287

Henriques AO, Glaser P, Piggot PJ, Moran CP, Jr. (1998) Control of cell shape and elongation by the rodA gene in Bacillus subtilis. *Mol Microbiol* **28**(2)**:** 235-247

Hett EC, Rubin EJ (2008) Bacterial growth and cell division: a mycobacterial perspective. *Microbiol Mol Biol Rev* **72**(1)**:** 126-156, table of contents

Hirota Y, Ryter A, Jacob F (1968) Thermosensitive mutants of E. coli affected in the processes of DNA synthesis and cellular division. *Cold Spring Harb Symp Quant Biol* **33:** 677-693

Hoch JA (1991) Genetic analysis in Bacillus subtilis. *Methods Enzymol* **204:** 305-320

Holland IB, Jones C (1985) The role of the FtsZ protein (SfiB) in UV-induced division inhibition and in the normal Escherichia coli cell division cycle. *Ann Inst Pasteur Microbiol* **136A**(1)**:** 165-171

Howard M (2004) A mechanism for polar protein localization in bacteria. *J Mol Biol* **335**(2)**:** 655-663

Howard-Flanders P, Simson E, Theriot L (1964) A Locus That Controls Filament Formation and Sensitivity to Radiation in Escherichia Coli K-12. *Genetics* **49:** 237-246

Hu Z, Gogol EP, Lutkenhaus J (2002) Dynamic assembly of MinD on phospholipid vesicles regulated by ATP and MinE. *Proc Natl Acad Sci U S A* **99**(10)**:** 6761-6766

Hu Z, Lutkenhaus J (1999) Topological regulation of cell division in Escherichia coli involves rapid pole to pole oscillation of the division inhibitor MinC under the control of MinD and MinE. *Mol Microbiol* **34**(1)**:** 82-90

Hu Z, Lutkenhaus J (2000) Analysis of MinC reveals two independent domains involved in interaction with MinD and FtsZ. *J Bacteriol* **182**(14)**:** 3965-3971

Hu Z, Mukherjee A, Pichoff S, Lutkenhaus J (1999) The MinC component of the division site selection system in Escherichia coli interacts with FtsZ to prevent polymerization. *Proc Natl Acad Sci U S A* **96**(26)**:** 14819-14824

Hua SS, Markovitz A (1972) Multiple regulator gene control of the galactose operon in Escherichia coli K-12. *J Bacteriol* **110**(3)**:** 1089-1099

Huecas S, Andreu JM (2004) Polymerization of nucleotide-free, GDP- and GTP-bound cell division protein FtsZ: GDP makes the difference. *FEBS Lett* **569**(1-3)**:** 43-48

Huisman O, D'Ari R (1981) An inducible DNA replication-cell division coupling mechanism in E. coli. *Nature* **290**(5809)**:** 797-799

Huisman O, D'Ari R, Gottesman S (1984) Cell-division control in Escherichia coli: specific induction of the SOS function SfiA protein is sufficient to block septation. *Proc Natl Acad Sci U S A* **81**(14)**:** 4490-4494

Ishikawa S, Kawai Y, Hiramatsu K, Kuwano M, Ogasawara N (2006) A new FtsZ-interacting protein, YlmF, complements the activity of FtsA during progression of cell division in Bacillus subtilis. *Mol Microbiol* **60**(6)**:** 1364-1380

Janion C (2008) Inducible SOS response system of DNA repair and mutagenesis in Escherichia coli. *Int J Biol Sci* **4**(6)**:** 338-344

Jensen SO, Thompson LS, Harry EJ (2005) Cell division in Bacillus subtilis: FtsZ and FtsA association is Z-ring independent, and FtsA is required for efficient midcell Z-Ring assembly. *J Bacteriol* **187**(18)**:** 6536-6544

Jones C, Holland IB (1985) Role of the SulB (FtsZ) protein in division inhibition during the SOS response in Escherichia coli: FtsZ stabilizes the inhibitor SulA in maxicells. *Proc Natl Acad Sci U S A* **82**(18)**:** 6045-6049

Jorgensen P, Tyers M (2004) How cells coordinate growth and division. *Curr Biol* **14**(23)**:** R1014-1027

Justice SS, Garcia-Lara J, Rothfield LI (2000) Cell division inhibitors SulA and MinC/MinD block septum formation at different steps in the assembly of the Escherichia coli division machinery. *Mol Microbiol* **37**(2)**:** 410-423

Kaltwasser M, Wiegert T, Schumann W (2002) Construction and application of epitope- and green fluorescent protein-tagging integration vectors for Bacillus subtilis. *Appl Environ Microbiol* **68**(5)**:** 2624-2628

Karimova G, Dautin N, Ladant D (2005) Interaction network among Escherichia coli membrane proteins involved in cell division as revealed by bacterial two-hybrid analysis. *J Bacteriol* **187**(7)**:** 2233-2243

Karmazyn-Campelli C, Fluss L, Leighton T, Stragier P (1992) The spoIIN279(ts) mutation affects the FtsA protein of Bacillus subtilis. *Biochimie* **74**(7-8)**:** 689-694

Katis VL, Wake RG, Harry EJ (2000) Septal localization of the membrane-bound division proteins of Bacillus subtilis DivIB and DivIC is codependent only at high temperatures and requires FtsZ. *J Bacteriol* **182**(12)**:** 3607-3611

Kjeldgaard NO, Maaloe O, Schaechter M (1958) The transition between different physiological states during balanced growth of Salmonella typhimurium. *J Gen Microbiol* **19**(3)**:** 607-616

Kleina LG, Miller JH (1990) Genetic studies of the lac repressor. XIII. Extensive amino acid replacements generated by the use of natural and synthetic nonsense suppressors. *J Mol Biol* **212**(2)**:** 295-318

Kolter R, Inuzuka M, Helinski DR (1978) Trans-complementation-dependent replication of a low molecular weight origin fragment from plasmid R6K. *Cell* **15**(4)**:** 1199-1208

Kuchibhatla A, Rasheed AS, Narayanan J, Bellare J, Panda D (2009) An Analysis of FtsZ Assembly Using Small Angle X-ray Scattering and Electron Microscopy. *Langmuir*

Kusumi A, Nakada C, Ritchie K, Murase K, Suzuki K, Murakoshi H, Kasai RS, Kondo J, Fujiwara T (2005) Paradigm shift of the plasma membrane concept from the two-dimensional continuum fluid to the partitioned fluid: high-speed single-molecule tracking of membrane molecules. *Annu Rev Biophys Biomol Struct* **34:** 351-378

Lambertsen L, Sternberg C, Molin S (2004) Mini-Tn7 transposons for site-specific tagging of bacteria with fluorescent proteins. *Environ Microbiol* **6**(7)**:** 726-732

Larsen RA, Cusumano C, Fujioka A, Lim-Fong G, Patterson P, Pogliano J (2007) Treadmilling of a prokaryotic tubulin-like protein, TubZ, required for plasmid stability in Bacillus thuringiensis. *Genes Dev* **21**(11)**:** 1340-1352

Larsen RA, Wilson MM, Guss AM, Metcalf WW (2002) Genetic analysis of pigment biosynthesis in Xanthobacter autotrophicus Py2 using a new, highly efficient transposon mutagenesis system that is functional in a wide variety of bacteria. *Arch Microbiol* **178**(3)**:** 193-201

Lau IF, Filipe SR, Soballe B, Okstad OA, Barre FX, Sherratt DJ (2003) Spatial and temporal organization of replicating Escherichia coli chromosomes. *Mol Microbiol* **49**(3)**:** 731-743

Lee S, Price CW (1993) The minCD locus of Bacillus subtilis lacks the minE determinant that provides topological specificity to cell division. *Mol Microbiol* **7**(4)**:** 601-610

Levin PA, Kurtser IG, Grossman AD (1999) Identification and characterization of a negative regulator of FtsZ ring formation in Bacillus subtilis. *Proc Natl Acad Sci U S A* **96**(17)**:** 9642-9647

Levin PA, Losick R (1996) Transcription factor Spo0A switches the localization of the cell division protein FtsZ from a medial to a bipolar pattern in Bacillus subtilis. *Genes Dev* **10**(4)**:** 478-488

Levin PA, Schwartz RL, Grossman AD (2001) Polymer stability plays an important role in the positional regulation of FtsZ. *J Bacteriol* **183**(18)**:** 5449-5452

Levin PA, Shim JJ, Grossman AD (1998) Effect of minCD on FtsZ ring position and polar septation in Bacillus subtilis. *J Bacteriol* **180**(22)**:** 6048-6051

Lewis M (2005) The lac repressor. *C R Biol* **328**(6)**:** 521-548

Lewis M, Chang G, Horton NC, Kercher MA, Pace HC, Schumacher MA, Brennan RG, Lu P (1996) Crystal structure of the lactose operon repressor and its complexes with DNA and inducer. *Science* **271**(5253)**:** 1247-1254

Li Z, Trimble MJ, Brun YV, Jensen GJ (2007) The structure of FtsZ filaments in vivo suggests a force-generating role in cell division. *EMBO J* **26**(22)**:** 4694-4708

Little JW (1984) Autodigestion of lexA and phage lambda repressors. *Proc Natl Acad Sci U S A* **81**(5)**:** 1375-1379

Little JW, Harper JE (1979) Identification of the lexA gene product of Escherichia coli K-12. *Proc Natl Acad Sci U S A* **76**(12)**:** 6147-6151

Liu Z, Mukherjee A, Lutkenhaus J (1999) Recruitment of ZipA to the division site by interaction with FtsZ. *Mol Microbiol* **31**(6)**:** 1853-1861

Lopilato J, Bortner S, Beckwith J (1986) Mutations in a new chromosomal gene of Escherichia coli K-12, pcnB, reduce plasmid copy number of pBR322 and its derivatives. *Mol Gen Genet* **205**(2)**:** 285-290

Lowe J (1998) Crystal structure determination of FtsZ from Methanococcus jannaschii. *J Struct Biol* **124**(2-3)**:** 235-243

Lowe J, Amos LA (1998) Crystal structure of the bacterial cell-division protein FtsZ. *Nature* **391**(6663)**:** 203-206

Lowe J, Amos LA (1999) Tubulin-like protofilaments in Ca2+-induced FtsZ sheets. *EMBO J* **18**(9)**:** 2364-2371

Lowe J, Amos LA (2000) Helical tubes of FtsZ from Methanococcus jannaschii. *Biol Chem* **381**(9-10)**:** 993-999

Lowe J, Amos LA (2009) Evolution of cytomotive filaments: the cytoskeleton from prokaryotes to eukaryotes. *Int J Biochem Cell Biol* **41**(2)**:** 323-329

Lutkenhaus J (2007) Assembly Dynamics of the Bacterial MinCDE System and Spatial Regulation of the Z Ring. *Annu Rev Biochem*

Lutkenhaus JF (1983) Coupling of DNA replication and cell division: sulB is an allele of ftsZ. *J Bacteriol* **154**(3)**:** 1339-1346

Lutkenhaus JF, Wolf-Watz H, Donachie WD (1980) Organization of genes in the ftsA-envA region of the Escherichia coli genetic map and identification of a new fts locus (ftsZ). *J Bacteriol* **142**(2)**:** 615-620

Ma X, Ehrhardt DW, Margolin W (1996) Colocalization of cell division proteins FtsZ and FtsA to cytoskeletal structures in living Escherichia coli cells by using green fluorescent protein. *Proc Natl Acad Sci U S A* **93**(23)**:** 12998-13003

Maddock JR, Shapiro L (1993) Polar location of the chemoreceptor complex in the Escherichia coli cell. *Science* **259**(5102)**:** 1717-1723

Manley S, Gillette JM, Patterson GH, Shroff H, Hess HF, Betzig E, Lippincott-Schwartz J (2008) High-density mapping of single-molecule trajectories with photoactivated localization microscopy. *Nat Methods* **5**(2)**:** 155-157

Margolin W (2000) Green fluorescent protein as a reporter for macromolecular localization in bacterial cells. *Methods* **20**(1)**:** 62-72

Margolin W (2005) FtsZ and the division of prokaryotic cells and organelles. *Nat Rev Mol Cell Biol* **6**(11)**:** 862-871

Margolin W (2006) Bacterial division: another way to box in the ring. *Curr Biol* **16**(20)**:** R881-884

Markiewicz P, Kleina LG, Cruz C, Ehret S, Miller JH (1994) Genetic studies of the lac repressor. XIV. Analysis of 4000 altered Escherichia coli lac repressors reveals essential and non-essential residues, as well as "spacers" which do not require a specific sequence. *J Mol Biol* **240**(5)**:** 421-433

Markovitz A (1964) Regulatory Mechanisms for Synthesis of Capsular Polysaccharide in Mucoid Mutants of Escherichia Coli K12. *Proc Natl Acad Sci U S A* **51:** 239-246

Marston AL, Errington J (1999) Selection of the midcell division site in Bacillus subtilis through MinD-dependent polar localization and activation of MinC. *Mol Microbiol* **33**(1)**:** 84-96

Marston AL, Thomaides HB, Edwards DH, Sharpe ME, Errington J (1998) Polar localization of the MinD protein of Bacillus subtilis and its role in selection of the mid-cell division site. *Genes Dev* **12**(21)**:** 3419-3430

Mazouni K, Domain F, Cassier-Chauvat C, Chauvat F (2004) Molecular analysis of the key cytokinetic components of cyanobacteria: FtsZ, ZipN and MinCDE. *Mol Microbiol* **52**(4)**:** 1145-1158

McEntee K, Weinstock GM, Lehman IR (1979) Initiation of general recombination catalyzed in vitro by the recA protein of Escherichia coli. *Proc Natl Acad Sci U S A* **76**(6)**:** 2615-2619

McKinney SA, Murphy CS, Hazelwood KL, Davidson MW, Looger LL (2009) A bright and photostable photoconvertible fluorescent protein. *Nat Methods* **6**(2)**:** 131-133

Merkulov GV, Boeke JD (1998) Libraries of green fluorescent protein fusions generated by transposition in vitro. *Gene* **222**(2)**:** 213-222

Michie KA, Monahan LG, Beech PL, Harry EJ (2006) Trapping of a spiral-like intermediate of the bacterial cytokinetic protein FtsZ. *J Bacteriol* **188**(5)**:** 1680-1690

Miller JH (1972) *Experiments in molecular genetics*, Cold Spring Harbor, NY.

Miller JH (1992) *A short course in bacterial genetics*, Cold Sprint Harbor, NY: Cold Spring Harbor Press.

Miraldi ER, Thomas PJ, Romberg L (2008) Allosteric models for cooperative polymerization of linear polymers. *Biophys J* **95**(5)**:** 2470-2486

Mitchell DR (2007) The evolution of eukaryotic cilia and flagella as motile and sensory organelles. *Adv Exp Med Biol* **607:** 130-140

Mitchison T, Kirschner M (1984) Dynamic instability of microtubule growth. *Nature* **312**(5991)**:** 237-242

Mitchison TJ (1992) Compare and contrast actin filaments and microtubules. *Mol Biol Cell* **3**(12)**:** 1309-1315

Mizusawa S, Court D, Gottesman S (1983) Transcription of the sulA gene and repression by LexA. *J Mol Biol* **171**(3)**:** 337-343

Mizusawa S, Gottesman S (1983) Protein degradation in Escherichia coli: the lon gene controls the stability of sulA protein. *Proc Natl Acad Sci U S A* **80**(2)**:** 358-362

Moller-Jensen J, Lowe J (2005) Increasing complexity of the bacterial cytoskeleton. *Curr Opin Cell Biol* **17**(1)**:** 75-81

Moreira IS, Fernandes PA, Ramos MJ (2006) Detailed microscopic study of the full zipA:FtsZ interface. *Proteins* **63**(4)**:** 811-821

Mount DW (1977) A mutant of Escherichia coli showing constitutive expression of the lysogenic induction and error-prone DNA repair pathways. *Proc Natl Acad Sci U S A* **74**(1)**:** 300-304

Mukherjee A, Lutkenhaus J (1994) Guanine nucleotide-dependent assembly of FtsZ into filaments. *J Bacteriol* **176**(9)**:** 2754-2758

Mulder E, Woldringh CL (1989) Actively replicating nucleoids influence positioning of division sites in Escherichia coli filaments forming cells lacking DNA. *J Bacteriol* **171**(8)**:** 4303-4314

Mullineaux CW, Nenninger A, Ray N, Robinson C (2006) Diffusion of green fluorescent protein in three cell environments in Escherichia coli. *J Bacteriol* **188**(10)**:** 3442-3448

Nelson BD, Manoil C, Traxler B (1997) Insertion mutagenesis of the lac repressor and its implications for structure-function analysis. *J Bacteriol* **179**(11)**:** 3721-3728

Nogales E, Downing KH, Amos LA, Lowe J (1998) Tubulin and FtsZ form a distinct family of GTPases. *Nat Struct Biol* **5**(6)**:** 451-458

Oliva MA, Cordell SC, Lowe J (2004) Structural insights into FtsZ protofilament formation. *Nat Struct Mol Biol* **11**(12)**:** 1243-1250

Oliva MA, Trambaiolo D, Lowe J (2007) Structural insights into the conformational variability of FtsZ. *J Mol Biol* **373**(5)**:** 1229-1242

Osawa M, Anderson DE, Erickson HP (2008) Reconstitution of contractile FtsZ rings in liposomes. *Science* **320**(5877)**:** 792-794

Osawa M, Erickson HP (2005) Probing the domain structure of FtsZ by random truncation and insertion of GFP. *Microbiology* **151**(Pt 12)**:** 4033-4043

Patrick JE, Kearns DB (2008) MinJ (YvjD) is a topological determinant of cell division in Bacillus subtilis. *Mol Microbiol* **70**(5)**:** 1166-1179

Perez F, Diamantopoulos GS, Stalder R, Kreis TE (1999) CLIP-170 highlights growing microtubule ends in vivo. *Cell* **96**(4)**:** 517-527

Peters PC, Migocki MD, Thoni C, Harry EJ (2007) A new assembly pathway for the cytokinetic Z ring from a dynamic helical structure in vegetatively growing cells of Bacillus subtilis. *Mol Microbiol* **64**(2)**:** 487-499

Phizicky EM, Roberts JW (1981) Induction of SOS functions: regulation of proteolytic activity of E. coli RecA protein by interaction with DNA and nucleoside triphosphate. *Cell* **25**(1)**:** 259-267

Pichoff S, Lutkenhaus J (2001) Escherichia coli division inhibitor MinCD blocks septation by preventing Z-ring formation. *J Bacteriol* **183**(22)**:** 6630-6635

Pichoff S, Lutkenhaus J (2002) Unique and overlapping roles for ZipA and FtsA in septal ring assembly in Escherichia coli. *EMBO J* **21**(4)**:** 685-693

Pichoff S, Lutkenhaus J (2005) Tethering the Z ring to the membrane through a conserved membrane targeting sequence in FtsA. *Mol Microbiol* **55**(6)**:** 1722-1734

Pichoff S, Lutkenhaus J (2007) Overview of cell shape: cytoskeletons shape bacterial cells. *Curr Opin Microbiol* **10**(6)**:** 601-605

Pinheiro LB, Gibbs MD, Vesey G, Smith JJ, Bergquist PL (2008) Fluorescent reference strains of bacteria by chromosomal integration of a modified green fluorescent protein gene. *Appl Microbiol Biotechnol* **77**(6)**:** 1287-1295

Popp D, Iwasa M, Narita A, Erickson HP, Maeda Y (2009) FtsZ condensates: an in vitro electron microscopy study. *Biopolymers* **91**(5)**:** 340-350

Prasher DC, Eckenrode VK, Ward WW, Prendergast FG, Cormier MJ (1992) Primary structure of the Aequorea victoria green-fluorescent protein. *Gene* **111**(2)**:** 229-233

Ramirez-Arcos S, Szeto J, Beveridge T, Victor C, Francis F, Dillon J (2001) Deletion of the cell-division inhibitor MinC results in lysis of Neisseria gonorrhoeae. *Microbiology* **147**(Pt 1)**:** 225-237

Raskin DM, de Boer PA (1999a) MinDE-dependent pole-to-pole oscillation of division inhibitor MinC in *Escherichia coli*. *J Bacteriol* **181:** 6419-6424

Raskin DM, de Boer PA (1999b) Rapid pole-to-pole oscillation of a protein required for directing division to the middle of *Escherichia coli*. *Proc Natl Acad Sci U S A* **96:** 4971-4976

Romberg L, Levin PA (2003) Assembly dynamics of the bacterial cell division protein FTSZ: poised at the edge of stability. *Annu Rev Microbiol* **57:** 125-154

Romberg L, Mitchison TJ (2004) Rate-limiting guanosine 5'-triphosphate hydrolysis during nucleotide turnover by FtsZ, a prokaryotic tubulin homologue involved in bacterial cell division. *Biochemistry* **43**(1)**:** 282-288

Romberg L, Simon M, Erickson HP (2001) Polymerization of Ftsz, a bacterial homolog of tubulin. is assembly cooperative? *J Biol Chem* **276**(15)**:** 11743-11753

Rothfield L, Taghbalout A, Shih YL (2005) Spatial control of bacterial division-site placement. *Nat Rev Microbiol* **3**(12)**:** 959-968

Rueda S, Vicente M, Mingorance J (2003) Concentration and assembly of the division ring proteins FtsZ, FtsA, and ZipA during the Escherichia coli cell cycle. *J Bacteriol* **185**(11)**:** 3344-3351

Rupp WD, Howard-Flanders P (1968) Discontinuities in the DNA synthesized in an excision-defective strain of Escherichia coli following ultraviolet irradiation. *J Mol Biol* **31**(2)**:** 291-304

Ryan KR, Shapiro L (2003) Temporal and spatial regulation in prokaryotic cell cycle progression and development. *Annu Rev Biochem* **72:** 367-394

Sako Y, Uyemura T (2002) Total internal reflection fluorescence microscopy for single-molecule imaging in living cells. *Cell Struct Funct* **27**(5)**:** 357-365

Schaechter M, Maaloe O, Kjeldgaard NO (1958) Dependency on medium and temperature of cell size and chemical composition during balanced grown of Salmonella typhimurium. *J Gen Microbiol* **19**(3)**:** 592-606

Scheffers DJ (2008) The effect of MinC on FtsZ polymerization is pH dependent and can be counteracted by ZapA. *FEBS Lett* **582**(17)**:** 2601-2608

Scheffers DJ, Driessen AJ (2002) Immediate GTP hydrolysis upon FtsZ polymerization. *Mol Microbiol* **43**(6)**:** 1517-1521

Scheffers DJ, Errington J (2004) PBP1 is a component of the Bacillus subtilis cell division machinery. *J Bacteriol* **186**(15)**:** 5153-5156

Scheffers DJ, Jones LJ, Errington J (2004) Several distinct localization patterns for penicillin-binding proteins in Bacillus subtilis. *Mol Microbiol* **51**(3)**:** 749-764

Scheffers DJ, Pinho MG (2005) Bacterial cell wall synthesis: new insights from localization studies. *Microbiol Mol Biol Rev* **69**(4)**:** 585-607

Schermelleh L, Carlton PM, Haase S, Shao L, Winoto L, Kner P, Burke B, Cardoso MC, Agard DA, Gustafsson MG, Leonhardt H, Sedat JW (2008) Subdiffraction multicolor imaging of the nuclear periphery with 3D structured illumination microscopy. *Science* **320**(5881)**:** 1332-1336

Schmidt KL, Peterson ND, Kustusch RJ, Wissel MC, Graham B, Phillips GJ, Weiss DS (2004) A predicted ABC transporter, FtsEX, is needed for cell division in Escherichia coli. *J Bacteriol* **186**(3)**:** 785-793

Schoemaker JM, Gayda RC, Markovitz A (1984) Regulation of cell division in Escherichia coli: SOS induction and cellular location of the sulA protein, a key to lon-associated filamentation and death. *J Bacteriol* **158**(2)**:** 551-561

Sharp MD, Pogliano K (2002) Role of cell-specific SpoIIIE assembly in polarity of DNA transfer. *Science* **295**(5552)**:** 137-139

Shen B, Lutkenhaus J (2009) The conserved C-terminal tail of FtsZ is required for the septal localization and division inhibitory activity of MinC(C)/MinD. *Mol Microbiol* **72**(2)**:** 410-424

Sheridan DL, Berlot CH, Robert A, Inglis FM, Jakobsdottir KB, Howe JR, Hughes TE (2002) A new way to rapidly create functional, fluorescent fusion proteins: random insertion of GFP with an in vitro transposition reaction. *BMC Neurosci* **3:** 7

Sheridan DL, Hughes TE (2004) A faster way to make GFP-based biosensors: two new transposons for creating multicolored libraries of fluorescent fusion proteins. *BMC Biotechnol* **4:** 17

Shibata T, DasGupta C, Cunningham RP, Radding CM (1979) Purified Escherichia coli recA protein catalyzes homologous pairing of superhelical DNA and single-stranded fragments. *Proc Natl Acad Sci U S A* **76**(4)**:** 1638-1642

Shih YL, Le T, Rothfield L (2003) Division site selection in Escherichia coli involves dynamic redistribution of Min proteins within coiled structures that extend between the two cell poles. *Proc Natl Acad Sci U S A* **100**(13)**:** 7865-7870

Shroff H, Galbraith CG, Galbraith JA, Betzig E (2008) Live-cell photoactivated localization microscopy of nanoscale adhesion dynamics. *Nat Methods* **5**(5)**:** 417-423

Shroff H, Galbraith CG, Galbraith JA, White H, Gillette J, Olenych S, Davidson MW, Betzig E (2007) Dual-color superresolution imaging of genetically expressed probes

within individual adhesion complexes. *Proc Natl Acad Sci U S A* **104**(51)**:** 20308-20313

Singh JK, Makde RD, Kumar V, Panda D (2007) A membrane protein, EzrA, regulates assembly dynamics of FtsZ by interacting with the C-terminal tail of FtsZ. *Biochemistry* **46**(38)**:** 11013-11022

Singh JK, Makde RD, Kumar V, Panda D (2008) SepF increases the assembly and bundling of FtsZ polymers and stabilizes FtsZ protofilaments by binding along its length. *J Biol Chem* **283**(45)**:** 31116-31124

Slater M, Schaechter M (1974) Control of cell division in bacteria. *Bacteriol Rev* **38**(2)**:** 199-221

Small E, Marrington R, Rodger A, Scott DJ, Sloan K, Roper D, Dafforn TR, Addinall SG (2007) FtsZ polymer-bundling by the Escherichia coli ZapA orthologue, YgfE, involves a conformational change in bound GTP. *J Mol Biol* **369**(1)**:** 210-221

Stricker J, Maddox P, Salmon ED, Erickson HP (2002) Rapid assembly dynamics of the Escherichia coli FtsZ-ring demonstrated by fluorescence recovery after photobleaching. *Proc Natl Acad Sci U S A* **99**(5)**:** 3171-3175

Suckow J, Markiewicz P, Kleina LG, Miller J, Kisters-Woike B, Muller-Hill B (1996) Genetic studies of the Lac repressor. XV: 4000 single amino acid substitutions and analysis of the resulting phenotypes on the basis of the protein structure. *J Mol Biol* **261**(4)**:** 509-523

Suefuji K, Valluzzi R, RayChaudhuri D (2002) Dynamic assembly of MinD into filament bundles modulated by ATP, phospholipids, and MinE. *Proc Natl Acad Sci U S A* **99**(26)**:** 16776-16781

Sun Q, Margolin W (1998) FtsZ dynamics during the division cycle of live Escherichia coli cells. *J Bacteriol* **180**(8)**:** 2050-2056

Szeto J, Ramirez-Arcos S, Raymond C, Hicks LD, Kay CM, Dillon JA (2001) Gonococcal MinD affects cell division in Neisseria gonorrhoeae and Escherichia coli and exhibits a novel self-interaction. *J Bacteriol* **183**(21)**:** 6253-6264

Szeto TH, Rowland SL, Rothfield LI, King GF (2002) Membrane localization of MinD is mediated by a C-terminal motif that is conserved across eubacteria, archaea, and chloroplasts. *Proc Natl Acad Sci U S A* **99**(24)**:** 15693-15698

Thanbichler M, Shapiro L (2008) Getting organized--how bacterial cells move proteins and DNA. *Nat Rev Microbiol* **6**(1)**:** 28-40

Thanedar S, Margolin W (2004) FtsZ exhibits rapid movement and oscillation waves in helix-like patterns in Escherichia coli. *Curr Biol* **14**(13)**:** 1167-1173

Trusca D, Scott S, Thompson C, Bramhill D (1998) Bacterial SOS checkpoint protein SulA inhibits polymerization of purified FtsZ cell division protein. *J Bacteriol* **180**(15)**:** 3946-3953

Turner JP (1940) The Question of the Cell Theory. *Science* **91**(2365)**:** 404-405

Van De Putte P, Van D, Roersch A (1964) The Selection of Mutants of Escherichia Coli with Impaired Cell Division at Elevated Temperature. *Mutat Res* **106:** 121-128

van den Ent F, Vinkenvleugel TM, Ind A, West P, Veprintsev D, Nanninga N, den Blaauwen T, Lowe J (2008) Structural and mutational analysis of the cell division protein FtsQ. *Mol Microbiol* **68**(1)**:** 110-123

Vasudevan P, Weaver A, Reichert ED, Linnstaedt SD, Popham DL (2007) Spore cortex formation in Bacillus subtilis is regulated by accumulation of peptidoglycan precursors under the control of sigma K. *Mol Microbiol* **65**(6)**:** 1582-1594

Vicente M, Rico AI (2006) The order of the ring: assembly of Escherichia coli cell division components. *Mol Microbiol* **61**(1)**:** 5-8

Vicente M, Rico AI, Martinez-Arteaga R, Mingorance J (2006) Septum enlightenment: assembly of bacterial division proteins. *J Bacteriol* **188**(1)**:** 19-27

Wade RH (2007) Microtubules: an overview. *Methods Mol Med* **137:** 1-16

Walker GC (1984) Mutagenesis and inducible responses to deoxyribonucleic acid damage in Escherichia coli. *Microbiol Rev* **48**(1)**:** 60-93

Walker JR, Pardee AB (1967) Conditional mutations involving septum formation in Escherichia coli. *J Bacteriol* **93**(1)**:** 107-114

Wang X, Huang J, Mukherjee A, Cao C, Lutkenhaus J (1997) Analysis of the interaction of FtsZ with itself, GTP, and FtsA. *J Bacteriol* **179**(17)**:** 5551-5559

Wang X, Reyes-Lamothe R, Sherratt DJ (2008) Visualizing genetic loci and molecular machines in living bacteria. *Biochem Soc Trans* **36**(Pt 4)**:** 749-753

Ward JE, Jr., Lutkenhaus J (1985) Overproduction of FtsZ induces minicell formation in E. coli. *Cell* **42**(3)**:** 941-949

Watanabe N, Mitchison TJ (2002) Single-molecule speckle analysis of actin filament turnover in lamellipodia. *Science* **295**(5557)**:** 1083-1086

Waterman-Storer C, Desai A, Salmon ED (1999) Fluorescent speckle microscopy of spindle microtubule assembly and motility in living cells. *Methods Cell Biol* **61:** 155-173

Waterman-Storer CM, Gregory J, Parsons SF, Salmon ED (1995) Membrane/microtubule tip attachment complexes (TACs) allow the assembly dynamics of plus ends to push and pull membranes into tubulovesicular networks in interphase Xenopus egg extracts. *J Cell Biol* **130**(5)**:** 1161-1169

Weart RB, Lee AH, Chien AC, Haeusser DP, Hill NS, Levin PA (2007) A metabolic sensor governing cell size in bacteria. *Cell* **130**(2)**:** 335-347

Weart RB, Levin PA (2003) Growth rate-dependent regulation of medial FtsZ ring formation. *J Bacteriol* **185**(9)**:** 2826-2834

Weart RB, Nakano S, Lane BE, Zuber P, Levin PA (2005) The ClpX chaperone modulates assembly of the tubulin-like protein FtsZ. *Mol Microbiol* **57**(1)**:** 238-249

Weiss DS (2004) Bacterial cell division and the septal ring. *Mol Microbiol* **54**(3)**:** 588-597

Wilson CJ, Zhan H, Swint-Kruse L, Matthews KS (2007) The lactose repressor system: paradigms for regulation, allosteric behavior and protein folding. *Cell Mol Life Sci* **64**(1)**:** 3-16

Witkin EM (1976) Ultraviolet mutagenesis and inducible DNA repair in Escherichia coli. *Bacteriol Rev* **40**(4)**:** 869-907

Woldringh CL, Mulder E, Huls PG, Vischer N (1991) Toporegulation of bacterial division according to the nucleoid occlusion model. *Res Microbiol* **142**(2-3)**:** 309-320

Wu F, Goldberg I, Filutowicz M (1992) Roles of a 106-bp origin enhancer and Escherichia coli DnaA protein in replication of plasmid R6K. *Nucleic Acids Res* **20**(4)**:** 811-817

Wu LJ, Errington J (2004) Coordination of cell division and chromosome segregation by a nucleoid occlusion protein in Bacillus subtilis. *Cell* **117**(7)**:** 915-925

Yanisch-Perron C, Vieira J, Messing J (1985) Improved M13 phage cloning vectors and host strains: nucleotide sequences of the M13mp18 and pUC19 vectors. *Gene* **33**(1)**:** 103-119

Yasbin RE, Cheo D, Bayles KW (1991) The SOB system of Bacillus subtilis: a global regulon involved in DNA repair and differentiation. *Res Microbiol* **142**(7-8)**:** 885-892

Youngman P, Perkins JB, Losick R (1984) A novel method for the rapid cloning in Escherichia coli of Bacillus subtilis chromosomal DNA adjacent to Tn917 insertions. *Mol Gen Genet* **195**(3)**:** 424-433

Yu D, Ellis HM, Lee EC, Jenkins NA, Copeland NG, Court DL (2000) An efficient recombination system for chromosome engineering in Escherichia coli. *Proc Natl Acad Sci U S A* **97**(11)**:** 5978-5983

Yu XC, Margolin W (1997) Ca2+-mediated GTP-dependent dynamic assembly of bacterial cell division protein FtsZ into asters and polymer networks in vitro. *EMBO J* **16**(17)**:** 5455-5463

Yu XC, Margolin W (1999) FtsZ ring clusters in min and partition mutants: role of both the Min system and the nucleoid in regulating FtsZ ring localization. *Mol Microbiol* **32**(2)**:** 315-326

Zhao CR, de Boer PA, Rothfield LI (1995) Proper placement of the Escherichia coli division site requires two functions that are associated with different domains of the MinE protein. *Proc Natl Acad Sci U S A* **92**(10)**:** 4313-4317

Zhou H, Lutkenhaus J (2004) The switch I and II regions of MinD are required for binding and activating MinC. *J Bacteriol* **186**(5)**:** 1546-1555

Zolkiewski M (2006) A camel passes through the eye of a needle: protein unfolding activity of Clp ATPases. *Mol Microbiol* **61**(5)**:** 1094-1100